# pH AND TEMPERATURE DEPENDENCE OF THE RATE OF DISSOLUTION OF $AgIO_3$

by

ÖMER LÜTFİ UYANIK

B.S. in Ch.E., M.E.T.U, 1974

M.S. in Ch.E., M.E.T.U, 1977



Submitted to the Institute for Graduate Studies in Science and Engineering in partial fulfillment of the requirements for the degree of

Doctor

of

Philosophy

Boğaziçi University

1984

# pH AND TEMPERATURE DEPENDENCE OF THE RATE OF DISSOLUTION OF $AgIO_3$

APPROVED BY

Prof.Dr.Vedat ENÖSTON
(Thesis Supervisor) .....

Prof.Dr.Yüksel İNEL .....

Prof.Dr.Cemil ŞENVAR .....

DATE OF APPROVAL:

28.2.1984

# ACKNOWLEDGEMENTS

I wish to express my deepest gratitude to my thesis supervisor Prof.Dr.Vedat Enüstün for his helpful comments and suggestions and his invaluable supervision throughout the course of this work.

I would also like to express my sincere appreciation to Prof.Dr.Yüksel İnel and to all other members of the Department of Chemistry for their valuable comments, criticisms and helpful suggestions.

I wish to thank my wife Nurseli Uyanık for her intense work in drawing the figures.

Finally, I am deeply grateful to Arcan Yalaz, the Technical Manager of İstanbul Kimya Sanayii, for his kindly assistance in the construction of the equipment.

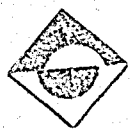

# pH AND TEMPERATURE DEPENDENCE OF THE RATE OF DISSOLUTION OF $AgIO_3$

In this thesis a theory based on a dissolution model was checked experimentally. The theory which is developed by B.V.Enüstün expresses the initial rate of dissolution for a 1:1 type ionic solid in terms of the model parameters by considering the electrochemical properties of the crystal/solution interface. The theory has been verified previously on the basis of some experimental work by observing the dependence of the initial dissolution rate of $AgIO_3$ on ionic strength in various media at $25^oC$.

In this work, the dissolution kinetics of $AgIO_3$ was investigated as a function of pH at $25^oC$, and temperature using a concentration cell with silver electrodes. It was observed that in acidic media, initial dissolution rate of $AgIO_3$ drops to an asymptotic value at high and medium pH's showing a Gouy type electrical double layer behavior due to the proton nature of $H^+$ ions.

The temperature dependence of the initial dissolution rate of $AgIO_3$ in distilled water follows an Arrhenius type relation with a reasonable value of activation enthalpy for dissolution.

The dependence of initial dissolution rate of $AgIO_3$ on ionic strength in various media at $25^{o}C$ was also followed and the results previously obtained have been reproduced.

Two important conclusions reached at the end of the work were that in the presence of small hydrated cations in the dissolution medium the electrical double layer behaves as a Gouy layer and in the presence of large hydrated cations it behaves as a Stern layer.

# GÜMÜŞ İYODATIN ÇÖZÜNME HIZININ pH VE SICAKLIĞA BAĞLILIĞI

Bu tezde bir çözünme modeline dayalı bir teori, deneysel olarak gerçeklendi. B.V.Enüstün tarafından geliştirilmiş olan teori, 1:1 tipi bir iyonik katının başlangıçtaki çözünme hızını, kristal/çözelti arayüzünün elektrokimyasal özelliklerini gözönüne alarak model parametreleri cinsinden ifade etmektedir. Teori, daha önce, $AgIO_3$'ın başlangıçtaki çözünme hızının ortamın iyon gücüne bağımlılığının çeşitli ortamlarda incelenmesiyle gerçeklenmişti.

Bu çalışmada, $AgIO_3$'ın çözünme kinetiğinin pH'a ve sıcaklığa göre değişimleri, gümüş elektrotlar içeren bir konsantrasyon pili ile incelendi. Asitli ortamda yürütülen çözünme deneyleri sonunda, $AgIO_3$'ın başlangıçtaki çözünme hızının, yüksek ve orta pH değerlerinde asimtotik olarak düşerek Gouy tipi bir elektriksel çift tabaka davranışına uyduğu gözlendi. Bu davranışa, $H^+$ iyonlarının proton tabiatının neden olduğu ileri sürüldü.

$AgIO_3$'ın saf sudaki çözünme hızının, sıcaklığa Arrhenius tipi bir ifade ile bağıntılı olduğu görüldü ve bu bağıntının grafiksel incelenmesinden, makul bir çözünme aktiflenme entalpisi değeri elde edildi.

$AgIO_3$'ın, 25°C'de başlangıçtaki çözünme hızının, ortamın iyon gücüne bağımlılığı da çeşitli ortamlarda incelenerek daha önce elde edilmiş olan sonuçlara varıldı.

Bu çalışmanın sonucunda ulaşılan iki önemli sonuçtan biri, çözünme ortamında küçük hidratize katyonların bulunması halinde, elektriksel çift tabakanın Gouy tipinde olduğu, diğeri ise çözünme ortamında büyük hidratize katyonların bulunması halinde elektriksel çift tabakanın Stern tipinde olduğudur.

# TABLE OF CONTENTS

# LIST OF TABLES

# LIST OF FIGURES

# LIST OF SYMBOLS

| | |
|---|---|
| $A$ | Surface area |
| $a$ | Activity of solution |
| $a_s$ | Activity of saturated solution |
| $a'$ | A parameter defined by Equation 2.26 |
| $b$ | A constant which is given in Equation 2.30 and is related to adsorption potential and thickness of Stern layer |
| $C$ | Concentration of dissolved substance |
| $C_{eq}$ | Concentration of saturated solution |
| $C_1$ | Initial concentration in the "delay in equilibriation" experiments |
| $C_2$ | Actual concentration in the "delay in equilibriation" experiments |
| $C_{\pm}^*$ | Surface concentration of the ion concerned at its transition state involved in dissolution |
| $D$ | Dielectric constant |
| $E$ | Applied potential |
| $E_m$ | Value of E which makes rate of dissolution maximum |
| $e$ | Unit electrical charge |
| $F$ | One Faraday of electricity |
| $\Delta G_{\pm}^*$ | Free energy of activation for the dissolution of the ion concerned |
| $\Delta H_{\pm}$ | Enthalpy change accompanying the movement of one mole of a surface ion by a distance x |
| $\Delta H_{\pm}^o$ | Enthalpy change during the movement of the ion from the surface into the solution at the zero surface potential |
| $\Delta H_{\pm}^c$ | Change in the crystal lattice enthalpy |
| $\Delta H_{\pm}^s$ | Change in the solvation enthalpy |
| $\Delta H_{\pm}^*$ | Activation enthalpy for the dissolution of the ion concerned |
| $(\Delta H_{\pm}^*)^o$ | Activation enthalpy for the dissolution of the ion concerned at zero surface potential |
| $\Delta H^*$ | Activation enthalpy for the dissolution at the steady value of surface potential |
| $h$ | Planck constant |

| | |
|---|---|
| $I$ | Ionic strength |
| $k$ | Initial specific rate of dissolution at the steady value of surface potential |
| $k_{\pm}$ | Initial specific rate of dissolution for the ion concerned |
| $k^{o}_{\pm}$ | Initial specific rate of dissolution for the ion concerned at zero surface potential |
| $k'$ | Rate constant for the dissolution in the "delay in equilibriation" experiments |
| $k_d$ | Rate constant for the delay in equilibriation at the silver electrode |
| $k_g$ | Initial specific rate of dissolution in Gouy layer |
| $k_s$ | Initial specific rate of dissolution in Stern layer |
| $k_1$ | Rate constant in Equation 1.1 |
| $k_4$ | Rate constant in Equation 1.4 |
| $k_5$ | Rate constant in Equation 1.5 |
| $k_6$ | Rate constant in Equation 1.6 |
| $k_7$ | Rate constant in Equation 1.7 |
| $k_8, k_9$ | Rate constants in Equation 1.8 |
| $k_B$ | Boltzmann constant |
| $N$ | Total number of sites on the surface |
| $N'$ | Number of sites on the activation plane |
| $N_d$ | Number of divisions on recorder output |
| $N_o$ | Avogadro number |
| $n$ | Number of moles of sites on the surface |
| $n'$ | Number of moles of ions in activation plane |
| $n_1$ | Exponent in Equation 1.1 |
| $n_s$ | Molar surface concentration of the solid |
| $p$ | Intercept of calibration function |
| $p'$ | Group of constants involving transference number of the anion, temperature and universal constants given in Equation A.3.1 |
| $q$ | Slope of calibration function |
| $R$ | Gas constant |
| $Rd$ | Rate of dissolution |
| $r$ | A parameter defined by Equation 2.24 |
| $r_a$ | Rate of ion adsorption |
| $r_d$ | Rate of ion desorption |

| | |
|---|---|
| $r_g$ | Value of parameter "r" defined by Equation 2.24 in case of Gouy layer |
| $r_s$ | Value of parameter "r" defined by Equation 2.24 in case of Stern layer |
| $r_+$ | Radius of cation ($Ag^+$) |
| $r_-$ | Radius of anion ($IO_3^-$) |
| $r_o$ | Sum of the radii of $Ag^+$ and $IO_3^-$ |
| $(r_+)_h$ | Hydrated radius of cation |
| S | Entropy |
| $\Delta S^*_\pm$ | Entropy of activation |
| T | Temperature |
| t | Time |
| $X^*_\pm$ | Mole fraction of the available sites occuppied by activated ions on the respective activation plane |
| x | Distance from the solid surface into solution |
| $x_\pm$ | Distance between the surface and activation plane |
| Z | Valency of the ion concerned |
| $\alpha_\pm$ | Short range relative potential drop defined by Equation 2.7 |
| $\eta$ | Viscosity of the solvent |
| $\varepsilon$ | Cell potential |
| $\gamma$ | Integration constant in Equatian A.4.8 |
| $\lambda_\pm$ | Limiting equivalent ionic conductance |
| $\Omega$ | Number of ways of distributing N' identical things on N labeled sites |
| $\psi$ | Surface potential |
| $\psi_x$ | Potential at any distance x |
| $\psi_\pm$ | Double layer potential at the distance x for the ion concerned |
| $\sigma$ | Specific surface of the solid |

# CHAPTER I

## REVIEW OF THE LITERATURE

During the first half of the twentieth century, research in crystal dissolution emphasized the transport of dissolved material between the crystal surface and the bulk of the solution. Research about the dissolution mechanism at the crystal surface has been conducted much more recently. This development started with the work of Jones[1] who found that the dissolution of $PbSO_4$ crystals in water was surface controlled and governed by a rate law of the following form

$$(1.1) \qquad R_d = k_1 A (C_{eq} - C)^{n_1}$$

where $R_d$ is the dissolution rate, A is the surface area, $C_{eq}$ is the salt solubility, C is the salt solution concentration, and $k_1$ and $n_1$ are constants. For the surface dissolution of nine sparingly soluble salts, the above equation has been confirmed and for symmetrical electrolytes like $PbSO_4$, $n_1$ has been found as 2; but for unsymmetrical 2:1 electrolytes like $Ba(IO_3)_2$, $n_1$ appeared to be 3. Models for the surface dissolution of crystals must rationalize the unusual solute concentration dependence of dissolution rates and the values found for the "reaction order" $n_1$ in Equation 1.1. According to this equation, the basic driving force for crystal dissolution is the deviation from the solubility equilibrium, $(C_{eq} - C)$. However, this form is expected on thermodynamic grounds only for almost saturated solutions with $n_i = 1$. Similarly, this concentration dependence cannot be explained by analogy with the kinetics of homogeneous solution reactions, as applied to a chemically controlled dissolution

reaction

$$(1.2) \qquad A_aB_b(s) \overset{H_2O}{\rightleftharpoons} aA^{b+}(aq) + bB^{a-}(aq)$$

If the dissolved ions are fully ionized and incorporated directly into the crystal in the reverse direction, then a concentration dependence of the type $(C_{eq}^{n_1} - C^{n_1})$ is expected. This type of a concentration dependence cannot be reduced to the form of Equation 1.1. For that reason, more complicated models are required for modelling these dissolution rates.

Linge[2] reported two dissolution models called (a) Screw Dislocation Model and (b) Adsorption Layer Model which have been derived from models proposed for crystal growth. These models have the following general ideas in common.

A. Crystal dissolution spreads from preferred locations (e.g., kinks in steplines) on the surface.

B. The crystal surface is in thermodynamic equilibrium with the crystal bulk, so that the reaction steps within the crystal lattice are not included into the kinetic analysis.

C. Since a direct single step transfer from kink sites to the solution adjacent to the surface is not energetically favored, ion motion on the surface must always be a consecutive reaction step in the crystal dissolution mechanism.

The surface reaction therefore consists of the following separate steps: (1) hydration of lattice ions at a kink site on the surface; (2) surface transport of lattice ions from kinks along and between steplines; (3) desorption of ions from points between steplines on the crystal surface into the adjacent solution phase in a rapid and reversible manner so that solute in the solution is effectively in

equilibrium with the solute on the crystal surface at points of desorption.

Screw dislocation model considers self-perpetuating steplines formed on the crystal surface by screw dislocations, which are a common form of crystal imperfection in nearperfect lattices. In dissolution, the steplines spiral down into the surface, forming conical pits and the fresh kink sites needed to sustain the reaction. Ion hydration at each kink takes place by a reversible reaction between the crystal and adsorbed solvent. Ions leave and reenter the crystal phase as separate entities, but the overall reaction rates for each type of ion are presumed to be strongly coupled that the same relaxation time can be used for modelling the separate cation and anion reactions. Therefore the reaction format is of the following type

$$(1.3) \qquad (A_aB_b)_c + h\ H_2O \rightleftharpoons (A_aB_b)_h$$

where $(A_aB_b)_c$ denotes a stoichiometric assembly of lattice ions at crystal kinks and $(A_aB_b)_h$ denotes a stoichiometric assembly of partly hydrated lattice ions adsorbed on the crystal surface. The net rate at which solute leaves kinks, which is the difference between the forward and reverse rate in Equation 1.3 becomes zero when the solution in contact with the crystal is saturated. In this way, the kinetics in a subsaturated solution is defined assuming that the intrinsic rates at which ions leave the crystal phase is constant. This assumption is valid if the solvent activity and the kink density (expressed per unit length of stepline) do not change in the course of the reaction. Considering the above kinetic argument and describing the solute transport between steplines and points of desorption on the crystal surface by Fick's Laws of diffusion with a constant surface diffusion coefficient, the rate of dissolution in a near saturated solution takes the form

$$(1.4) \qquad R_d = k_4\ A(C_{eq} - C)^2$$

applicable to the dissolution of symmetrical electrolytes in near-saturated solutions. However, it is obvious that the dissolution rates of unsymmetrical electrolytes cannot be explained by this model for any arbitrary condition. The details of the screw dislocation model and the derivation of Equation 1.4 are given in several papers[2,3,4].

The basic ideas of adsorption layer model were developed by Davies and Jones[5] for crystal growth and later adapted for crystal dissolution[2]. The central feature in this model is an adsorption layer within which ion surface diffusion is presumed to be rapid, and the hydration reaction at crystal kinks solely controls the dissolution rate. The model assumes that: (i) an ion layer of constant composition always covers wet crystals; and (ii) that net dissolution occurs only in the event of simultaneous hydration of equivalent amounts of oppositely charged ions. The rate of ion adsorption ($r_a$) from the adjoining solution is proportional to C and because of the constancy of the composition of the ion layer, the rate of ion desorption ($r_d$) from the layer is constant. Since $r_d = r_a$ in a saturated solution the net rate of layer depletion ($r_n$) in subsaturated solutions would be

$$(1.5) \qquad r_n = r_d - r_a = k_5 (C_{eq} - C)$$

The net rate of hydration of the cations and anions at kinks must each separately have the same mathematical form as Equation 1.5. Noting that the probability of simultaneous release of equivalent amounts of oppositely charged ions into the solution per unit surface area is the product of the separate events which can lead to ion-hydration, the rate of dissolution of the lattice $A_aB_b$ in water is expressed as

$$(1.6) \qquad R_d = k_6 A (C_{eq} - C)^{a+b}$$

which agrees with the experimental results obtained for symmetrical (a + b = 2) and unsymmetrical (a + b = 3) salts

for the whole of the reaction ($0 \leqq C \leqq C_{eq}$). This makes the adsorption layer model powerful in most cases. The details of the adsorption layer model are given in Davies and Jones' paper[5].

Electrochemical concepts have a better prospect for defining the form of the relationship between cation and anion rates for crystal dissolution when the ionic concentration terms deviate from their stoichiometric value, e.g., as is the case for impure crystals, or when one or both of the lattice ions is separately introduced into the dissolving solution from another source. The central idea in the electrochemical theory is that the transfer of ions from the kinks at the crystal surface is explicitly dependent on the electrical potential just like any electron charge transfer step. Although the phase boundary potential of a freely dissolving crystal is defined by the equivalence of the cation and anion flux at the steady state, a closed analysis of the rate-solution concentration dependence cannot be achieved unless arbitrary assumptions are proposed for the potential-concentration dependence during the reaction. The theories advanced thus far have therefore not been useful for treating conventional dissolution rate data (i.e., for examining a measured rate-concentration dependence).

Thus far, these electrochemical ideas have been applied mainly for interpreting the influence of applied electrical potentials on initial dissolution rates of semiconductors (e.g., of metal oxides). Even for this restricted case, arbitrary assumptions must be introduced which effectively predefine the ionic interaction. Engell[6] assumed that (1) the solvent concentration at kink sites does not change during the dissolution; (2) with an applied potential E, the electrical potential across the phase boundary $\psi$, can be changed proportionally; (3) the surface population of solute is constant. These assumptions led to a rate law of the form

(1.7) $$R_d = \exp (k_7 E)$$

if the crystal activity coefficients are not dependent on the potential. Vermilyea[7] obtained a rate equation, using the first two assumptions of Engell and further assuming that the sum of cation and anion sites in a crystal lattice is always constant, in the following form

(1.8) $$R_d = [\exp (k_8 E) + \exp (-k_9 E)]^{-1}$$

Equation 1.8 predicts a maximum in the dissolution rate at a certain value ($E_m$) of E, but transforms into the same mathematical form as Equation 1.7 when E is sufficiently large (i.e., $|E| >> E_m$). However, $E_m$ values cannot be calculated independently and the experimental distinction between Engell and Vermilyea treatments is therefore vague.

Some experimental results[6,8] confirm the exponential dependence of $R_d$ on electrical potential. There seems to be only one example available where a dissolution rate maximum is just apparent: this refers to the dissolution of lithiated NiO in sulphuric acid solutions as reported by Lee and Yeager[8]. On the other hand, Landsberg et al.[9] have shown that the dissolution rate of ZnO in alkali is independent of potential. These contradictions do not clarify how the electrochemical concepts should be applied to ionic crystals.

# CHAPTER II

# THEORETICAL BASIS OF THE PRESENT WORK

## 2.1. INTRODUCTION

In a more recent theory developed by Enüstün[10], independent motion of ions and its electrochemical consequences were considered in relation to coupling of dissolution of each type of ion and thus formulating the overall dissolution rate. As the experimental results of the present work were evaluated on the basis of this model the underlying theory will be given in this chapter.

The dissolution of an MA type ionic solid can be represented in terms of the transition state concept as

$$\underset{\text{solid surface}}{\text{ion on the}} \rightleftharpoons \underset{\text{ion}}{\text{activated}} \longrightarrow \underset{\text{ion}}{\text{dissolved}}$$

Then the specific rate of dissolution (per unit surface area) $k_+$ of the cation $M^{z+}$ and $k_-$ of the anion $A^{z-}$ can be expressed in the following manner

$$(2.1) \qquad k_{\pm} = (k_B\, T/h)C^*_{\pm}$$

where $C^*_{\pm}$ is the surface concentration of the ion concerned at its transition state involved in dissolution, T is the absolute temperature, $k_B$ and h are Boltzmann and Planck constants respectively.

The development of the theory is based on the

following assumptions

(a) The dissolution process is not diffusion controlled. In other words diffusion is so rapid that it does not affect the dissolution rate.

(b) The dissolution medium is sufficiently dilute with respect to all dissolved species.

(c) The activated cations and anions are situated on two planes parallel to the solid surface at short distances from the surface, and the number of sites available for activated ions on one plane is equal to that of ions of that kind on the solid surface.

(d) The dissolving solid is in the form of a perfect crystal.

(e) There is not any ion common with the dissolving solid, in the medium.

(f) The hydration energy of the cation $M^{z+}$ is greater than that of the anion $A^{z-}$.

## 2.2. TRANSITION STATE FOR DISSOLUTION

In order to evaluate C*, the formation of an energy barrier for dissolution between the solid surface and the solution on the basis of a simple model for the transition state is considered.

When the system is at the zero point of charge, the enthalpy change $\Delta H^{o}_{\pm}$ accompanying the passage of one mole of an ion from the solid surface to the solution can be expressed as

(2.2) $$\Delta H^{o}_{\pm} = \Delta H^{c}_{\pm} + \Delta H^{s}_{\pm}$$

where $\Delta H^{c}_{\pm}$ is the change in the crystal lattice enthalpy and $\Delta H^{s}_{\pm}$ is the enthalpy change due to solvation(hydration). It is a known fact that $\Delta H^{c}_{\pm}$ is always positive and $\Delta H^{s}_{\pm}$ is always negative.

All these enthalpy changes plotted as functions of the perpendicular distance of displacement x of an ion from the solid surface towards the solution are shown schematically in Figure 2.1.

$\Delta H^{c}_{\pm}$ curve represents the Coulombic interaction on an ion which is moving into the solution phase. A single curve like this is assumed to represent both $\Delta H^{c}_{+}$ and $\Delta H^{c}_{-}$ (This assumption is valid at least in the case of a simple cubic crystal).

As an ion moves away from the solid surface by such a short distance that hydration is not significant yet, $\Delta H^{s}_{\pm}$ is nearly zero. If it travels further towards solution, $\Delta H^{s}_{\pm}$ starts to become important due to partial hydration. When it enters the solution substantially, contribution of $\Delta H^{s}_{\pm}$ will increase, especially when the clearance between this ion and the neighboring ions on the solid surface becomes large enough for the passage of the water molecules to build up the first hydration shell. Further on, $\Delta H^{s}_{\pm}$ will level off because of the completion of multilayer hydration.

$\Delta H^{o}_{+}$ and $\Delta H^{o}_{-}$ curves which are the algebraic sums of the corresponding $\Delta H^{c}_{\pm}$ and $\Delta H^{s}_{\pm}$ curves exhibit maxima at the points where the $\Delta H^{s}_{\pm}$ contribution starts to become important. Each maximum defines the transition state of the ion concerned and the peak heights of $\Delta H^{o}_{+}$ and $\Delta H^{o}_{-}$ are the activation enthalpies $(\Delta H^{*}_{+})^{o}$ and $(\Delta H^{*}_{-})^{o}$ for the dissolution of the cation and anion respectively, at zero surface potential. As mentioned in assumption (c) these maxima occur at short distances $x_{+}$ and $x_{-}$ from the surface at which the activation planes are

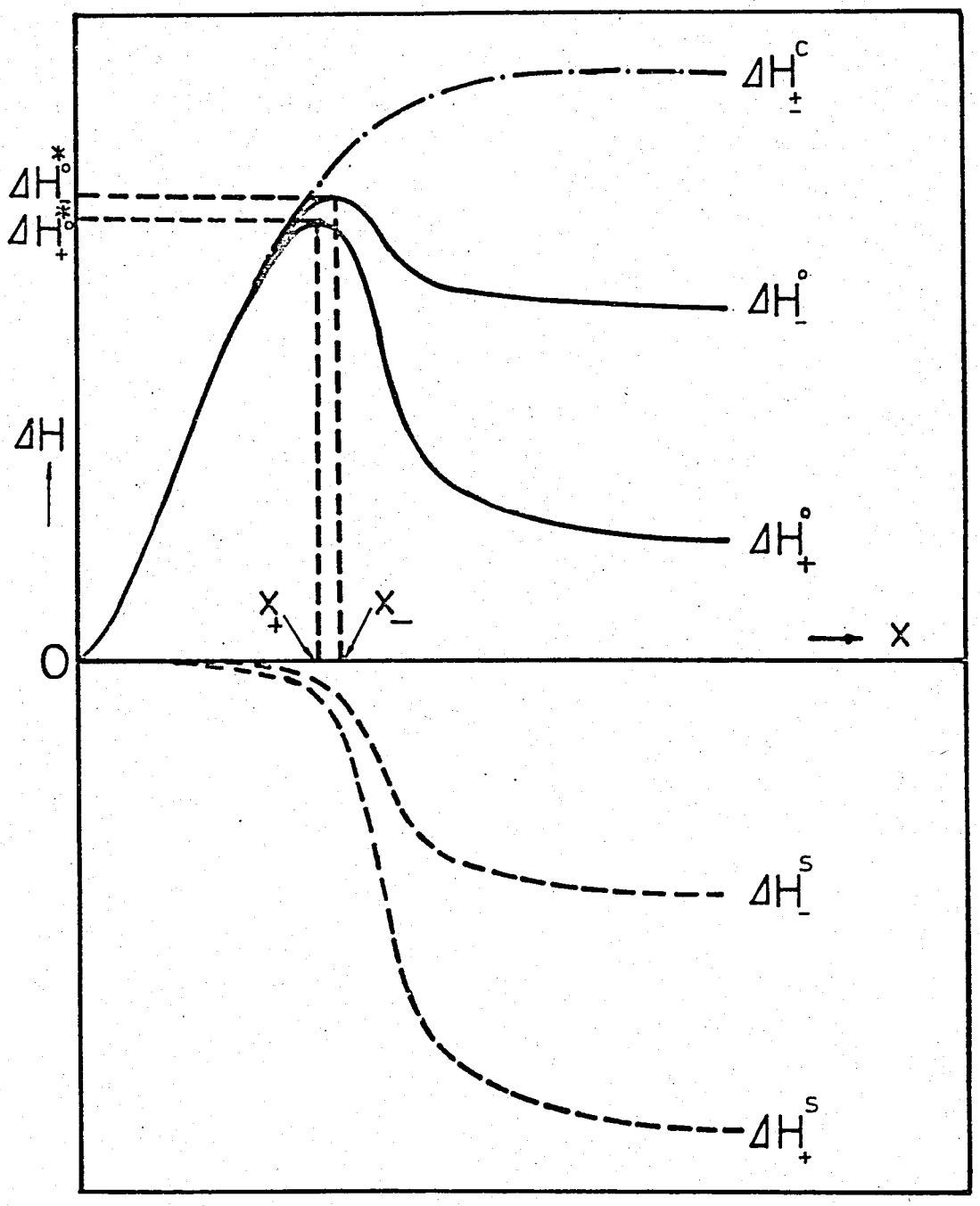


FIGURE 2.1. Enthalpy Changes as a Function of Distance of Separation at Zero Point of Charge.

located; and for each type of ion the number of occupiable sites on the corresponding activation plane is equal to that on the solid surface. On the other hand, assumption (b) can be related to the transition state as follows: The dissolution medium covering both the surface phase (defined to include the two planes of activation) and the solution phase is dilute enough with respect to all dissolved species not to affect $\Delta H_{\pm}^{s}$ nor the random distribution of the activated ions over the whole surface. A consequence of this assumption is that $\Delta H_{\pm}^{o}$ is independent of the composition of both phases.

One final remark about the transition state is that because of assumption (f), $|\Delta H_{+}^{s}| > |\Delta H_{-}^{s}|$. (This is illustrated in Figure 2.1). As can be seen from the figure, when assumption (f) holds (as is generally the case),

$$(\Delta H_{+}^{*})^{o} < (\Delta H_{-}^{*})^{o} \tag{2.3}$$

and

$$x_{+} < x_{-} \tag{2.4}$$

## 2.3. ELECTRICAL DOUBLE LAYER POTENTIAL

When the solid surface possess an electrical potential $\psi$ relative to the solution the enthalpy change $\Delta H_{\pm}$ accompanying the movement of one mole of a surface ion by a distance x is given by

$$\Delta H_{\pm}(x) = \Delta H_{\pm}^{o}(x) \mp z F(\psi - \psi_{x}) \tag{2.5}$$

where z is the valency of the ion concerned, F is one Faraday and $\psi_x$ is the potential at distance x. If the function $\psi_x$ is is known, $\Delta H_{\pm}(x)$ can be plotted from the $\Delta H_{\pm}^{o}(x)$ curves of Figure 2.1. Such a construction is shown schematically in Figure 2.2, using a given (negative) potential profile $\psi_x$ and assuming that the electrical double layer extends beyond the

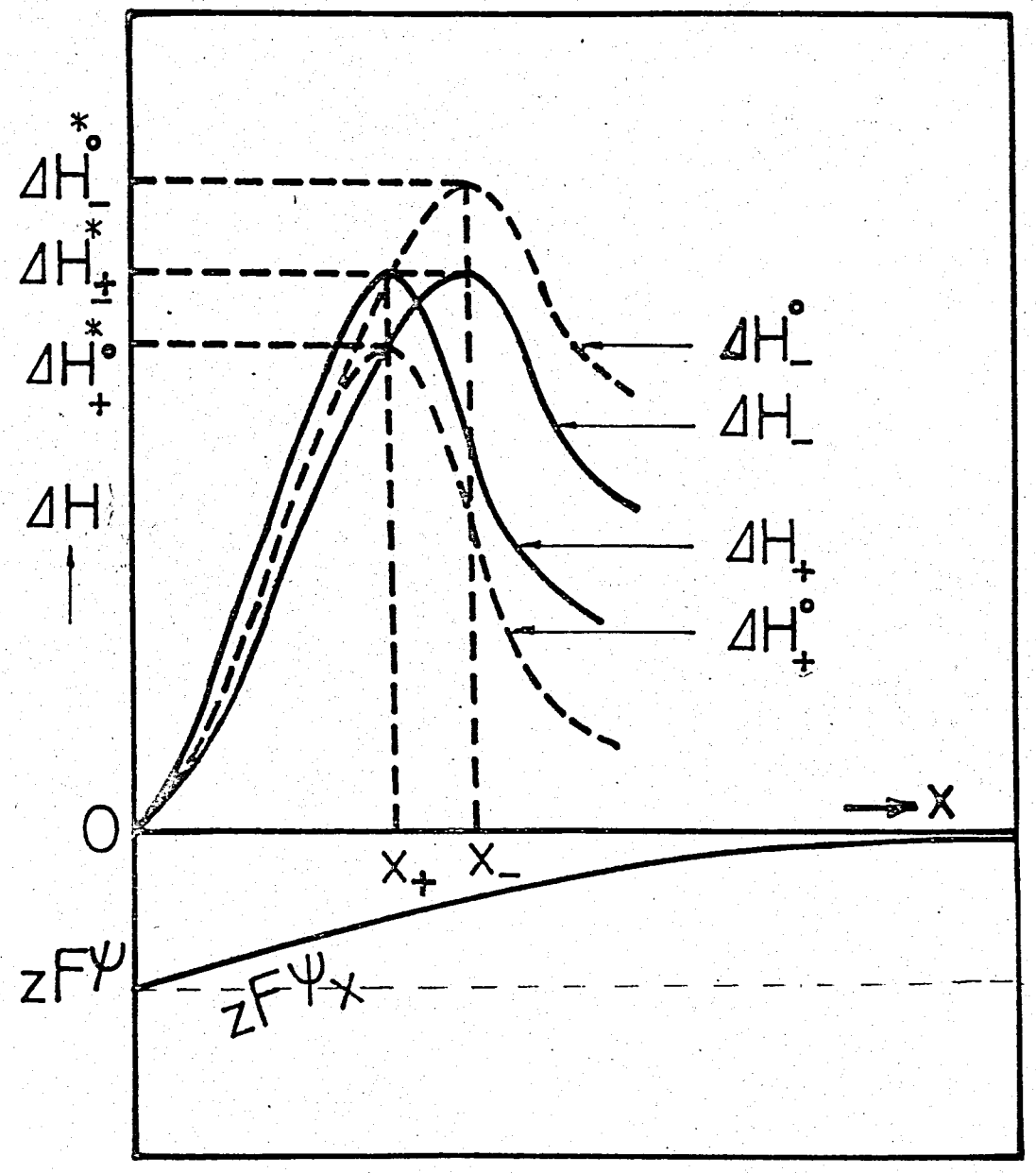


FIGURE 2.2. Enthalpy Changes as a Function of Distance of Separation at a Surface Potential $\psi$.

energy barriers.

The activation enthalpies are expressed in accordance with Equation 2.5 as

$$\Delta H^{*}_{\pm} = (\Delta H^{*}_{\pm})^{o} \mp zF\,(\psi - \psi_{\pm}) \qquad (2.6)$$

where $\psi_{\pm}$ is the double layer potential at the distance $x_{\pm}$ for the ion concerned, and since the double layer is assumed to extend beyond the energy barries $\psi_{\pm} \neq 0$.

A quantity called "short range relative potential drop" for the cation and anion is defined by

$$\alpha_{\pm} = (\psi - \psi_{\pm})/\psi \qquad (2.7)$$

Unless the counter ions in the surface phase are involved in a charge reversing specific adsorption, $|\psi_x|$ is a decreasing function of x, and approaches zero as $x \to \infty$. For that reason, $\alpha$ must have positive values less than unity, and since $x_{+} < x_{-}$

$$\alpha_{+} < \alpha_{-} \qquad (2.8)$$

## 2.4. ENTROPY OF ACTIVATION FOR DISSOLUTION

The entropy of activation, $\Delta S^{*}_{\pm}$, is the differential entropy change on transferring one mole of an ion from the solid surface to the activation plane. It is independent of the surface potential. Ignoring the contributions other than the configurational, a statistical analysis on the basis of assumptions (b), (c) and (d) gives

$$\Delta S^{*}_{\pm} \fallingdotseq -R\,\ell n\left[X^{*}_{\pm}/(1-X^{*}_{\pm})\right] \qquad (2.9)$$

where R is the gas constant and $X^{*}_{\pm}$ is the mole fraction of the available sites occupied by the activated ions on the respective activation plane. (The derivation of Equation 2.9

is given in Appendix I). Equation 2.9 can be simplified further on grounds of the diluteness of the surface phase with respect to activated ions, to the following form.

(2.10) $\Delta S^*_{\pm} = -R \ell n X^*_{\pm}$

## 2.5. RATE OF DISSOLUTION AND THE DOUBLE LAYER

The free energy of activation $\Delta G^*$ is given by

(2.11) $\Delta G^*_{\pm} = \Delta H^*_{\pm} - T\Delta S^*_{\pm}$

Substitution of Equation 2.10 into Equation 2.11 gives

(2.12) $\Delta G^*_{\pm} = \Delta H^*_{\pm} + RT \ell n X^*_{\pm}$

As stated in Section 2.1 an equilibrium exists between the ions on the solid surface and the activated ions, in accordance with the transition state theory. Therefore, $\Delta G^*_{\pm} = 0$. With this condition, Equation 2.12 gives

(2.13) $X^*_{\pm} = \exp(-\Delta H^*_{\pm}/RT)$

$X^*_{\pm}$ can be related to $C^*_{\pm}$ in Equation 2.1 through

(2.14) $C^*_{\pm} = n_s X^*_{\pm}$

where $n_s$ is the molar surface concentration of the solid. Combining Equations 2.1, 2.13 and 2.14 the specific rate of dissolution is obtained in the following form

(2.15) $k_{\pm} = (k_B T/h)\, n_s \exp(-\Delta H^*_{\pm}/RT)$

The specific rate of dissolution at the zero point of charge, $k^*_{\pm}$, is then expressed as follows

(2.16) $k^o_{\pm} = (k_B T/h)\, n_s \exp\left[-(\Delta H^*_{\pm})^o/RT\right]$

Combination of Equations 2.15, 2.16 and 2.6 results in

$$(2.17) \qquad k_{\pm} = k_{\pm}^{o} \exp\left[\pm zF(\psi - \psi_{\pm})/RT\right]$$

Equation 2.17 can further be simplified by using Equation 2.7, to the following form

$$(2.18) \qquad k_{\pm} = k_{\pm}^{o} \exp\left[\pm zF\alpha_{\pm}\psi/RT\right]$$

In the case of an ionic solid placed into an aqueous medium containing no common ion with the solid itself, the only process to be considered is the continuous dissolution of surface ions (Crystallization can be neglected in a system which is so far from saturation).

In the light of Equation 2.3, Equation 2.16 indicates that

$$(2.19) \qquad k_{-}^{o} < k_{+}^{o}$$

Equation 2.19 shows that, at the time of placement of the solid into the aqueous medium (a situation at which $\psi = 0$), the cations will dissolve faster than anions. As a result of this, the solid surface will start having a negative potential and, because of Equation 2.17, soon $\psi$ will assume a steady value to provide

$$(2.20) \qquad k_{+} = k_{-} = k$$

With the condition in Equation 2.20, Equation 2.15 implies that

$$(2.21) \qquad \Delta H_{+}^{*} = \Delta H_{-}^{*}$$

This result is shown in Figure 2.2 with equal peak heights of $\Delta H_{+}$ and $\Delta H_{-}$ curves.

The steady value of $\psi$ mentioned above can be obtained

from Equations 2.20 and 2.18 as

$$(2.22) \qquad \psi = \left[RT/zF(\alpha_+ + \alpha_-)\right] \ln(k_-^o/k_+^o)$$

The specific rate of dissolution, k, can be expressed by eliminating $\psi$ between the conjugate equations 2.18 as follows

$$(2.23) \qquad k = k_+ = k_- = (k_+^o)^r (k_-^o)^{1-r}$$

where

$$(2.24) \qquad r = \alpha_-/(\alpha_+ + \alpha_-)$$

Because of the potential acquired by the surface, an electrical double layer is formed which is composed of a surface charge resulted from the ions on the surface and a charge in solution resulted from the distribution of counter-ions (cations) away from the surface. As a result of the electrical double layer formed, a potential profile develops. The $\alpha_+$ and $\alpha_-$ values depend on this profile because of Equation 2.7. Hence the potential profile developed affects r through Equation 2.24 and the specific rate of dissolution k through Equation 2.23.

As far as the energy barriers (activation planes) are concerned, two types of potential profiles are possible:

(I) If the closest distance of approach of the hydrated counter-ion (cation) is much smaller than the distance between the surface and the energy barriers, the potential profile in this region will be of Gouy type for which mathematical analysis gives a concave downwards shape obeying the following function[11]

$$(2.25) \qquad \psi_x = \psi \exp(-a'x)$$

where

$$(2.26) \qquad a' = (8\pi e^2/DRT)^{1/2} \cdot (I)^{1/2}$$

In Equation 2.26, e is the charge of an electron, D is the dielectric constant of the medium and I is the ionic strength of the solution. It is observed from the definition of a' that as ionic strength increases a' also increases and correspondingly the slope of the exponential potential profile becomes steeper.

The value of the parameter r in the case of a Gouy layer is obtained from Equations 2.24, 2.7 and 2.25 as

$$(2.27) \qquad r_g = \left[1-\exp(-a'x_-)\right] / \left[2-\exp(-a'x_+)-\exp(-a'x_-)\right]$$

The analysis of the expression obtained by substituting Equation 2.27 into Equation 2.23 shows that the rate of dissolution in a Gouy layer, $k_g$, depends on the ionic strength of the solution in such a manner that rate decreases as ionic strength increases.

Mathematical analysis of the problem from the point of view of activation enthalpies (using Figure 2.2) shows that at zero ionic strength the activation enthalpies are at their minimum limiting value equal to

$$(2.28) \qquad (\Delta H_+^*)_{min.} = (\Delta H_-^*)_{min.} = \frac{x_-}{x_+ + x_-}(\Delta H_+^*)^o + \frac{x_+}{x_+ + x_-}(\Delta H_-^*)^o$$

and therefore the rate of dissolution is maximum. As the ionic strength increases the activation enthalpies also increase and dissolution rate decreases. At infinite ionic strength, activation enthalpies increase up to the arithmetic mean of $(\Delta H_+^*)^o$ and $(\Delta H_-^*)^o$ as shown by Equation 2.29

$$(2.29) \qquad (\Delta H_+^*)_{max} = (\Delta H_-^*)_{max} = \frac{1}{2}(\Delta H_+^*)^o + \frac{1}{2}(\Delta H_-^*)^o$$

and the dissolution rate is minimum.

(II) If the radius of the hydrated counter-ion (cation) is larger than the distance between the surface and the energy barriers and if there is a strong electrostatic interaction between the counter-ion and the surface the electrical double layer formed will be a Stern layer for which the potential profile is linear all the way from the surface past the energy barriers as in the following form

$$\psi_x = \psi(1 - bx) \tag{2.30}$$

where b is a positive constant related to the adsorption potential and thickness of the Stern layer[11].

The value of the parameter r in the case of a Stern layer is obtained from Equations 2.24, 2.7 and 2.30 as

$$r_s = x_-/(x_+ + x_-) \tag{2.31}$$

Since $r_s$ does not depend on ionic strength, there is no dependence of the rate of dissolution in a Stern layer, $k_s$, on ionic strength. At zero ionic strength, i.e., for $a' = 0$, the value of $r_g$ calculated from Equation 2.27 becomes equal to $r_s$ given by Equation 2.31. Thus, whatever the ionic strength of the solution is, the rate of dissolution in a Stern layer will be equal to that in a Gouy layer at zero ionic strength. This is equivalent to saying that the activation enthalpies in case of Stern layer are at their minimum value given by Equation 2.28, for a Gouy layer at zero ionic strength.

## 2.6. CONCLUSIONS FROM THE THEORY

From the foregoing discussion of the theory the following conclusions can be reached which should be checked experimentally:

(a) Presence of small hydrated cations should decrease

the dissolution rate. As the ionic strength increases, the dissolution rate should fall asymptotically to a limiting value.

(b) Presence of large hydrated cations should have no effect on the dissolution rate.

(c) In the presence of small and large hydrated cations, it is expected that large hydrated polyvalent cations will preferably form a Stern adsorption layer which is impervious to small hydrated monovalent cations. Therefore, in a mixed medium containing such polyvalent cations, the dissolution rate should be independent of the ionic strength.

## 2.7. PREVIOUS ATTEMPTS TO VERIFY THE THEORY

As stated in Section 2.6 the theoretical conclusions reached lend themselves to experimental checking. For this purpose the dissolution of $AgIO_3$ was followed in a series of experiments by Enüstün and Ayranci[12].

For the verification of conclusion (a), they have needed experimental data in a dissolution medium containing cations small enough to enter the gap between the negatively charged solid surface and the energy barriers to start a Gouy layer in this gap, and inert enough not to interact electrostatically with the surface to cause a strong Stern adsorption. $K^+$ ion was found to serve both purposes. (Its large crystallographic radius causes its hydrated radius to be small and its small charge causes it to be electrostatically inert). They have conducted experiments in media containing $KNO_3$ at different concentrations and obtained the initial dissolution rate as a function of ionic strength. It has been observed that at low and medium ionic strengths the trend of the plot is consistent with theoretical conclusion

(a), i.e., as the ionic strength increases, the dissolution rate decreases to an asymptotic value and then remains constant. At high ionic strengths, however, rate increases up to about its value in distilled water most probably because of the invalidity of assumption (b) of the theory in concentrated media.

For the verification of conclusion (b), experimental data obtained in a dissolution medium containing cations which remain beyond the energy barriers and cause an effective Stern adsorption was necessary. $Al^{3+}$ ion was found to be suitable because of its large hydrated radius and large charge (since the crystallographic radius of $Al^{3+}$ is rather small its hydrated radius is large and its large charge cause it to be electrostatically active). They have conducted experiments in media containing $Al_2(SO_4)_3$ at different concentrations. Their rate v.s. ionic strength plot revealed that at low and medium ionic strengths, as the ionic strength increases the dissolution rate showed an asymptotic decrease which is much smaller than that in $KNO_3$ media. This indicated the presence of a Stern layer produced by $Al^{3+}$ ions outside the energy barriers and a Gouy layer character in the inner parts which was possibly caused by $H^+$ ions resulted from the hydrolysis of $Al^{3+}$ ions. At high ionic strengths an increase in rate was observed as in the previous case.

For testing conclusion (c), they have carried out experiments with $Al^{3+}$ adsorbed $AgIO_3$ samples in dissolution media containing $KNO_3$ at different concentrations. The adsorption of $Al^{3+}$ was carried out in such a manner that the dissolution system contained very small amount of $Al^{3+}$ (less than $10^{-8}$ M). The rate of dissolution in such a system was observed to be nearly equal to that in distilled water irrespective of $K^+$ concentration. This result was in agreement with theoretical conclusion (c). $Al^{3+}$ ions produced a Stern layer outside the energy barriers and there was practically no $H^+$ ion which can penetrate into this layer, since the $Al^{3+}$ concentration was very small.

## 2.8. PURPOSE OF THE PRESENT WORK

In the experiments carried out for the verification of conclusion (b), i.e., experiments in $Al_2(SO_4)_3$ media, the falling trend of dissolution rate with increasing ionic strength was supposed to be caused by the presence of $H^+$ ions in layers underneath an adsorbed immobile layer of $Al^{3+}$. In order to check this proposal and also investigate the mechanism by which $H^+$ ions enter through the hydration shell of $Al^{3+}$ ions adsorbed on the surface, a systematic study of the effect of $H^+$ ions on the rate of dissolution was necessary. In the present study, the effect of pH on the rate of dissolution of $AgIO_3$ was investigated to illuminate this problem. The experiments were planned to cover the dissolution of $AgIO_3$, $Al^{3+}$ adsorbed $AgIO_3$, and $Fe^{3+}$ adsorbed $AgIO_3$ in acidic media.

On the other hand, the temperature dependence of the initial dissolution rate of $AgIO_3$, which was not handled in the previous study was also investigated in order to check Equation 2.15 and also to calculate the activation enthalpy for the dissolution of $AgIO_3$ in distilled water.

Before going into the experiments planned for this study, the dissolution experiments with $AgIO_3$ in $KNO_3$ media, and $Al_2(SO_4)_3$ media and also the dissolution of $Al^{3+}$ adsorbed $AgIO_3$ in $KNO_3$ media were repeated in order to check the reproducibility of the method.

# CHAPTER III
# EXPERIMENTAL

## 3.1. EXPERIMENTAL APPARATUS

The schematic diagram of the apparatus is shown in Figure 3.1. The basic parts of the apparatus are a concentration cell placed in a water bath kept at constant temperature a potentiometer and a recorder.

The concentration cell used was

$$Ag\ |AgIO_3(C)||AgIO_3(C_s)|Ag$$

consisting of two silver electrodes immersed in two silver iodate solutions of different concentrations. One of the solutions was 200 ml saturated $AgIO_3$ solution (of concentration $C_s$) which constituted the reference half cell. The other was a 200 ml of a solution having a $AgIO_3$ concentration C, which constituted the sample half cell. In order to agitate the solution in the sample half cell during the experiments, there was a glass paddle stirrer driven by a DC motor at 0.85 volt. The stirrer consisted of a 2 cm diameter glass paddle attached to a 8 cm glass tube. A salt bridge consisting of a U-tube containing saturated $NH_4NO_3$ solution constituted the liquid junction between two solutions. The arms of the U-tube were 10 cm long and their inside diameters were 1 cm. The U-tube had also an upper extension of 3 cm long and with the same diameter. Ground joints were provided for the tips of the salt bridge. The whole cell was placed in a 20 lt water bath kept at constant temperature by a thermostat assembly.

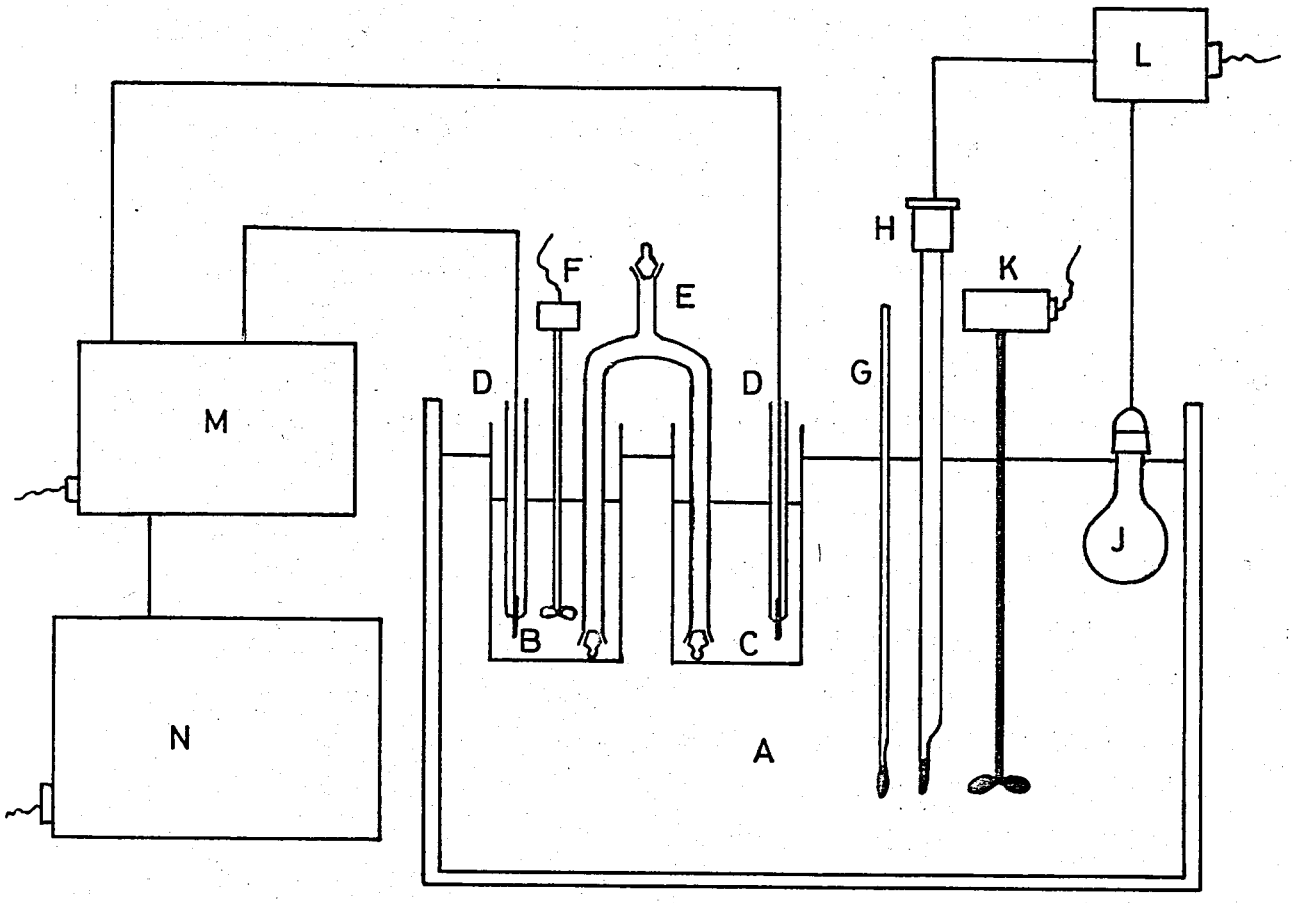


A: Water bath
B: Sample half cell
C: Reference half cell
D: Silver electrodes
E: Salt bridge
F: Glass paddle stirrer
G: Thermometer
H: Contact thermometer
J: Heater
K: Water bath stirrer
L: Relay
M: Potentiometer
N: Recorder

FIGURE 3.1. The Schematic Diagram of the Apparatus.

The emf developed by the concentration cell was measured by a potentiometer (Fisher Accumet pH Meter Model 210). The measured emf's were recorded by a strip chart recorder.(Linear 300 Series Recorder)

## 3.2. MATERIALS USED

The dissolving material was $AgIO_3$. In selecting $AgIO_3$ as the dissolving material the following requirements were aimed at[12].

(a) The substance should be an ionic solid of type MA.

(b) The dissolution rate should be sufficiently small such that it does not compete with the rate of diffusion and although it is taken in a large quantity so as to keep the surface area constant the dissolution rate is easily measured experimentally.

(c) The substance should have a large enough crystal size to expose a constant surface area during dissolution.

(d) The substance should exhibit sufficient solubility to follow the dissolution easily.

(e) The substance should be such that its dissolution rate can be measured by a simple and accurate method.

(f) The substance should contain an anion which is as large as possible to ascertain the validity of $|\Delta H_+^S| > |\Delta H_-^S|$.

The $AgIO_3$ sample used was a white powder which was taken from a stock previously prepared[12]. The stock was prepared from

$AgNO_3$ and $KIO_3$ solutions by precipitating and then dissolving the precipitate in dilute $NH_3$ solution and finally crystallizing $AgIO_3$ while the solution is being evaporated slowly. $AgIO_3$ has a rhombic bipyramidal crystal structure and its density is 5.525 gr/cm$^3$ measured at 16.5$^oC$[13]. The solubility data is tabulated[13] in Table 3.1.

TABLE 3.1. Solubility Data of $AgIO_3$ in $H_2O$

| t($^oC$) | 10 | 20 | 25 | 30 | 35 |
|---|---|---|---|---|---|
| $C_s$($Mx10^6$) | 0.97 | 1.463 | 1.785 | 2.152 | 2.587 |

The salt bridge is filled with saturated $NH_4NO_3$ solution. The $NH_4NO_3$ used was obtained from Riedel De Haënag Company. The solubility of $NH_4NO_3$ in water at 25$^oC$ is 217 gr/100 gr $H_2O$[14].

The silver electrodes are silver plated platinum wires. For silver plating, the chemicals used were $AgNO_3$ and KCN which were manufactured by Merck Company.

In the dissolution media of the experiments, $KNO_3$ (Riedel-De Haënag), $Al_2(SO_4)_3 \cdot 18\ H_2O$ (Fisher Scientific Co.), $CH_3COOH$ (E.Merck), $HNO_3$ (Pür Kimya) were used.

$Al_2(SO_4)_3 \cdot 18\ H_2O$ was also used for the preparation of the $Al^{3+}$ adsorbed $AgIO_3$ sample from a $2 \times 10^{-2}$ M solution and for the preparation of the $Fe^{3+}$ adsorbed $AgIO_3$, $Fe(NO_3)_3$ (Riedel-De Haënag) was used as $10^{-2}$ M solution.

## 3.3. EXPERIMENTAL PROCEDURE

### 3.3.1. Electrode Preparation

The silver electrodes were prepared by plating two platinum wires with silver. For the preparation of an

electrode, a Pt wire of 1 mm diameter and 1.5 cm long was connected to the end of a 10 cm glass tube 5 mm in inside diameter. The connection was accomplished as follows. The Pt wire was inserted slightly into the tube from one end and that end was sealed on a bunsen flame. In this way, Pt wire had been attached to the tube by keeping a few milimeters of the wire inside the tube. Then a few pieces of solder were put into the tube from the open end. A 10-13 cm long Cu wire was inserted till it touched the closed end. At this stage, by heating the tube at the closed end, the Pt wire became soldered to the Cu wire.

Ag plating was accomplished in silver bath containing potassium silver cyanide ($KAg(CN)_2$) solution. The procedure for its preparation is as follows: By slowly adding 0.1 M KCN solution to 0.1 M $AgNO_3$ solution a white AgCN precipitate was obtained. The precipitate was separated from the solution, washed with water and finally dissolved in KCN solution, thus resulting in a $KAg(CN)_2$ solution. The Pt electrode to be plated was dipped into this solution as cathode and another Pt electrode having a larger surface was used as anode. By conducting electrolysis for 10 minutes under a potential of 1.5 volts, Ag electrode was obtained.

### 3.3.2. Preparation of Saturated $AgIO_3$ Solution

An amount of $AgIO_3$ in excess of that corresponding to saturation was put into a container containing a certain volume of water. The saturated $AgIO_3$ solution was prepared by stirring the solution inside the container by a glass paddle stirrer for 6 hours in a water bath kept at the desired temperature.

### 3.3.3. Preparation of $Al^{+3}$ Adsorbed $AgIO_3$ and $Fe^{+3}$ Adsorbed $AgIO_3$ Samples

In order to obtain $Al^{3+}$ adsorbed $AgIO_3$, first a solution of $Al_2(SO_4)_3 \cdot 18H_2O$ containing $10^{-2}$ M $Al^{3+}$ was prepared. Then 1 gr $AgIO_3$ was wetted with 1 ml of this solution and dried by means of a filter paper after 30 seconds. The remaining material was placed in an oven at 110°C and left there for 6 hours for complete drying.

$Fe^{3+}$ adsorbed $AgIO_3$ was obtained in a similar manner, this time by wetting 1 gr $AgIO_3$ with 1 ml solution of $Fe(NO_3)_3$ containing $10^{-2}$M $Fe^{3+}$. The drying of the sample was carried out in exactly the same way as in $Al^{3+}$ adsorption on $AgIO_3$.

### 3.3.4. Dissolution Experiments

The dissolution experiments were conducted (A) At 25°C in media differing in composition; (B) At temperatures between 25°C and 40°C in distilled water.

Before starting the experimental work, the $AgIO_3$ sample was analyzed for its moisture content. Upon heating for 6 hours at 110°C in oven, no weight loss was observed, indicating that the sample was free of moisture.

Before each experimental run was started, the water bath was brought to the desired temperature by means of the heating unit of the thermostat assembly. For each run, 20 mg of $AgIO_3$ was weighed on an analytical balance (Mettler H 80) having a sensitivity of 0.1 mg, and put into a dry beaker of 250 ml capacity. It was immersed into the water bath together with the beaker containing reference half cell solution (saturated $AgIO_3$ solution) and the reference electrode. The salt bridge was placed inside the beakers. The other electrode and the glass paddle stirrer were dipped into the beaker containing the $AgIO_3$ sample to be dissolved. The dissolution

medium in each run was a 200 ml solution of desired composition and it was prepared before the above preparations were done.

At the start of a dissolution experiment first the recorder chart was started to move at a certain speed. The potentiometer and the stirrer were put into operation while the 200 ml solution (dissolution medium) was being poured quickly over the $AgIO_3$ powder. In this way an experiment was started and it was stopped after 100-120 seconds. Within this period a recorder output was obtained.

The stirring rate should be neither too low to cause the diffusional effects to become important so as to affect the dissolution rate nor too high to cause splashing. The DC motor driving the stirrer was operated at 0.85 volt, a value satisfying both of these requirements.

Obtaining concentration-time data from the recorder output of a dissolution experiment would be possible if there was a correlation between the recorder reading and $AgIO_3$ concentration in the dissolution medium. For this purpose a series of calibration experiments for each dissolution run were done. Each calibration experiment was performed at various $AgIO_3$ concentrations in a solution having the same composition as the dissolution medium. This was accomplished by diluting the saturated $AgIO_3$ solution to an extent such that it resulted in a solution the $AgIO_3$ concentration of which was equal to that of the calibration experiment when mixed with an equal volume of a solution which was twice as concentrated as the dissolution medium.

In a calibration experiment the calibration solution at a certain $AgIO_3$ concentration was placed as the sample half cell into the water bath at constant temperature and the emf of the cell measured by the potentiometer was recorded on the recorder chart. By repeating this procedure at five different $AgIO_3$ concentrations, in this way, a calibration

plot was obtained for each dissolution experiment (See Appendix III).

# CHAPTER IV
# RESULTS AND DISCUSSION

## 4.1. TREATMENT OF THE EXPERIMENTAL DATA

For each dissolution experiment the data was obtained in the form of a recorder output, i.e., number of divisions, $N_d$, v.s. time, t. Then the corresponding calibration experiment was performed as explained in Section 3.3.4. The points on the calibration plot were fitted to a straight line by linear least square analysis, and a calibration function in the form of $\log C = p + qN_d$ was obtained where p and q are constants. A sample calculation for calibration function is given in Appendix III. By means of the calibration function, the recorder output was converted to C v.s. t data and plotted. In the next step, the initial slope of each plot was calculated. This calculation offered a certain difficulty such that the points on each plot fell on a straight line through the origin only within a very short region at the middle section of the curve. This can be explained as follows. At earlier stages of dissolution since $Ag^+$ concentration is small the electrode delays in reaching equilibrium. At later stages, on the other hand, the dissolution rate decreases as the saturation concentration is approached. Both effects cause the concentrations found to be lower than the values if they would fall on a straight line through the origin. The initial slope was obtained by extrapolating the straight line to the origin.

These initial slopes were used in constructing the plots showing the dependence of initial rate of dissolution

on ionic strength and pH and also the dependence of the initial rate of dissolution in distilled water on temperature. Each point on these plots corresponds to a certain initial slope provided that these slopes are converted to the units of moles $AgIO_3$/sec-gr $AgIO_3$. The conversion from the units of moles $AgIO_3$/lt-sec to moles $AgIO_3$/sec-gr $AgIO_3$ was accomplished by considering the volume of the dissolution medium and the initial amount of $AgIO_3$ in the medium.

A sample calculation for the initial dissolution rate is given in Appendix III.

At this stage a check was made to see whether the delay in passing from an electrode equilibrium for one concentration to that for a higher concentration was significant compared to the rate of dissolution in the intermediate stages of dissolution. For this purpose first a $AgIO_3$ solution of concentration $C_1$ was put into the sample cell and the recorder was run to draw a baseline. Then a $AgIO_3$ solution of certain volume and concentration was quickly poured into the sample cell to give rise to a final solution of concentration $C_2$. The baseline at $C_1$ suddenly changed to that at $C_2$ through a steep line. The kinetic treatment of the situation was made by the analysis of this line and it was observed that rate of dissolution is very much smaller compared to delay of the electrode in reaching a new equilibrium. The analysis was repeated for a few ($C_1$, $C_2$) pairs and the same conclusion was reached. Therefore no correction was made for the delay of the electrode in reaching a new equilibrium. The details of the kinetic treatment and a sample calculation is given in Appendix IV.

## 4.2. DISSOLUTION OF $AgIO_3$ IN $KNO_3$ MEDIA

The dissolution kinetics of $AgIO_3$ was followed in $KNO_3$ solutions of concentrations ranging from $10^{-6}$ M to $10^{-1}$ M. The results of these experiments are given in Tables 4.2.1

through 4.2.7. (The calibration data for each $KNO_3$ concentration is given in Table A.2.1). The c v.s t data for the dissolution of $AgIO_3$ in $KNO_3$ media are plotted in Figures 4.2.1 through 4.2.7.

The initial rates of dissolution of $AgIO_3$ in $KNO_3$ media were calculated from the initial slopes of the corresponding c v.s t plots. The ionic strengths, I, of the solutions were calculated from

$$(4.1) \qquad I = \frac{1}{2} \Sigma C_i Z_i^2$$

where $C_i$ is the molar concentration and $Z_i$ is the charge of the ionic species in the solution. Since $KNO_3$ is a 1:1 type ionic salt, ionic strength of a $KNO_3$ solution is nearly equal to its molar concentration. The initial dissolution rates of $AgIO_3$ in $KNO_3$ media are tabulated in Table 4.2.8. The data of Table 4.2.8. are plotted in Figure 4.1.a.

TABLE 4.2.1. Dissolution Data of $AgIO_3$ in Distilled $H_2O$ at $25^oC$

Calibration Function: $\log C = -3.859 - 0.0793\ N_d$

| Time, t (sec) | Number of Divisions on Recorder Output, $N_d$ | Concentration of $AgIO_3$, C, ($Mx10^6$) |
|---|---|---|
| 8 | 33.6 | 0.30 |
| 16 | 25.5 | 1.32 |
| 24 | 22.1 | 2.43 |
| 32 | 20.1 | 3.50 |
| 40 | 18.7 | 4.56 |
| 48 | 17.7 | 5.46 |
| 56 | 16.8 | 6.44 |
| 64 | 16.1 | 7.30 |
| 72 | 15.4 | 8.28 |
| 80 | 14.9 | 9.09 |
| 88 | 14.5 | 9.72 |
| 96 | 14.2 | 10.24 |

TABLE 4.2.2. Dissolution Data of $AgIO_3$ in $10^{-6}$ M $KNO_3$ Solution ($I=10^{-6}$) at $25^oC$

Calibration Function: $\log C = -3.764 - 0.0733\ N_d$

| Time, t (sec) | Number of Divisions on Recorder Output, $N_d$ | Concentration of $AgIO_3$, C, ($Mx10^6$) |
|---|---|---|
| 9 | 37.3 | 0.32 |
| 13 | 32.1 | 0.77 |
| 17 | 28.7 | 1.36 |
| 21 | 27.2 | 1.76 |
| 25 | 25.6 | 2.30 |
| 33 | 23.9 | 3.03 |
| 41 | 22.8 | 3.68 |
| 49 | 21.5 | 4.54 |
| 57 | 20.7 | 5.23 |
| 65 | 20.0 | 5.90 |
| 73 | 19.4 | 6.52 |
| 77 | 19.1 | 6.90 |
| 85 | 18.5 | 7.54 |
| 93 | 18.1 | 8.14 |
| 101 | 17.6 | 8.80 |
| 109 | 17.3 | 9.25 |

TABLE 4.2.3. Dissolution Data of $AgIO_3$ in $10^{-5}$ M $KNO_3$ Solution ($I=10^{-5}$) at $25^oC$

Calibration Function: $\log C = -3.990 - 0.0643\ N_d$

| Time, t (sec) | Number of Divisions on Recorder Output, $N_d$ | Concentration of $AgIO_3$, C, ($Mx10^6$) |
|---|---|---|
| 9 | 39.0 | 0.32 |
| 15 | 31.9 | 0.91 |
| 21 | 28.6 | 1.48 |
| 30 | 26.2 | 2.12 |
| 42 | 24.2 | 2.85 |
| 48 | 23.3 | 3.23 |
| 54 | 22.5 | 3.65 |
| 60 | 21.9 | 4.02 |
| 69 | 20.9 | 4.61 |
| 78 | 20.1 | 5.19 |
| 87 | 19.5 | 5.72 |
| 96 | 19.0 | 6.18 |
| 105 | 18.6 | 6.50 |

TABLE 4.2.4. Dissolution Data of $AgIO_3$ in $10^{-4}$ M $KNO_3$ Solution ($I=10^{-4}$) at $25^oC$

Calibration Function: $\log C = -3.980 - 0.077\ N_d$

| Time, t (sec) | Number of Divisions on Recorder Output, $N_d$ | Concentration of $AgIO_3$, C, ($Mx10^6$) |
|---|---|---|
| 6 | 34.1 | 0.24 |
| 14 | 27.0 | 0.85 |
| 23 | 24.5 | 1.37 |
| 32 | 22.4 | 1.97 |
| 44 | 20.9 | 2.56 |
| 56 | 19.6 | 3.24 |
| 68 | 18.5 | 3.91 |
| 80 | 17.6 | 4.59 |
| 92 | 16.9 | 5.26 |
| 104 | 16.2 | 5.92 |
| 116 | 15.7 | 6.48 |

TABLE 4.2.5. Dissolution Data of $AgIO_3$ in $10^{-3}$ M $KNO_3$ Solution ($I=10^{-3}$) at $25^{o}C$

Calibration Function: $\log C = -3.944 - 0.067\ N_d$

| Time, t (sec) | Number of Divisions on Recorder Output, $N_d$ | Concentration of $AgIO_3$, C, ($Mx10^6$) |
|---|---|---|
| 6 | 42.2 | 0.17 |
| 12 | 33.8 | 0.62 |
| 18 | 29.7 | 1.18 |
| 24 | 27.9 | 1.55 |
| 30 | 26.3 | 1.98 |
| 36 | 25.2 | 2.36 |
| 45 | 23.9 | 2.87 |
| 57 | 22.5 | 3.57 |
| 69 | 21.3 | 4.28 |
| 81 | 20.3 | 4.98 |
| 93 | 19.4 | 5.69 |
| 105 | 18.7 | 6.38 |
| 117 | 18.0 | 7.06 |

TABLE 4.2.6. Dissolution Data of $AgIO_3$ in $10^{-2}$ M $KNO_3$ Solution ($I=10^{-2}$) at $25^{o}C$

Calibration Function: $\log C = -3.851 - 0.079\ N_d$

| Time, t (sec) | Number of Divisions on Recorder Output, $N_d$ | Concentration of $AgIO_3$, C, ($Mx10^6$) |
|---|---|---|
| 11 | 31.5 | 0.46 |
| 17 | 27.2 | 1.01 |
| 23 | 25.0 | 1.51 |
| 29 | 23.5 | 1.96 |
| 35 | 22.4 | 2.41 |
| 41 | 21.5 | 2.82 |
| 47 | 20.9 | 3.17 |
| 53 | 20.1 | 3.64 |
| 59 | 19.5 | 4.09 |
| 71 | 18.6 | 4.78 |
| 83 | 17.8 | 5.56 |
| 101 | 16.9 | 6.51 |
| 113 | 16.4 | 7.18 |
| 125 | 16.0 | 7.75 |

TABLE 4.2.7. Dissolution Data of $AgIO_3$ in $10^{-1}$ M $KNO_3$ Solution ($I=10^{-1}$) at $25^oC$

Calibration Function: $\log C = -3.804 - 0.074\ N_d$

| Time, t (sec) | Number of Divisions on Recorder Output, $N_d$ | Concentration of $AgIO_3$, C, ($Mx10^6$) |
|---|---|---|
| 11 | 30.0 | 0.92 |
| 17 | 27.0 | 1.55 |
| 23 | 24.5 | 2.36 |
| 29 | 22.7 | 3.22 |
| 35 | 21.6 | 3.86 |
| 41 | 20.6 | 4.58 |
| 47 | 19.9 | 5.20 |
| 53 | 19.2 | 5.87 |
| 62 | 18.4 | 6.70 |
| 68 | 17.9 | 7.33 |
| 74 | 17.4 | 7.95 |
| 80 | 17.0 | 8.50 |
| 86 | 16.7 | 8.99 |
| 92 | 16.4 | 9.51 |

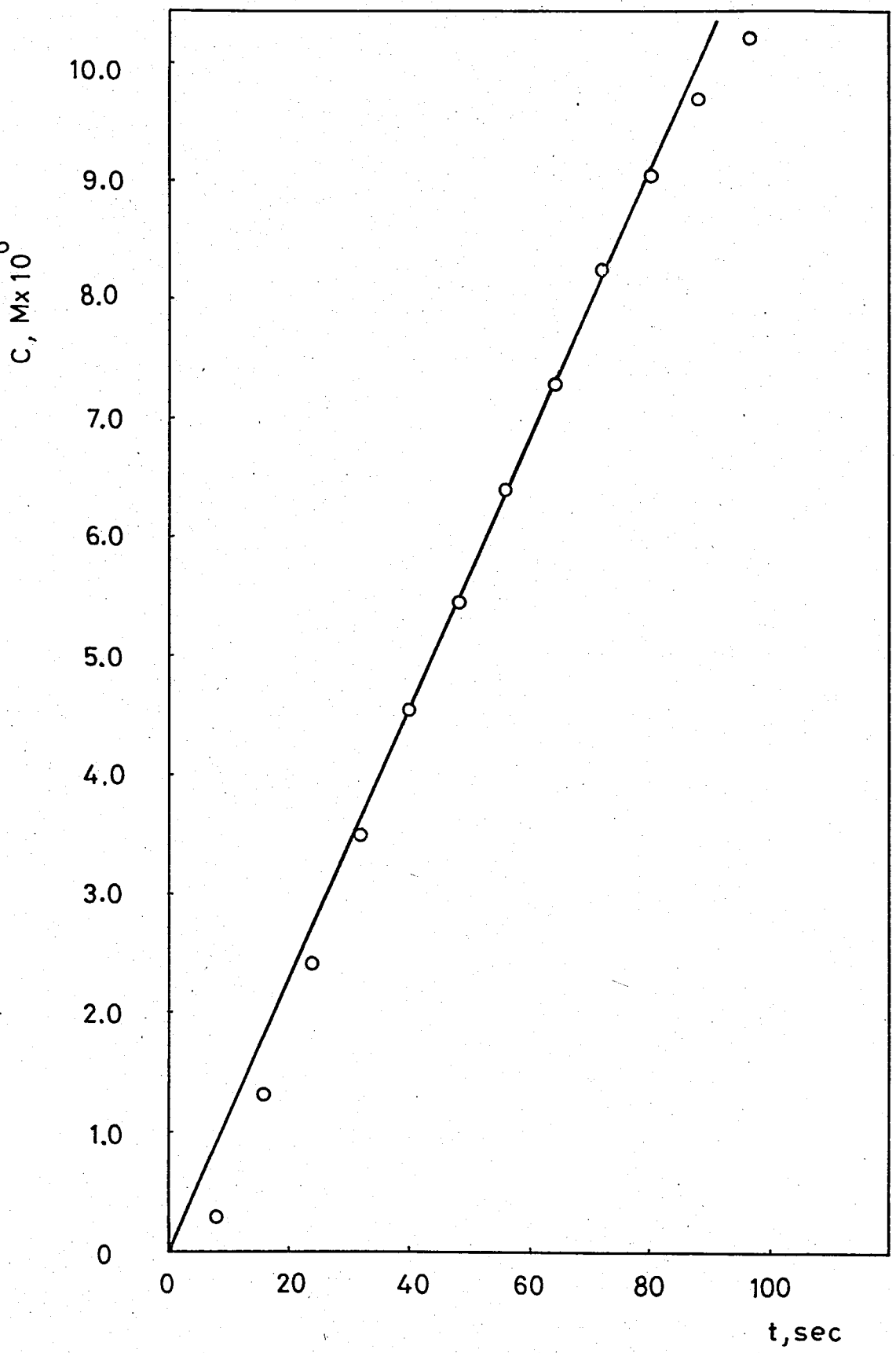


FIGURE 4.2.1. C v.s t Plot for the Dissolution of $AgIO_3$ in Distilled $H_2O$ at $25^oC$.

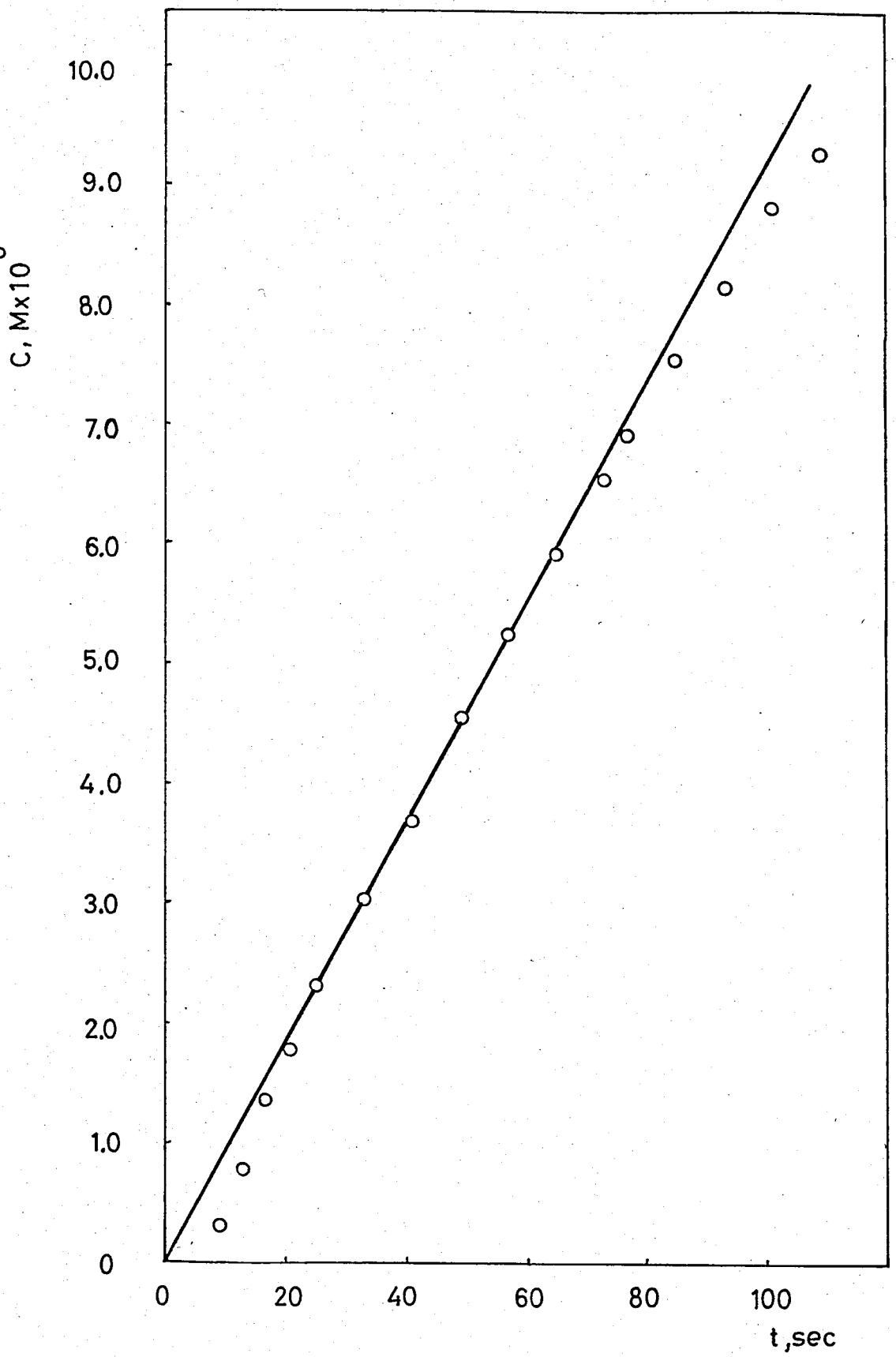


FIGURE 4.2.2. C v.s t Plot for the Dissolution of $AgIO_3$ in $10^{-6}$ M $KNO_3$ Solution ($I=10^{-6}$) at 25°C.

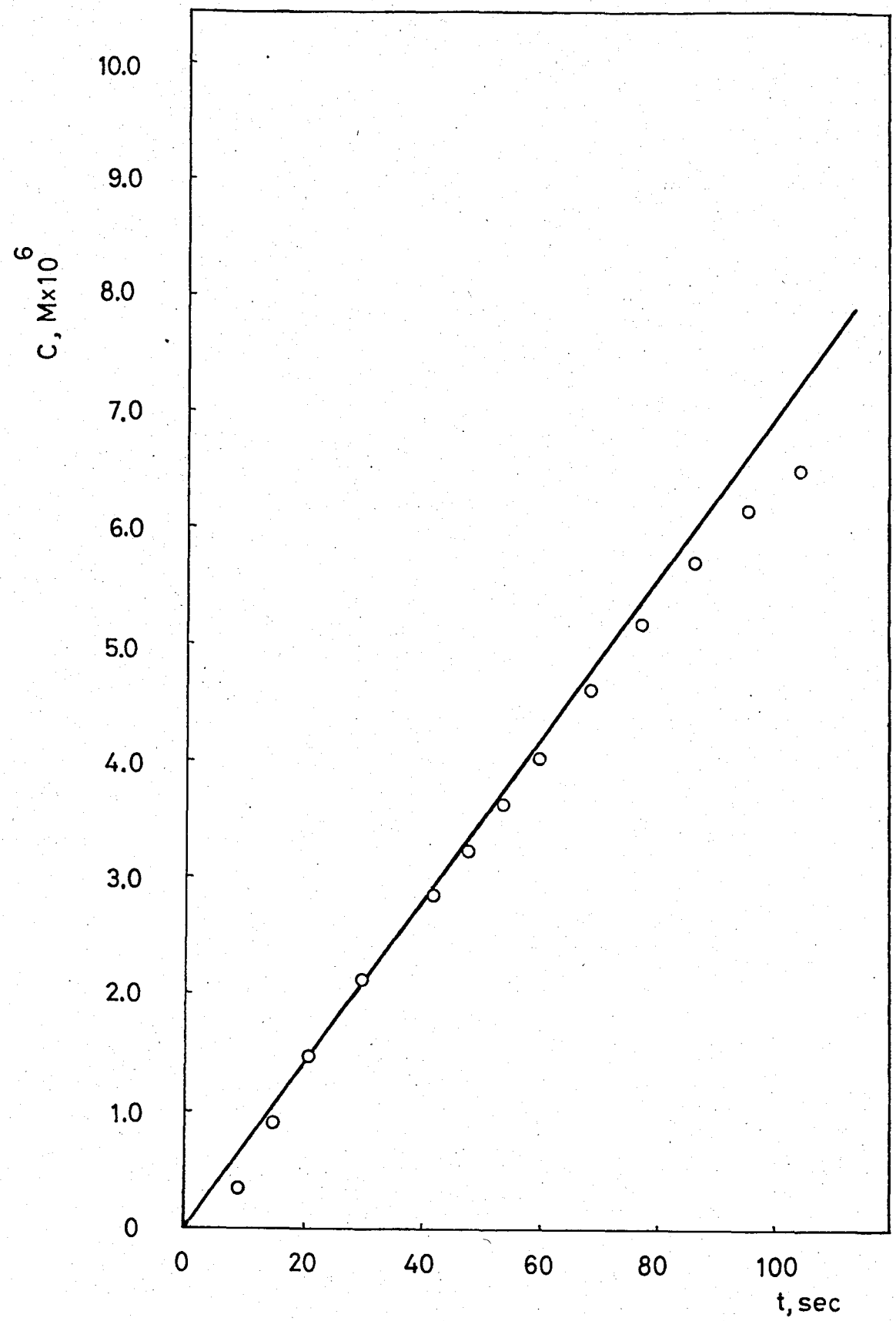


FIGURE 4.2.3. C v.s t Plot for the Dissolution of $AgIO_3$ in $10^{-5}$ M $KNO_3$ Solution ($I=10^{-5}$) at 25°C.

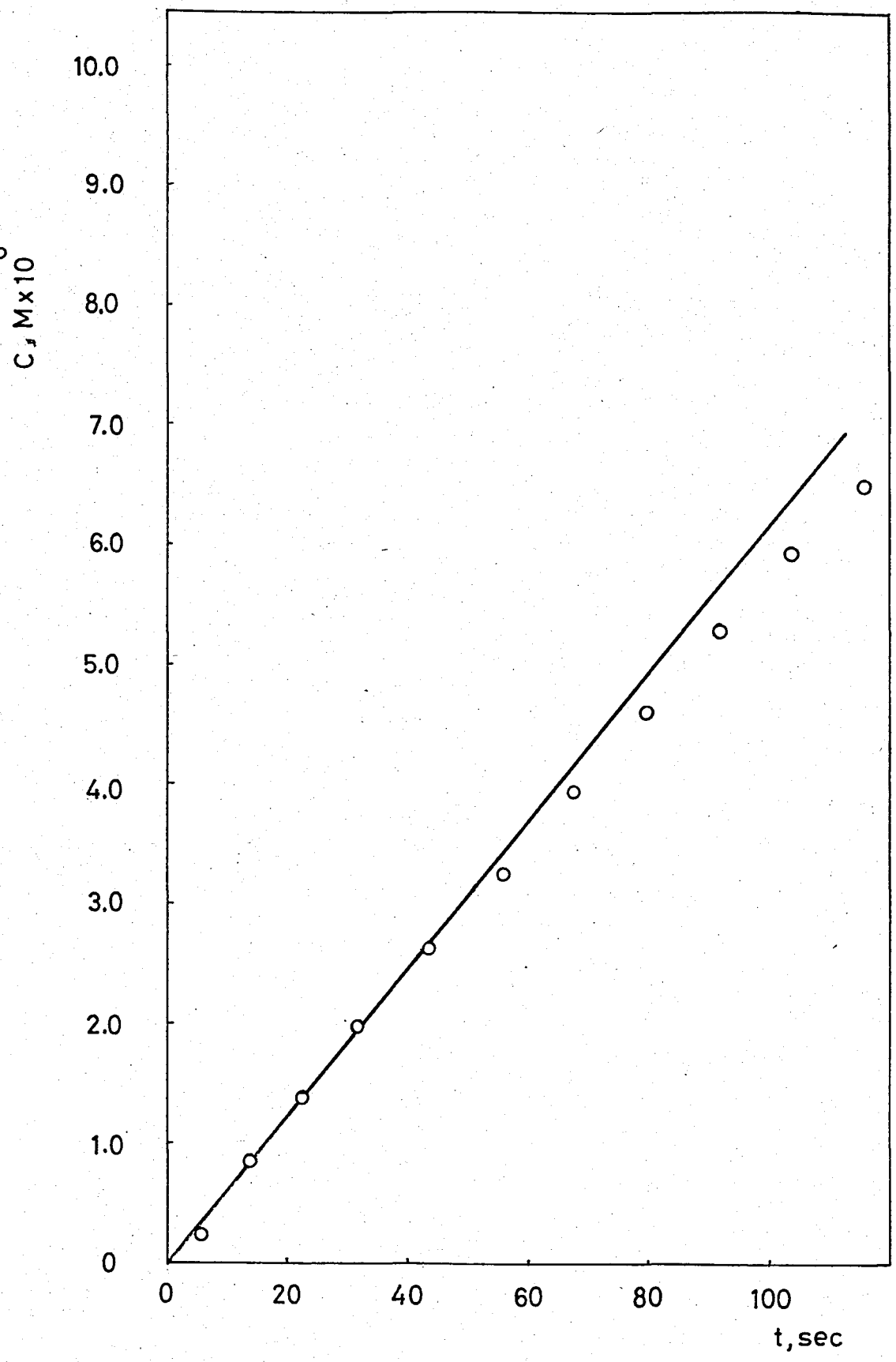


FIGURE 4.2.4: C v.s t Plot for the Dissolution of $AgIO_3$ in $10^{-4}$ M $KNO_3$ Solution ($I=10^{-4}$) at 25°C.

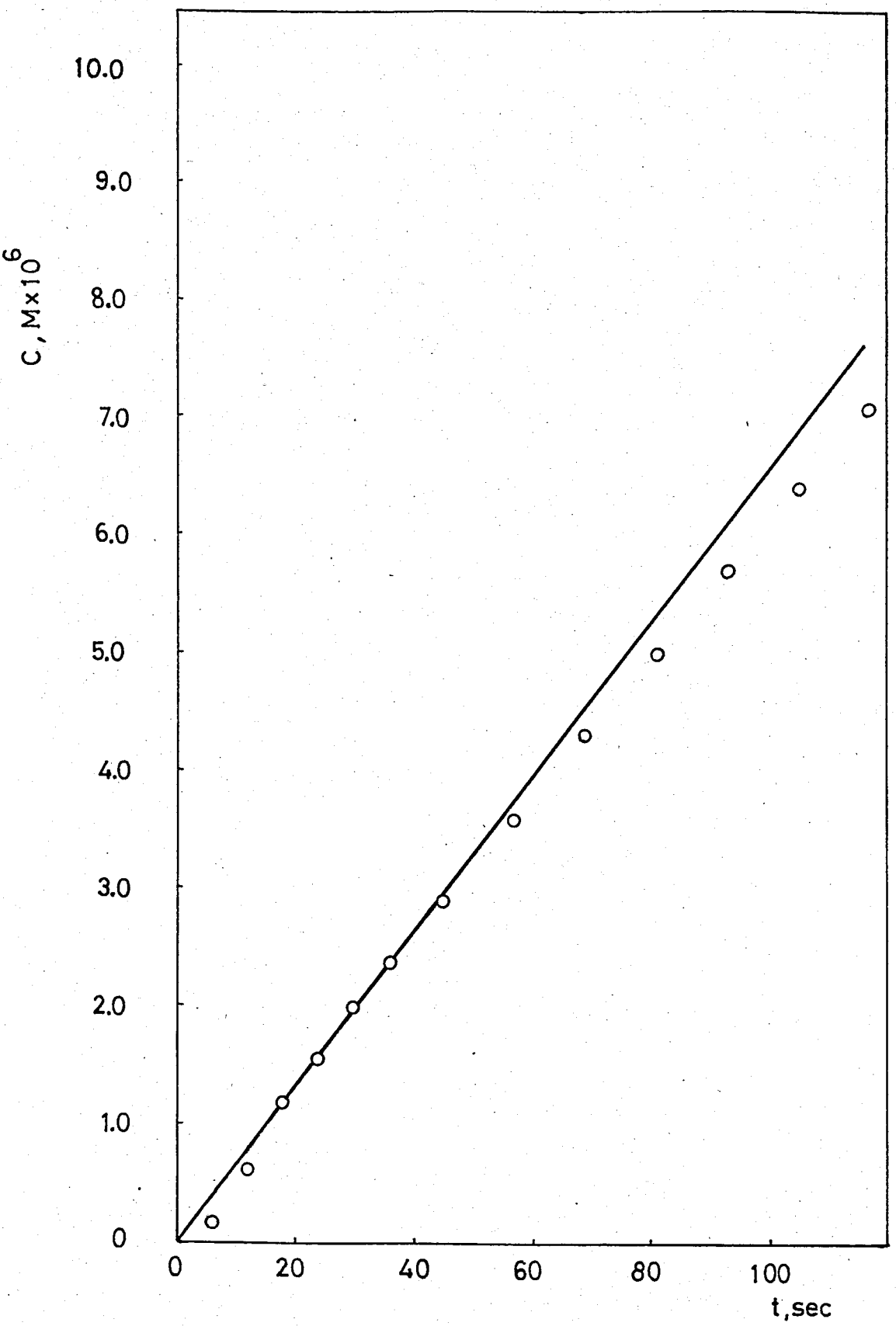


FIGURE 4.2.5. C v.s t Plot for the Dissolution of $AgIO_3$ in $10^{-3}$ M $KNO_3$ Solution ($I=10^{-3}$) at 25°C.

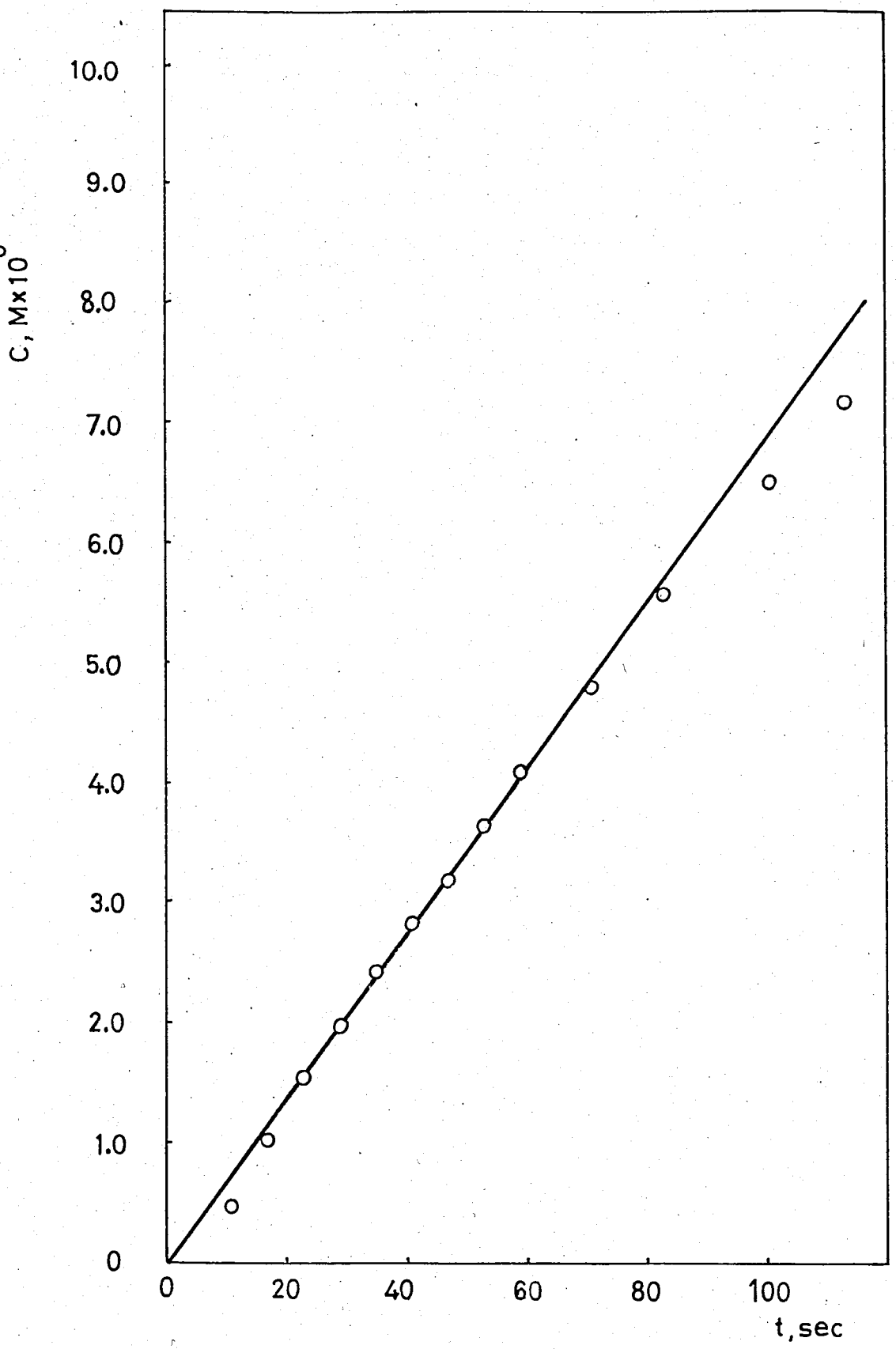


FIGURE 4.2.6. C v.s t Plot for the Dissolution of $AgIO_3$ in $10^{-2}$ M $KNO_3$ Solution ($I=10^{-2}$) at 25°C.

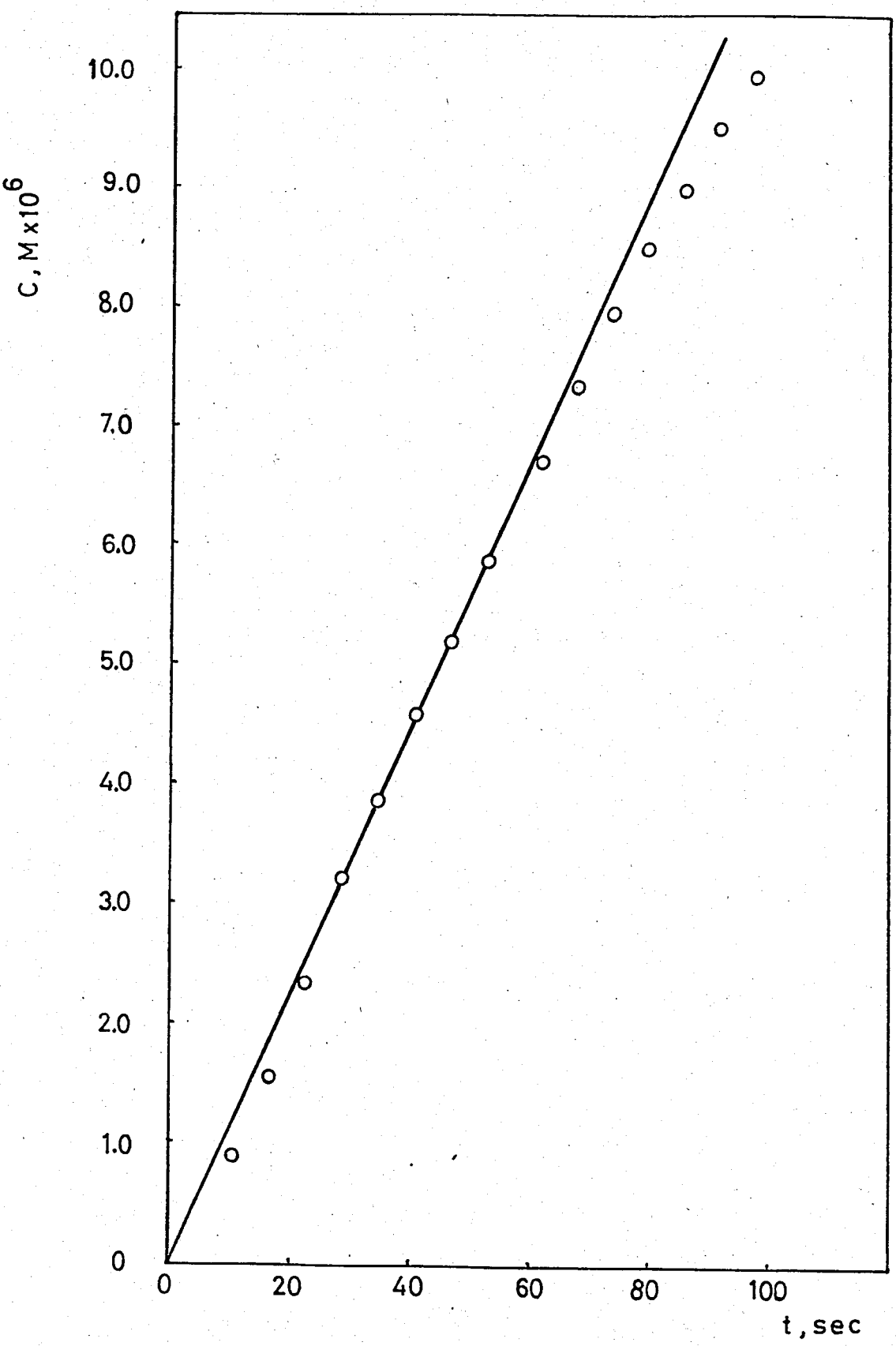


FIGURE 4.2.7. C v.s t Plot for the Dissolution of $AgIO_3$ in $10^{-1}$ M $KNO_3$ Solution ($I=10^{-1}$) at 25°C.

TABLE 4.2.8. Initial Dissolution Rates of $AgIO_3$ in $KNO_3$ Media at $25^oC$

| Ionic Strength I | Initial Dissolution Rate, $R_d$, (mol $sec^{-1}$ $gr^{-1}$) x $10^6$ |
|---|---|
| $10^{-6.4}$ (Distilled $H_2O$) | 1.14 |
| $10^{-6}$ | 0.95 |
| $10^{-5}$ | 0.70 |
| $10^{-4}$ | 0.62 |
| $10^{-3}$ | 0.65 |
| $10^{-2}$ | 0.69 |
| $10^{-1}$ | 1.11 |

In Figure 4.1.a the starting point of the curve is that corresponding to dissolution in distilled water. From pH measurements, the ionic strength of the distilled water was observed to be $10^{-6.4}$ although the theoretical value is $10^{-7}$. This is because of the $CO_2$ absorption from the atmosphere under the experimental conditions. The initial dissolution rate of $AgIO_3$ in distilled water under the same experimental conditions was calculated to be $1.14 \times 10^{-6}$ mol $sec^{-1}gr^{-1}$ (See Appendix III).

An investigation of Figure 4.1-a shows that rate of dissolution drops about 45 per cent from its value in distilled water up to an ionic strength of $10^{-4}$, and then remains constant up to an ionic strength of about $10^{-2}$. However at $I = 10^{-2}$, the dissolution rate starts to increase and reaches its value in distilled water at around $I = 10^{-1}$. The same trend with the same per cent rate drop was obtained by Enüstün and Ayranci[12] for the dissolution of $AgIO_3$ in $KNO_3$ media at $25^oC$ although their absolute values of the rates were slightly higher than those of this work probably because of aging of the $AgIO_3$ crystals for approximately five years.

The trend of Figure 4.1-a at low and medium ionic strengths is consistent with theoretical conclusion (a), i.e., the dissolution rate decreases to an asymptotic value as the ionic strength increases. The trend at high ionic strengths, however, shows a strong deviation from the theory. This deviation may be caused by two reasons. One of them is that at high ionic strengths assumption (b) of the theory (dilute medium assumption) will no longer be valid. The other reason may be the fact that the double layer deviates from Gouy character and gradually behaves as a Stern layer in this region. How this picture comes about can be explained in the following way. At high ionic strengths, the potential drop at the start of a Gouy layer is very large. This means that many counter $K^+$ ions should penetrate into the narrow region between the solid wall and the energy barriers. This is physically impossible, therefore most of these ions should be collected, almost at the same concentration in the outer layer beyond the energy barriers. Then the potential profile may take the linear shape resembling that of Stern layer[12].

## 4.3. DISSOLUTION OF $AgIO_3$ in $Al_2(SO_4)_3$ MEDIA

The dissolution kinetics of $AgIO_3$ was followed in $Al_2(SO_4)_3$ solutions of concentrations ranging from $5x10^{-7}$ M to $5x10^{-3}$ M. The results of these experiments are given in Tables 4.3.1 through 4.3.5. (The calibration data for each $Al_2(SO_4)_3$ concentration is given in Table A.2.2). The c v.s t data for the dissolution of $AgIO_3$ in $Al_2(SO_4)_3$ media are platted in Figures 4.3.1 through 4.3.5.

The initial rates of dissolution of $AgIO_3$ in $Al_2(SO_4)_3$ media were calculated from the initial slopes of the corresponding c v.s t plots. The ionic strengths of $Al_2(SO_4)_3$ solutions calculated from Equation 4.1 ranges from $7.5x10^{-6}$ to $7.5x10^{-2}$. The initial dissolution rates of $AgIO_3$ in $Al_2(SO_4)_3$ media are tabulated in Table 4.3.6. The data of Table 4.3.6. are plotted in Figure 4.1-b.

TABLE 4.3.1. Dissolution Data of $AgIO_3$ in $5 \times 10^{-7}$ M $Al_2(SO_4)_3$ Solution ($I = 7.5 \times 10^{-6}$) at $25^oC$

Calibration Function: $\log C = -3.845 - 0.0706\ N_d$

| Time, t (sec) | Number of Divisions on Recorder Output, $N_d$ | Concentration of $AgIO_3$, C, ($M \times 10^6$) |
|---|---|---|
| 13 | 31.2 | 0.90 |
| 17 | 28.7 | 1.35 |
| 21 | 26.8 | 1.83 |
| 29 | 24.5 | 2.66 |
| 37 | 23.0 | 3.40 |
| 45 | 21.9 | 4.05 |
| 53 | 21.0 | 4.73 |
| 57 | 20.6 | 5.05 |
| 65 | 19.9 | 5.66 |
| 73 | 19.2 | 6.30 |
| 81 | 18.6 | 6.96 |
| 89 | 18.0 | 7.65 |
| 97 | 17.5 | 8.33 |
| 105 | 17.1 | 8.80 |

TABLE 4.3.2. Dissolution Data of $AgIO_3$ in $5 \times 10^{-6}$ M $Al_2(SO_4)_3$ Solution ($I = 7.5 \times 10^{-5}$) at 25°C

Calibration Function: $\log C = -3.723 - 0.081\ N_d$

| Time, t (sec) | Number of Divisions on Recorder Output, $N_d$ | Concentration of $AgIO_3$, C, ($M \times 10^6$) |
|---|---|---|
| 10 | 30.9 | 0.60 |
| 14 | 28.0 | 1.03 |
| 18 | 26.4 | 1.38 |
| 26 | 24.1 | 2.11 |
| 34 | 22.7 | 2.75 |
| 42 | 21.6 | 3.40 |
| 50 | 20.7 | 4.01 |
| 58 | 19.9 | 4.63 |
| 66 | 19.3 | 5.22 |
| 74 | 18.7 | 5.82 |
| 82 | 18.2 | 6.42 |
| 90 | 17.7 | 7.05 |
| 98 | 17.3 | 7.61 |
| 106 | 16.9 | 8.11 |

TABLE 4.3.3. Dissolution Data of $AgIO_3$ in $5 \times 10^{-5}$ M $Al_2(SO_4)_3$ Solution ($I = 7.5 \times 10^{-4}$) at $25^{o}C$

Calibration Function: $\log C = -3.586 - 0.0906\ N_d$

| Time, t (sec) | Number of Divisions on Recorder Output, $N_d$ | Concentration of $AgIO_3$, C, ($M \times 10^6$) |
|---|---|---|
| 14 | 27.0 | 0.92 |
| 18 | 25.4 | 1.30 |
| 22 | 24.5 | 1.56 |
| 30 | 22.6 | 2.32 |
| 38 | 21.3 | 3.15 |
| 46 | 20.2 | 3.87 |
| 54 | 19.5 | 4.45 |
| 62 | 18.8 | 5.09 |
| 70 | 18.4 | 5.64 |
| 78 | 17.8 | 6.29 |
| 86 | 17.4 | 6.88 |
| 94 | 17.0 | 7.48 |
| 102 | 16.6 | 8.01 |

TABLE 4.3.4. Dissolution Data of $AgIO_3$ in $5 \times 10^{-4}$ M $Al_2(SO_4)_3$ Solution ($I=7.5 \times 10^{-3}$) at $25^{o}C$

Calibration Function: $\log C = -3.716 - 0.0892\ N_d$

| Time, t (sec) | Number of Divisions on Recorder Output, $N_d$ | Concentration of $AgIO_3$, C, ($M \times 10^6$) |
|---|---|---|
| 12 | 27.4 | 0.69 |
| 16 | 25.5 | 1.02 |
| 20 | 24.0 | 1.38 |
| 28 | 22.1 | 2.04 |
| 36 | 20.6 | 2.81 |
| 44 | 19.6 | 3.40 |
| 52 | 18.9 | 3.96 |
| 60 | 18.2 | 4.55 |
| 68 | 17.6 | 5.15 |
| 76 | 17.2 | 5.66 |
| 84 | 16.8 | 6.15 |
| 92 | 16.4 | 6.62 |
| 100 | 16.0 | 7.19 |

TABLE 4.3.5. Dissolution Data of $AgIO_3$ in $5 \times 10^{-3}$ M $Al_2(SO_4)_3$ Solution ($I=7.5 \times 10^{-2}$) at $25^{o}C$

Calibration Function: $\log C = -3.520 - 0.103\ N_d$

| Time, t (sec) | Number of Divisions on Recorder Output, $N_d$ | Concentration of $AgIO_3$, C, ($M \times 10^6$) |
|---|---|---|
| 10 | 28.1 | 0.39 |
| 14 | 25.2 | 0.77 |
| 18 | 23.3 | 1.21 |
| 22 | 22.1 | 1.59 |
| 30 | 20.5 | 2.35 |
| 38 | 19.3 | 3.14 |
| 46 | 18.5 | 3.79 |
| 54 | 17.7 | 4.52 |
| 62 | 17.2 | 5.11 |
| 74 | 16.5 | 6.00 |
| 82 | 16.2 | 6.52 |
| 90 | 15.8 | 7.17 |
| 98 | 15.4 | 7.81 |
| 106 | 15.1 | 8.40 |

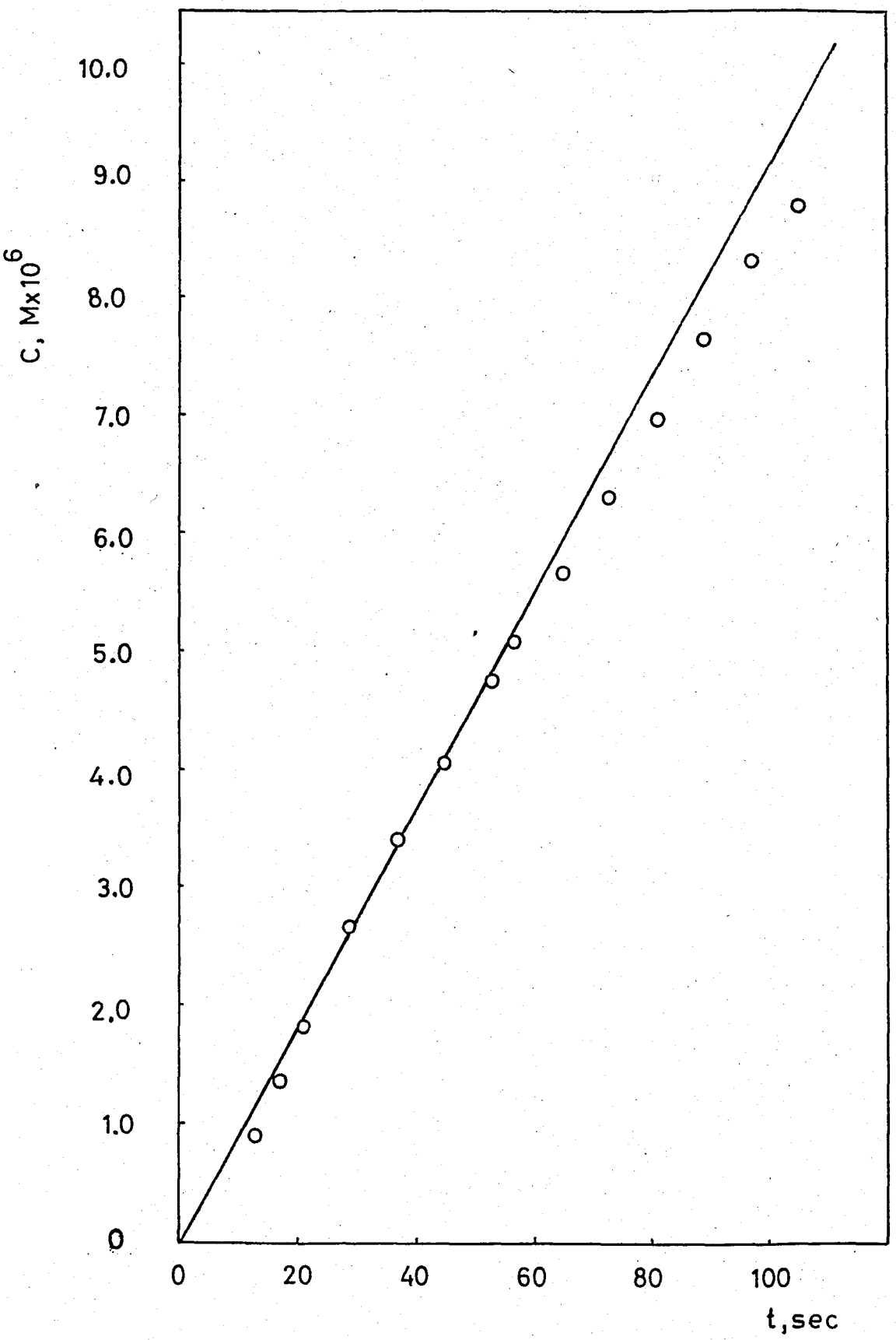


FIGURE 4.3.1. C v.s t Plot for the Dissolution of $AgIO_3$ in $5x10^{-7}$ M $Al_2(SO_4)_3$ Solution ($I=7.5x10^{-6}$) at 25°C.

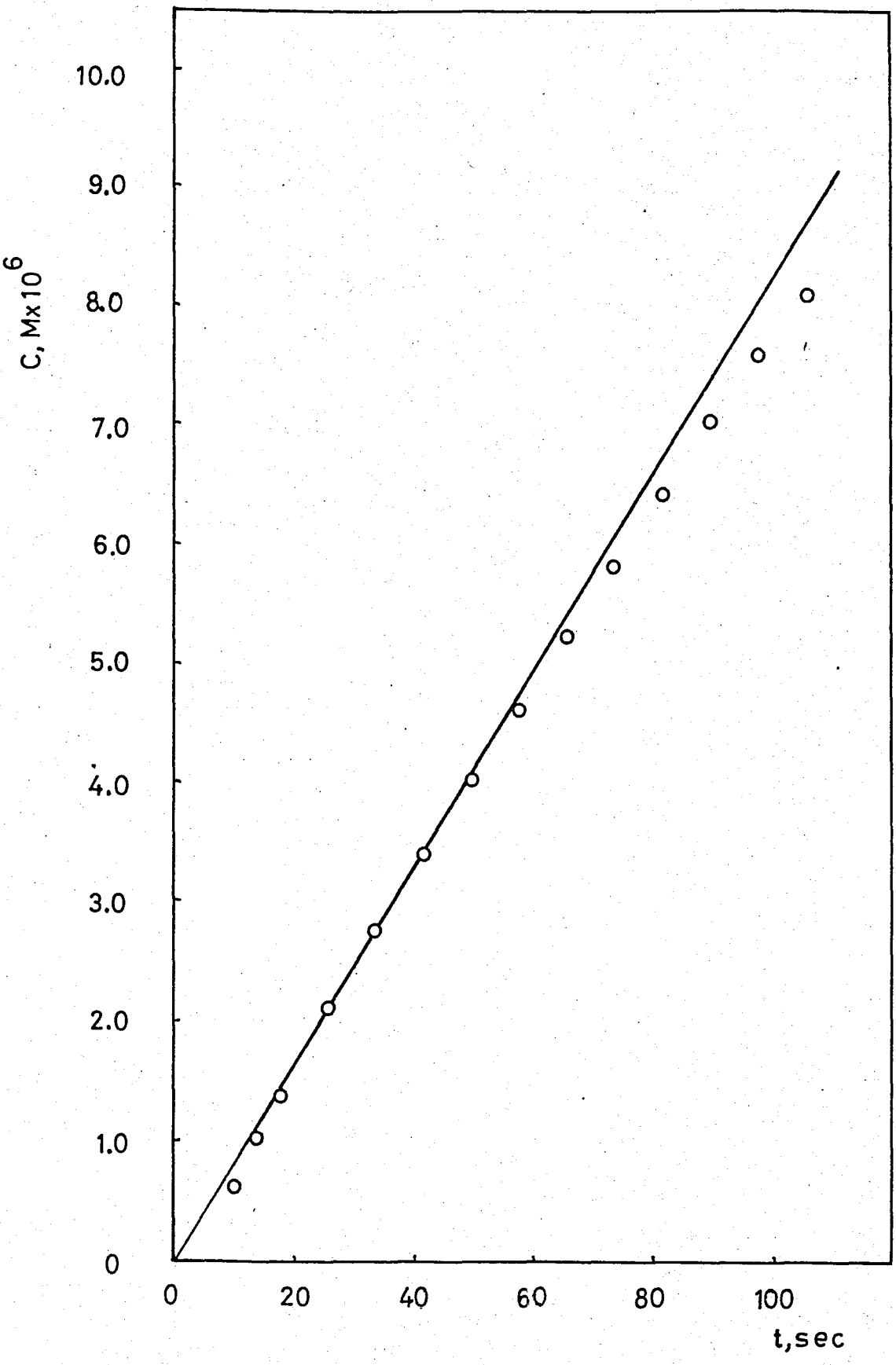


FIGURE 4.3.2. C v.s t Plot for the Dissolution of $AgIO_3$ in $5x10^{-6}$ M $Al_2(SO_4)_3$ Solution ($I=7.5x10^{-5}$) at 25°C.

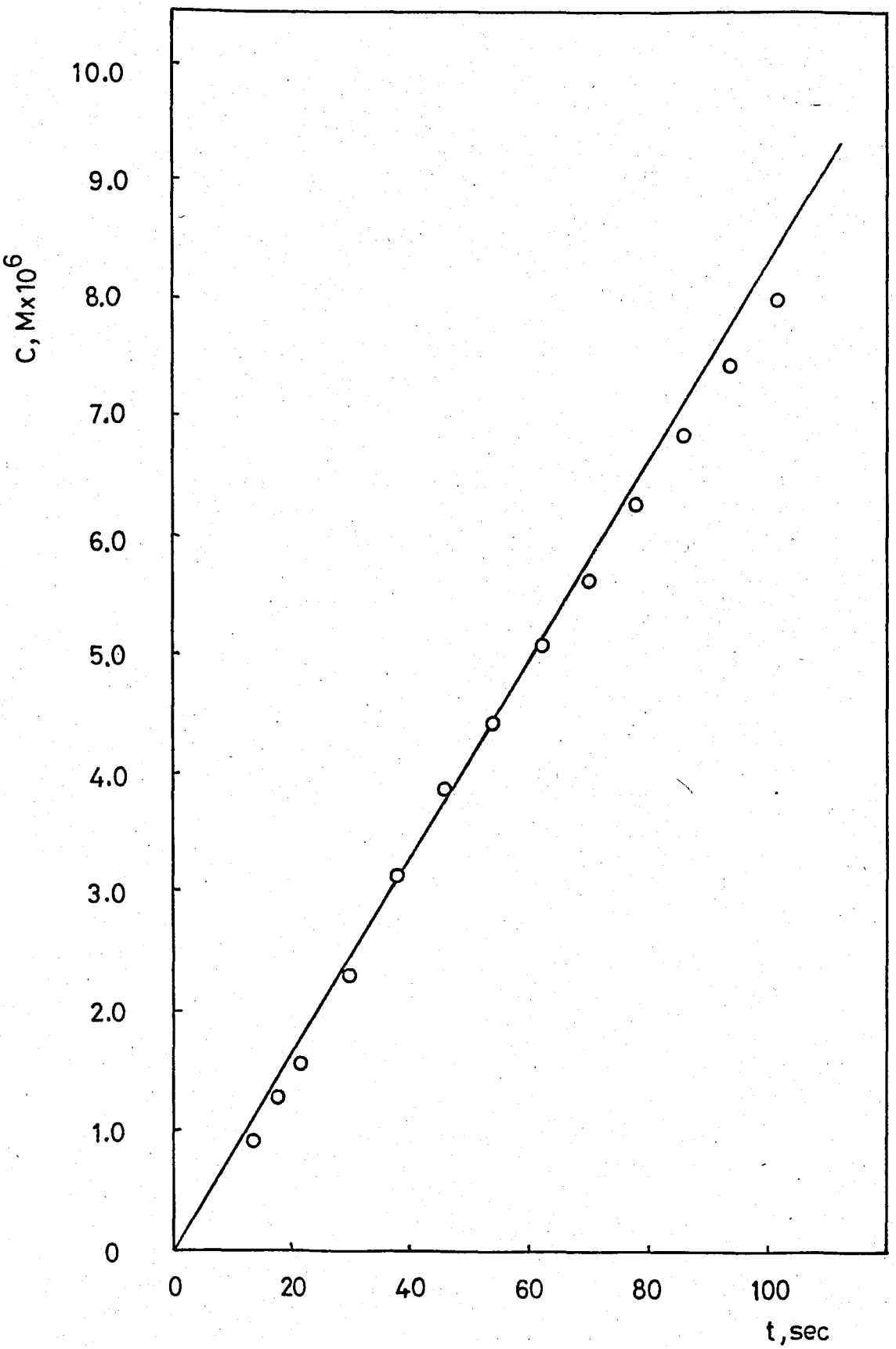


FIGURE 4.3.3. C v.s t Plot for the Dissolution of $AgIO_3$ in $5x10^{-5}$ M $Al_2(SO_4)_3$ Solution ($I=7.5x10^{-4}$) at 25°C.

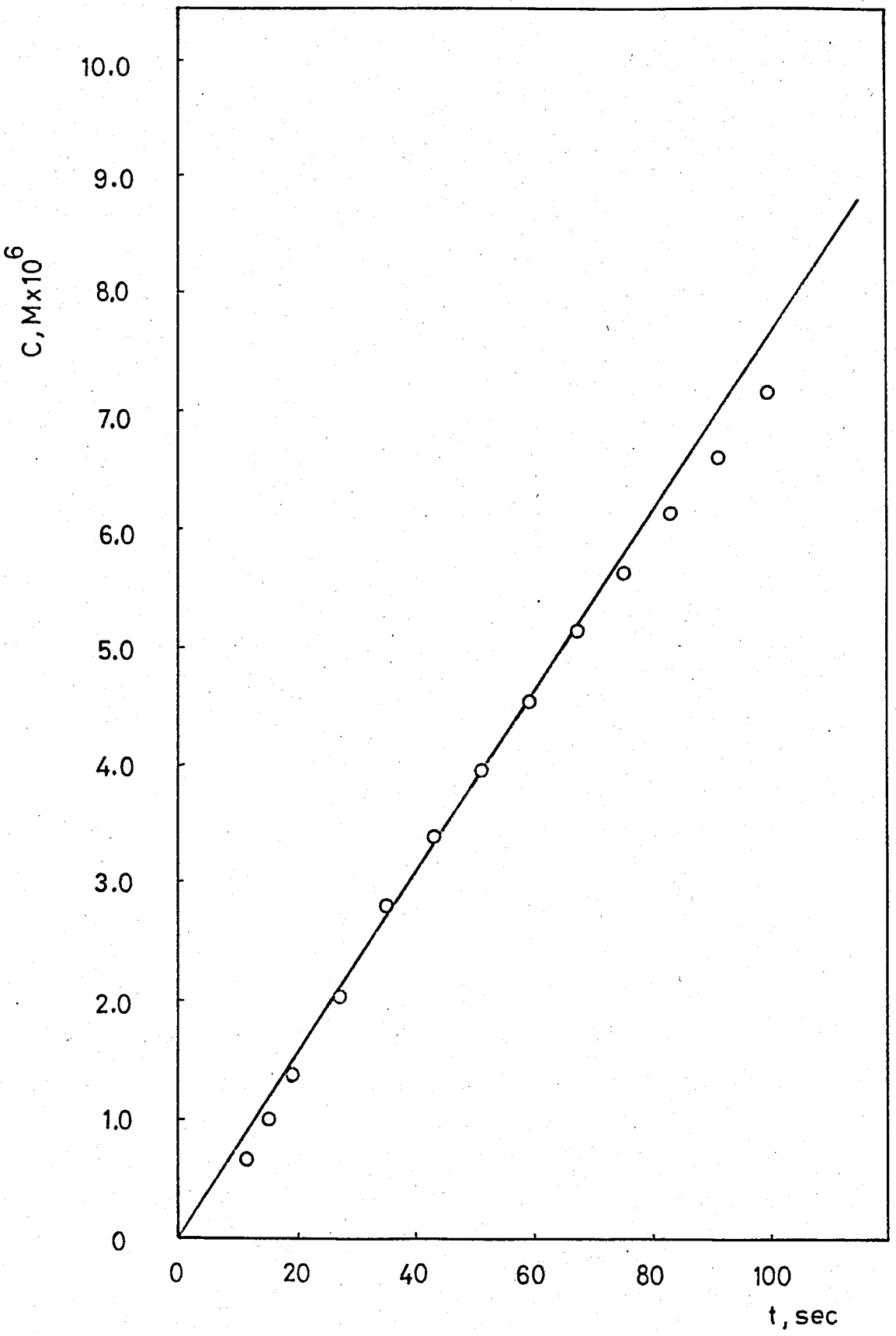


FIGURE 4.3.4. C v.s t Plot for the Dissolution of $AgIO_3$ in $5 \times 10^{-4}$ M $Al_2(SO_4)_3$ Solution ($I = 7.5 \times 10^{-3}$) at 25°C.

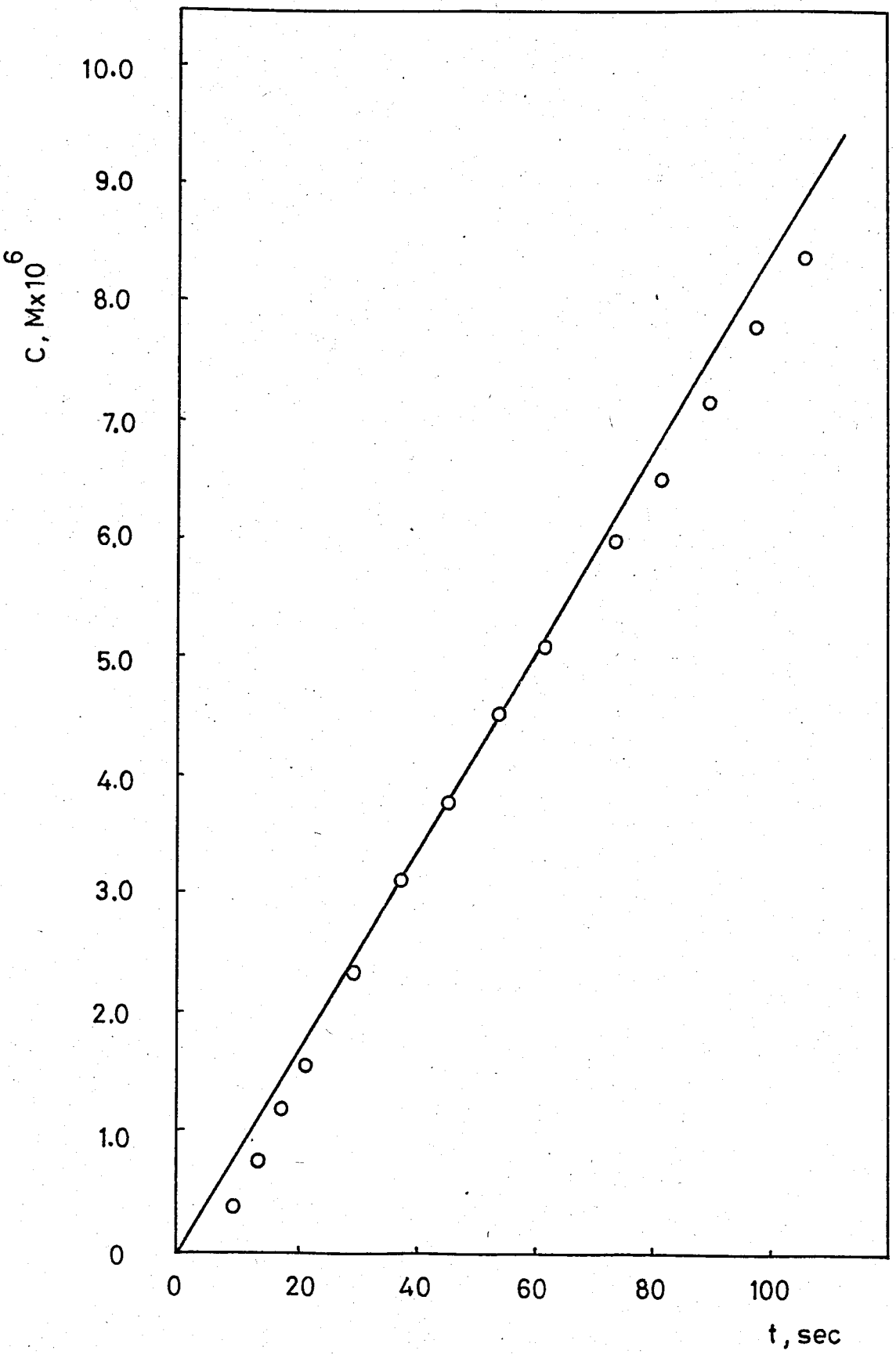


FIGURE 4.3.5. C v.s t Plot for the Dissolution of $AgIO_3$ in $5x10^{-3}$ M $Al_2(SO_4)_3$ Solution ($I=7.5x10^{-2}$) at 25°C.

TABLE 4.3.6. Initial Dissolution Rates of $AgIO_3$ in $Al_2(SO_4)_3$ Media at 25°C

| Ionic Strength I | Initial Dissolution Rate, $R_d$, (mol $sec^{-1} gr^{-1}$)$\times 10^6$ |
|---|---|
| $7.5 \times 10^{-6}$ | 0.92 |
| $7.5 \times 10^{-5}$ | 0.81 |
| $7.5 \times 10^{-4}$ | 0.84 |
| $7.5 \times 10^{-3}$ | 0.79 |
| $7.5 \times 10^{-2}$ | 0.84 |

In Figure 4.1-b the starting point of the curve is that corresponding to dissolution in distilled water. The trend in this case is similar to that in $KNO_3$ media except the drop in rate is less pronounced. The rate of dissolution decreases by 27 per cent of its value in distilled water at around an ionic strength of $10^{-4}$ and then remains constant up to about $I = 10^{-2}$. Finally it starts to increase towards its distilled water value. A similar trend with a per cent rate drop of 20 per cent was previously obtained by Enüstün and Ayrancı[12].

The meaning of the lesser decrease in rate in $Al_2(SO_4)_3$ solutions compared to that in $KNO_3$ media is that in the media containing $Al^{3+}$ ions, the double layer extends beyond the energy barriers forming a Stern layer but in the inner parts it shows some Gouy character. This character may be attributed to the presence of $H^+$ ions which are produced as a result of the hydrolysis of $Al^{3+}$ ions. The mechanism by which $H^+$ ions may penetrate into the layer produced by $Al^{3+}$ ions will be further investigated.(See Section 4.6).

## 4.4. DISSOLUTION OF $Al^{3+}$ ADSORBED $AgIO_3$ IN $KNO_3$ MEDIA

The dissolution kinetics of $Al^{3+}$ adsorbed $AgIO_3$ was followed in $KNO_3$ solutions of concentrations ranging from $10^{-6}$ M to $10^{-2}$ M. The $Al^{3+}$ adsorption on $AgIO_3$ was accomplished by following the procedure given in Section 3.3.3 and in this way the system contained less than $10^{-8}$ M $Al^{3+}$ under experimental conditions (this value corresponds to complete adsorption of $Al^{3+}$ from the solution). The results of these experiments are given in Tables 4.4.1 through 4.4.5 (The calibration data used for this set was the same as that of the dissolution of $AgIO_3$ in $KNO_3$ media which is given in Table A.2.2). The C v.s t data for the dissolution of $Al^{3+}$ adsorbed $AgIO_3$ in $KNO_3$ media are plotted in Figures 4.4.1 through 4.4.5.

The initial rates of dissolution of $Al^{3+}$ adsorbed $AgIO_3$ in $KNO_3$ media were calculated from the initial slopes of the corresponding C v.s t plots. The ionic strengths of $KNO_3$ solutions are the same as in Section 4.2., i.e., they are identical with the molar concentrations of the solutions. The initial dissolution rates of $Al^{3+}$ adsorbed $AgIO_3$ in $KNO_3$ media are tabulated together with the corresponding ionic strengths in Table 4.4.6. The data of Table 4.4.6 are plotted in Figure 4.1-c.

TABLE 4.4.1. Dissolution Data of $Al^{3+}$ Adsorbed $AgIO_3$ in $10^{-6}$ M $KNO_3$ Solution ($I=10^{-6}$) at 25°C

Calibration Function: $\log C = -3.764 - 0.0733\ N_d$

| Time, t (sec) | Number of Divisions on Recorder Output, $N_d$ | Concentration of $AgIO_3$, C, ($Mx10^6$) |
|---|---|---|
| 12 | 30.7 | 0.97 |
| 15 | 29.2 | 1.25 |
| 18 | 27.2 | 1.75 |
| 21 | 25.5 | 2.31 |
| 27 | 23.6 | 3.21 |
| 33 | 22.5 | 3.86 |
| 39 | 21.5 | 4.55 |
| 45 | 20.7 | 5.25 |
| 51 | 19.8 | 6.05 |
| 57 | 19.2 | 6.74 |
| 63 | 18.6 | 7.45 |
| 69 | 18.2 | 7.97 |
| 75 | 17.8 | 8.52 |
| 81 | 17.5 | 9.06 |
| 87 | 17.1 | 9.57 |
| 93 | 16.8 | 10.16 |

TABLE 4.4.2. Dissolution Data of $Al^{3+}$ Adsorbed $AgIO_3$ in $10^{-5}$ M $KNO_3$ Solution ($I=10^{-5}$) at 25°C

Calibration Function: $\log C = -3.990 - 0.0643\ N_d$

| Time, t (sec) | Number of Divisions on Recorder Output, $N_d$ | Concentration of $AgIO_3$, C, ($Mx10^6$) |
|---|---|---|
| 8 | 38.6 | 0.34 |
| 11 | 33.2 | 0.75 |
| 14 | 29.5 | 1.30 |
| 20 | 26.2 | 2.11 |
| 26 | 24.2 | 2.85 |
| 32 | 22.6 | 3.60 |
| 38 | 21.6 | 4.17 |
| 44 | 20.7 | 4.77 |
| 50 | 19.8 | 5.43 |
| 56 | 19.1 | 6.05 |
| 65 | 18.2 | 6.91 |
| 71 | 17.6 | 7.55 |
| 77 | 17.1 | 8.19 |
| 83 | 16.6 | 8.75 |
| 89 | 16.2 | 9.30 |
| 95 | 15.8 | 9.91 |

TABLE 4.4.3. Dissolution Data of $Al^{3+}$ Adsorbed $AgIO_3$ in $10^{-4}$ M $KNO_3$ Solution ($I=10^{-4}$) at $25^{o}C$

Calibration Function: $\log C = -3.980 - 0.077\ N_d$

| Time, t (sec) | Number of Divisions on Recorder Output, $N_d$ | Concentration of $AgIO_3$, C, ($Mx10^6$) |
|---|---|---|
| 9 | 30.9 | 0.44 |
| 12 | 26.8 | 0.90 |
| 15 | 24.3 | 1.41 |
| 21 | 21.6 | 2.26 |
| 27 | 19.9 | 3.09 |
| 33 | 18.9 | 3.70 |
| 39 | 18.0 | 4.34 |
| 45 | 17.1 | 5.07 |
| 51 | 16.4 | 5.76 |
| 60 | 15.7 | 6.49 |
| 66 | 15.2 | 7.06 |
| 72 | 14.8 | 7.60 |
| 78 | 14.4 | 8.21 |
| 84 | 14.0 | 8.75 |
| 90 | 13.8 | 9.13 |
| 96 | 13.4 | 9.68 |

TABLE 4.4.4. Dissolution Data of $Al^{3+}$ Adsorbed $AgIO_3$ in $10^{-3}$ M $KNO_3$ Solution ($I=10^{-3}$) at $25^{o}C$

Calibration Function: $\log C = -3.944 - 0.067\ N_d$

| Time, t (sec) | Number of Divisions on Recorder Output, $N_d$ | Concentration of $AgIO_3$, C, ($Mx10^6$) |
|---|---|---|
| 9 | 35.9 | 0.45 |
| 12 | 30.7 | 1.00 |
| 15 | 27.9 | 1.55 |
| 21 | 24.9 | 2.44 |
| 27 | 23.5 | 3.06 |
| 33 | 21.9 | 3.88 |
| 39 | 21.0 | 4.45 |
| 45 | 20.0 | 5.20 |
| 54 | 19.1 | 6.04 |
| 60 | 18.6 | 6.50 |
| 66 | 18.0 | 7.07 |
| 72 | 17.6 | 7.57 |
| 78 | 17.2 | 8.02 |
| 84 | 16.9 | 8.47 |
| 90 | 16.6 | 8.83 |
| 96 | 16.4 | 9.05 |

TABLE 4.4.5. Dissolution Data of $Al^{3+}$ Adsorbed $AgIO_3$ in $10^{-2}$ M $KNO_3$ Solution ($I=10^{-2}$) at 25°C

Calibration Function: $\log C = -3.851 - 0.079\ N_d$

| Time, t (sec) | Number of Divisions on Recorder Output, $N_d$ | Concentration of $AgIO_3$, C, ($Mx10^6$) |
|---|---|---|
| 9 | 33.7 | 0.31 |
| 15 | 27.1 | 1.02 |
| 21 | 23.4 | 2.00 |
| 27 | 21.2 | 3.02 |
| 33 | 19.8 | 3.84 |
| 39 | 18.8 | 4.62 |
| 45 | 18.1 | 5.30 |
| 51 | 17.4 | 5.94 |
| 57 | 16.8 | 6.67 |
| 66 | 16.1 | 7.60 |
| 72 | 15.7 | 8.20 |
| 78 | 15.3 | 8.75 |
| 84 | 15.1 | 9.06 |
| 90 | 14.8 | 9.58 |
| 96 | 14.6 | 9.89 |
| 102 | 14.4 | 10.30 |

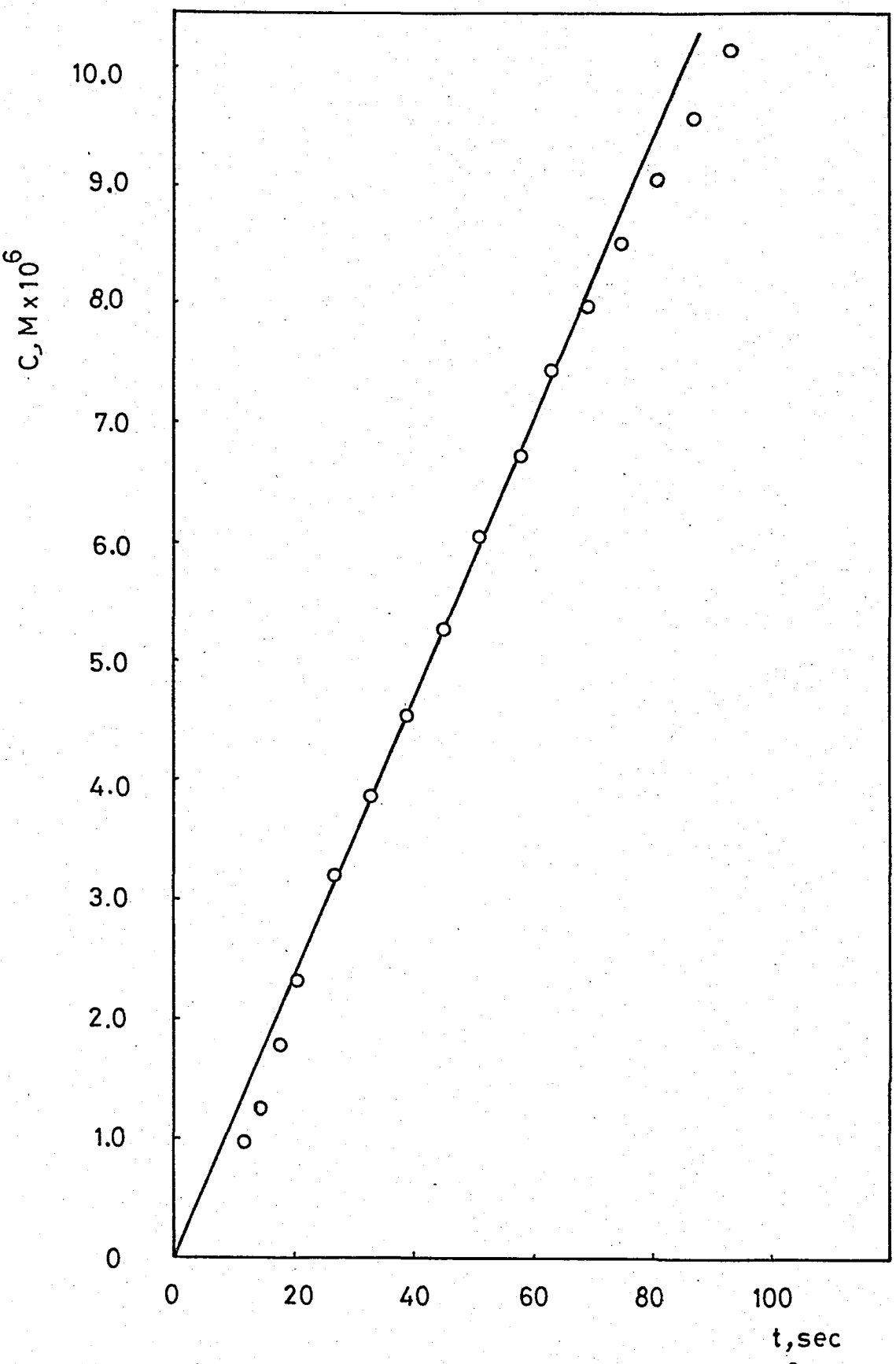


FIGURE 4.4.1. C v.s t Plot for the Dissolution of $Al^{3+}$ Adsorbed $AgIO_3$ in $10^{-6}$ M $KNO_3$ Solution ($I=10^{-6}$) at $25^{o}C$.

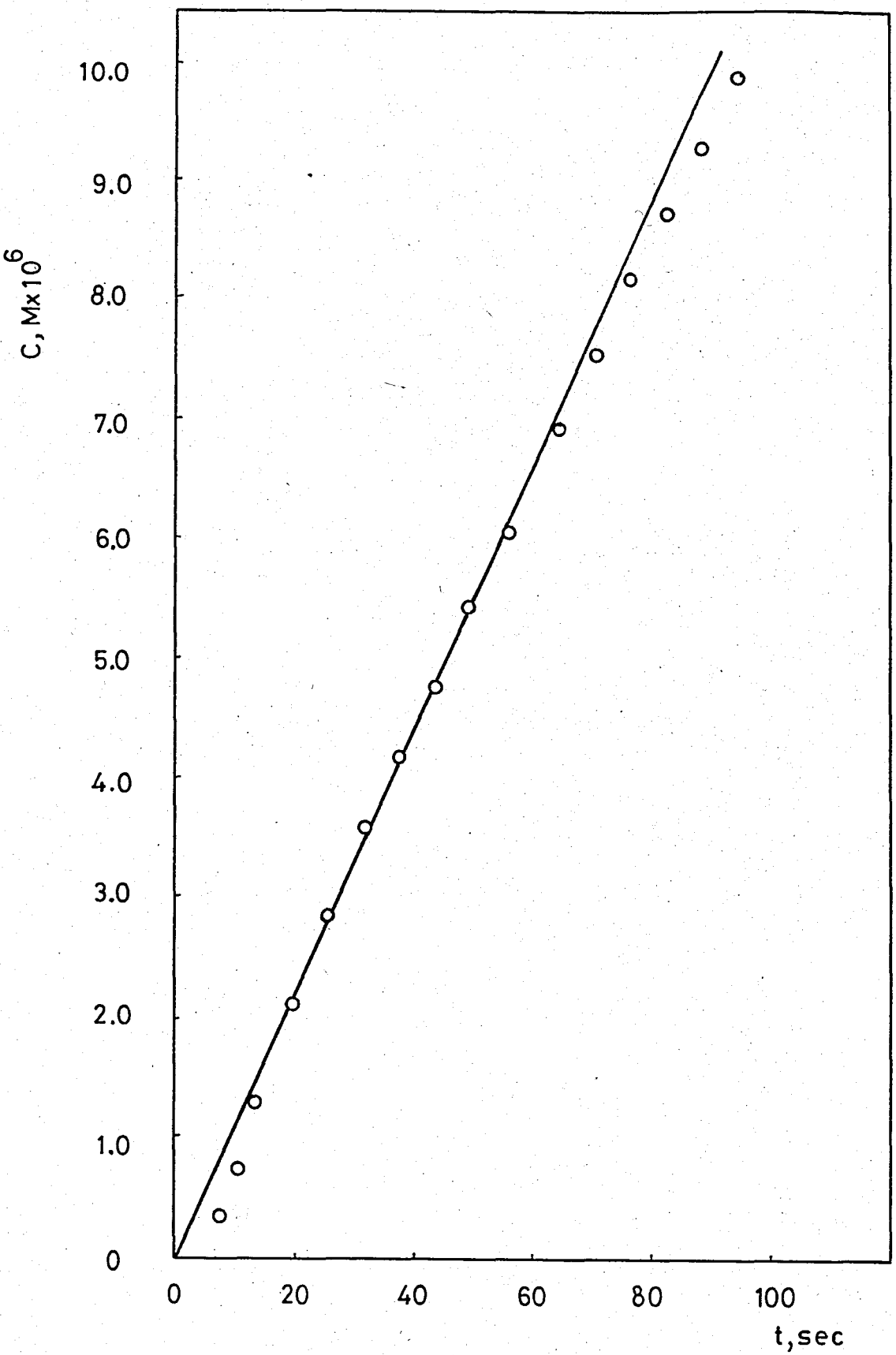


FIGURE 4.4.2. C v.s t Plot for the Dissolution of $Al^{3+}$ Adsorbed $AgIO_3$ in $10^{-5}$ M $KNO_3$ Solution ($I=10^{-5}$) at $25^{o}C$.

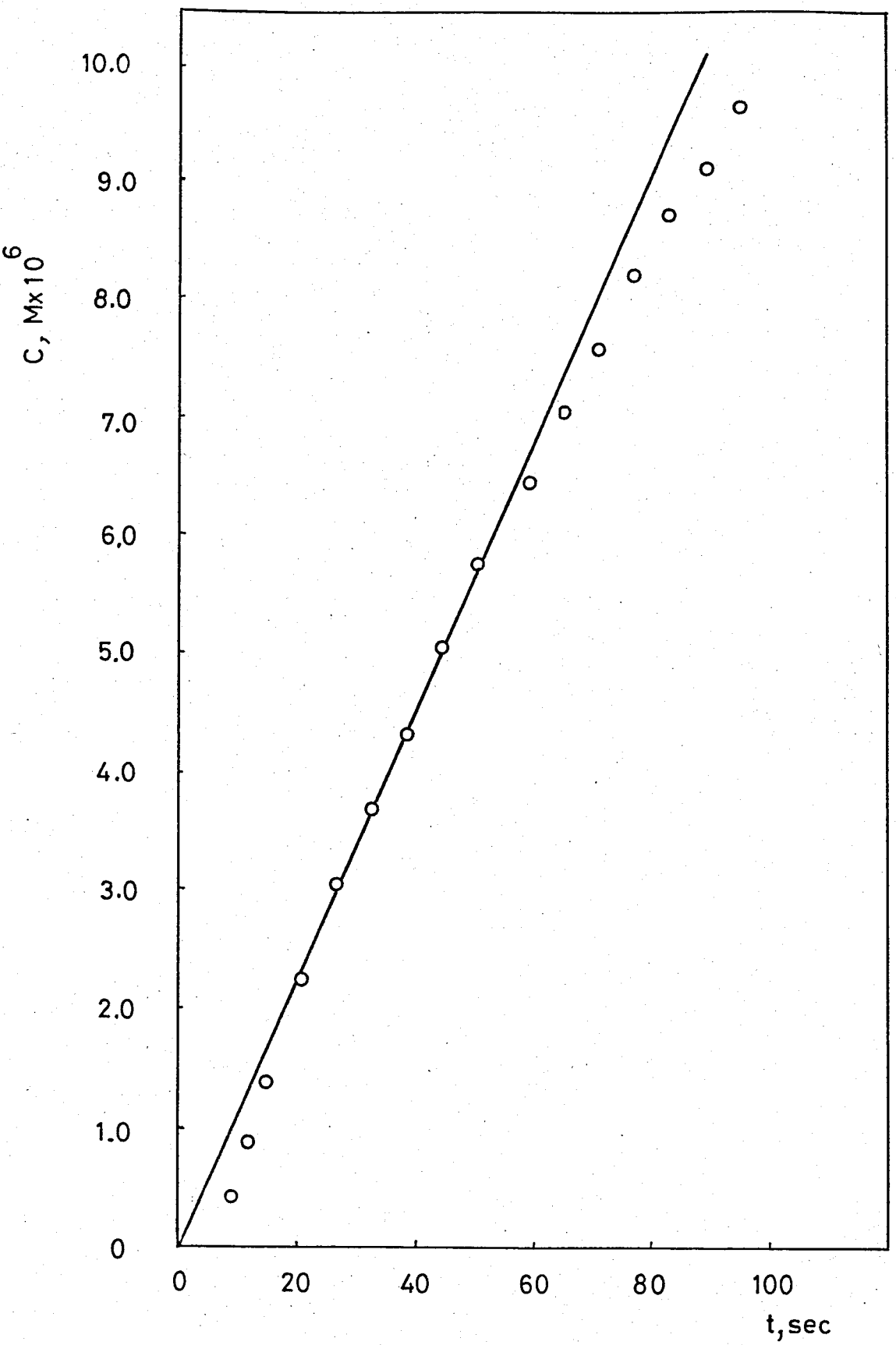


FIGURE 4.4.3. C v.s t Plot for the Dissolution of $Al^{3+}$ Adsorbed $AgIO_3$ in $10^{-4}$ M $KNO_3$ Solution ($I=10^{-4}$) at 25°C.

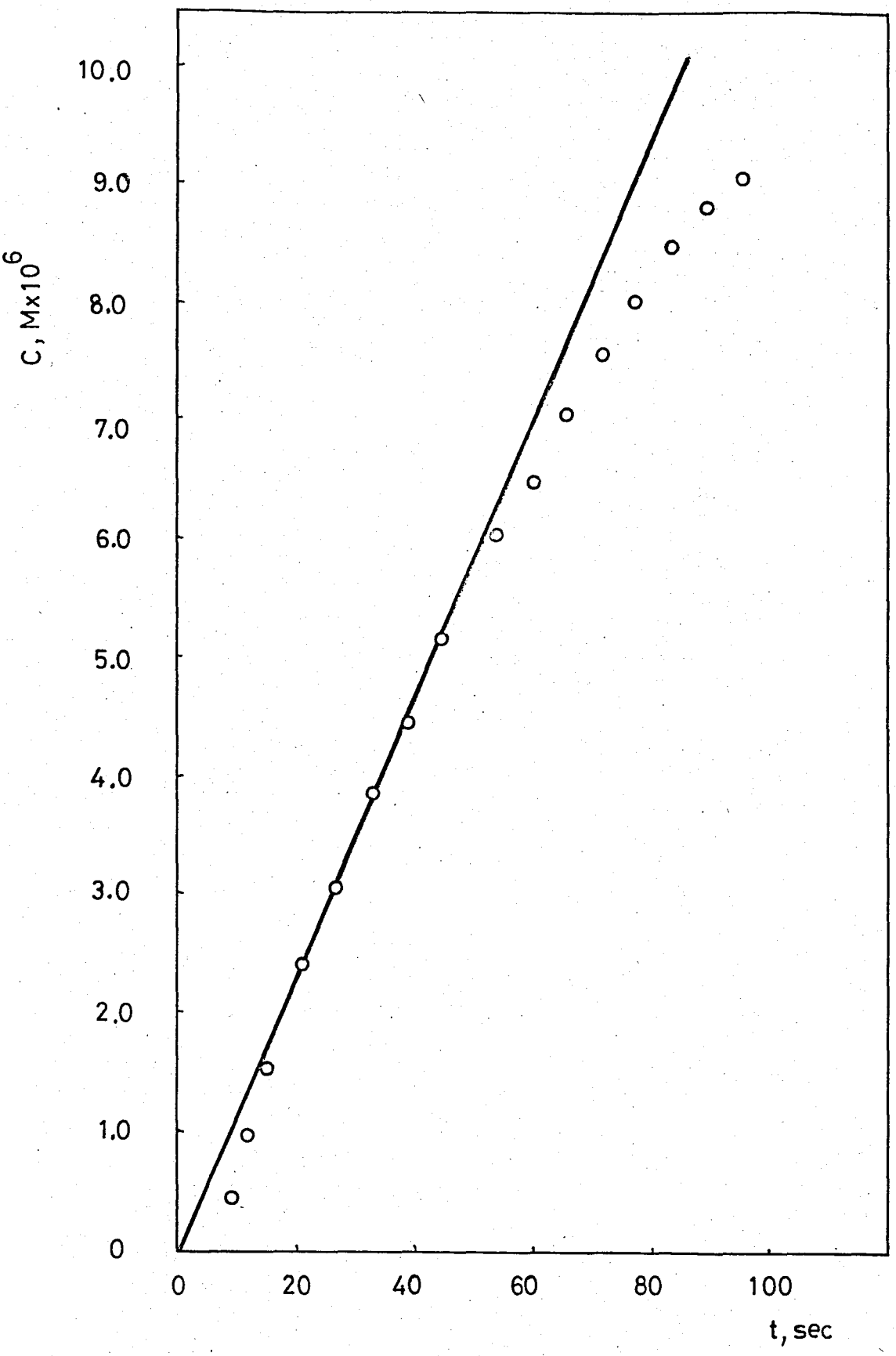


FIGURE 4.4.4. C v.s t Plot for the Dissolution of $Al^{3+}$ Adsorbed $AgIO_3$ in $10^{-3}$ M $KNO_3$ Solution ($I=10^{-3}$) at $25^{o}C$.

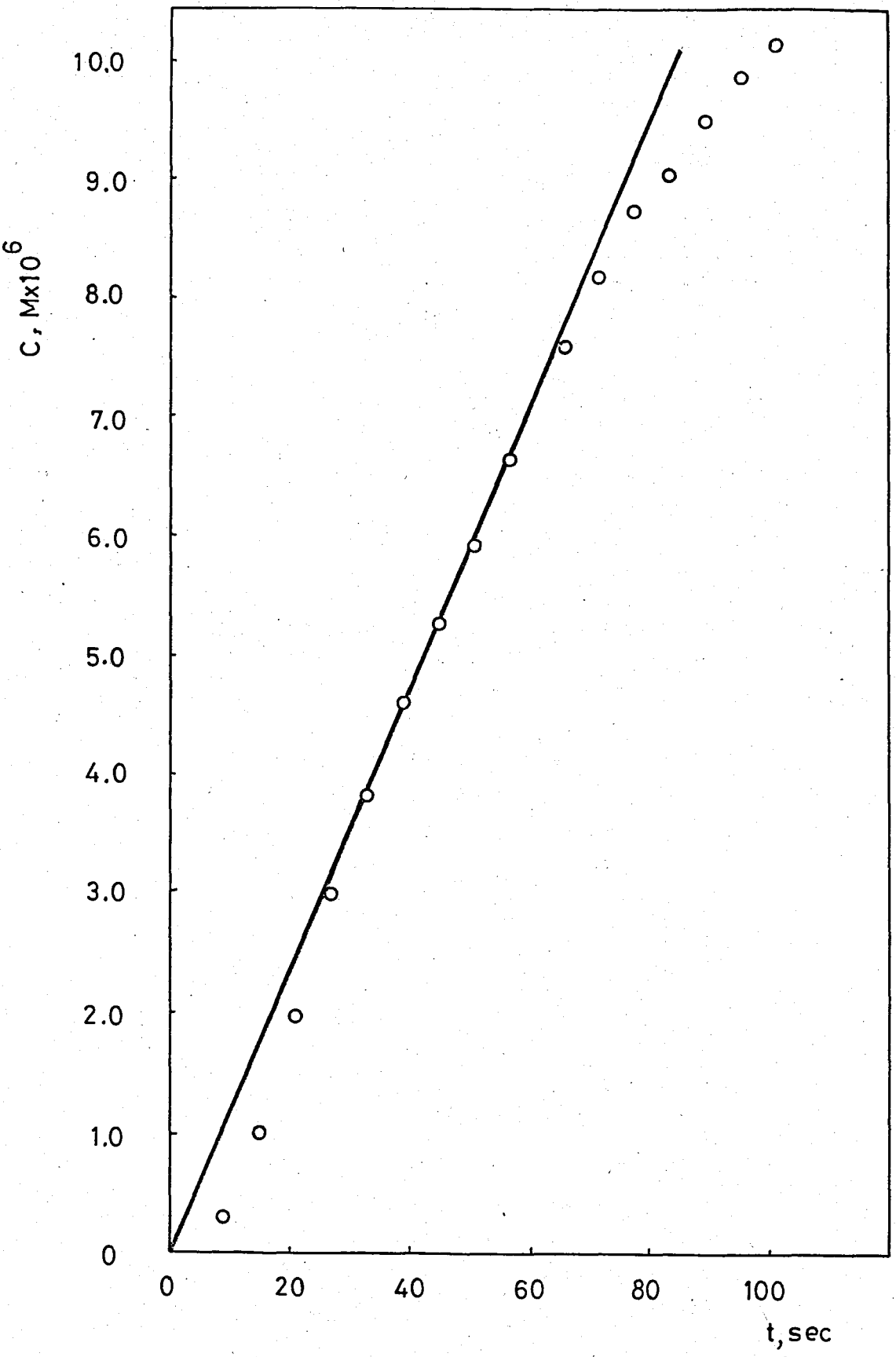


FIGURE 4.4.5. C v.s t Plot for the Dissolution of $Al^{3+}$ Adsorbed $AgIO_3$ in $10^{-2}$ M $KNO_3$ Solution ($I=10^{-2}$) at $25^{o}C$.

TABLE 4.4.6. Initial Dissolution Rates of $Al^{3+}$ Adsorbed $AgIO_3$ in $KNO_3$ Media at 25°C

| Ionic Strength I | Initial Dissolution Rate, $R_d$, (mol $sec^{-1}gr^{-1}$)x$10^6$ |
|---|---|
| $10^{-6}$ | 1.17 |
| $10^{-5}$ | 1.10 |
| $10^{-4}$ | 1.12 |
| $10^{-3}$ | 1.16 |
| $10^{-2}$ | 1.18 |

An examination of Figure 4.1-c shows that in a system containing only a trace amount of $Al^{3+}$ in the presence of $K^+$ ions, the rate of dissolution is nearly identical with that in distilled water, irrespective of $K^+$ concentration. The same type of behavior was observed by Enüstün and Ayranci[12] for this system.

This observation is in perfect agreement with theoretical conclusion (c). The $Al^{3+}$ content of the system is so small that practically no excess $H^+$ due to hydrolysis of $Al^{3+}$ ions is present to penetrate through the Stern layer produced by $Al^{3+}$ outside the energy barriers. Obviously, the penetration of $K^+$ ions is also out of question. Thus, the Stern character of the double layer is dominant.

## 4.5. DISSOLUTION OF $Fe^{+3}$ ADSORBED $AgIO_3$ IN $KNO_3$ MEDIA

The dissolution behavior of $Fe^{3+}$ adsorbed $AgIO_3$ in $KNO_3$ media was investigated to check the applicability of the theory further. The $Fe^{3+}$ adsorption on $AgIO_3$ was accomplished by following the procedure given in Section 3.3.3. and in this way the system contained less than $10^{-8}$ M $Fe^{3+}$ under experimental conditions (this number corresponds to complete adsorption of $Fe^{3+}$ from the solution). The ionic strengths of

the $KNO_3$ solutions used range from $10^{-6}$ to $10^{-2}$. One further dissolution experiment for this case is the dissolution of $Fe^{3+}$ adsorbed $AgIO_3$ in distilled water. The results of these experiments are given in Tables 4.5.1 through 4.5.6. (The calibration data used for this set was the same as that of the dissolution of $AgIO_3$ in $KNO_3$ media which is given in Table A.2.1). The C v.s t data for the dissolution of $Fe^{3+}$ adsorbed $AgIO_3$ in $KNO_3$ media are plotted in Figures 4.5.1 through 4.5.6.

The initial dissolution rates of $Fe^{3+}$ adsorbed $AgIO_3$ in $KNO_3$ media calculated from the initial slopes of the corresponding C v.s t plots are tabulated in Table 4.5.7. The data of Table 4.5.7 are plotted in Figure 4.1-d.

TABLE 4.5.1. Dissolution Data of $Fe^{3+}$ Adsorbed $AgIO_3$ in Distilled $H_2O$ at $25^oC$

Calibration Function: $\log C = -3.859 - 0.079\ N_d$

| Time, t (sec) | Number of Divisions on Recorder Output, $N_d$ | Concentration of $AgIO_3$, C, ($Mx10^6$) |
|---|---|---|
| 12 | 29.8 | 0.61 |
| 20 | 25.5 | 1.34 |
| 28 | 23.0 | 2.11 |
| 36 | 21.3 | 2.85 |
| 44 | 20.3 | 3.43 |
| 52 | 19.3 | 4.11 |
| 60 | 18.5 | 4.80 |
| 68 | 17.9 | 5.35 |
| 76 | 17.2 | 6.03 |
| 84 | 16.8 | 6.55 |
| 92 | 16.3 | 7.10 |
| 100 | 15.9 | 7.68 |
| 108 | 15.5 | 8.26 |
| 116 | 15.1 | 8.80 |

TABLE 4.5.2. Dissolution Data of $Fe^{3+}$ Adsorbed $AgIO_3$ in $10^{-6}$ M $KNO_3$ Solution ($I=10^{-6}$) at 25°C

Calibration Function: $\log C = -3.764 - 0.0733 N_d$

| Time, t (sec) | Number of Divisions on Recorder Output, $N_d$ | Concentration of $AgIO_3$, C, ($Mx10^6$) |
|---|---|---|
| 10 | 35.9 | 0.40 |
| 18 | 31.1 | 0.91 |
| 22 | 29.4 | 1.21 |
| 26 | 27.8 | 1.59 |
| 34 | 26.0 | 2.13 |
| 42 | 24.8 | 2.61 |
| 50 | 23.8 | 3.10 |
| 58 | 23.0 | 3.56 |
| 66 | 22.2 | 4.08 |
| 74 | 21.6 | 4.50 |
| 82 | 21.1 | 4.91 |
| 90 | 20.5 | 5.42 |
| 98 | 20.0 | 5.84 |
| 106 | 19.6 | 6.25 |

TABLE 4.5.3. Dissolution Data of $Fe^{3+}$ Adsorbed $AgIO_3$ in $10^{-5}$ M $KNO_3$ Solution ($I=10^{-5}$) at $25^{o}C$

Calibration Function: $\log C = -3.990 - 0.0643\ N_d$

| Time, t (sec) | Number of Divisions on Recorder Output, $N_d$ | Concentration of $AgIO_3$, C, ($Mx10^6$) |
|---|---|---|
| 17 | 35.3 | 0.55 |
| 21 | 32.0 | 0.90 |
| 25 | 28.8 | 1.44 |
| 29 | 27.2 | 1.82 |
| 37 | 25.3 | 2.42 |
| 45 | 24.0 | 2.92 |
| 53 | 23.0 | 3.39 |
| 61 | 22.1 | 3.86 |
| 73 | 21.1 | 4.52 |
| 81 | 20.5 | 4.95 |
| 89 | 19.9 | 5.36 |
| 97 | 19.4 | 5.79 |
| 105 | 19.0 | 6.11 |
| 113 | 18.6 | 6.49 |

TABLE 4.5.4. Dissolution Data of $Fe^{3+}$ Adsorbed $AgIO_3$ in $10^{-4}$ M $KNO_3$ Solution ($I=10^{-4}$) at $25^{o}C$

Calibration Function: $\log C = -3.980 - 0.077\ N_d$

| Time, t (sec) | Number of Divisions on Recorder Output, $N_d$ | Concentration of $AgIO_3$, C, ($Mx10^6$) |
|---|---|---|
| 12 | 30.1 | 0.50 |
| 16 | 27.2 | 0.85 |
| 20 | 25.3 | 1.17 |
| 28 | 23.0 | 1.79 |
| 36 | 21.6 | 2.28 |
| 44 | 20.3 | 2.85 |
| 52 | 19.6 | 3.24 |
| 64 | 18.5 | 3.96 |
| 72 | 17.9 | 4.42 |
| 80 | 17.4 | 4.82 |
| 88 | 16.9 | 5.26 |
| 96 | 16.4 | 5.77 |
| 104 | 16.1 | 6.06 |
| 112 | 15.7 | 6.47 |
| 120 | 15.4 | 6.86 |

TABLE 4.5.5. Dissolution Data of $Fe^{3+}$ Adsorbed $AgIO_3$ in $10^{-3}$ M $KNO_3$ Solution ($I=10^{-3}$) at $25^{o}C$

Calibration Function: $\log C = -3.944 - 0.067\ N_d$

| Time, t (sec) | Number of Divisions on Recorder Output, $N_d$ | Concentration of $AgIO_3$, C, ($Mx10^6$) |
|---|---|---|
| 14 | 33.9 | 0.61 |
| 22 | 29.3 | 1.25 |
| 30 | 26.5 | 1.91 |
| 38 | 24.8 | 2.49 |
| 46 | 23.4 | 3.09 |
| 54 | 22.3 | 3.66 |
| 62 | 21.5 | 4.12 |
| 70 | 20.8 | 4.64 |
| 78 | 20.1 | 5.14 |
| 86 | 19.6 | 5.57 |
| 94 | 19.1 | 6.02 |
| 102 | 18.6 | 6.45 |
| 110 | 18.2 | 6.86 |
| 118 | 17.9 | 7.20 |

TABLE 4.5.6. Dissolution Data of $Fe^{3+}$ Adsorbed $AgIO_3$ in $10^{-2}$ M $KNO_3$ Solution ($I=10^{-2}$) at $25^{o}C$

Calibration Function: $\log C = -3.851 - 0.079\ N_d$

| Time, t (sec) | Number of Divisions on Recorder Output, $N_d$ | Concentration of $AgIO_3$, C, ($Mx10^6$) |
|---|---|---|
| 7 | 36.1 | 0.20 |
| 13 | 28.8 | 0.75 |
| 19 | 25.4 | 1.40 |
| 25 | 23.4 | 2.02 |
| 31 | 22.1 | 2.54 |
| 37 | 21.2 | 3.00 |
| 43 | 20.5 | 3.40 |
| 52 | 19.5 | 4.10 |
| 58 | 18.9 | 4.55 |
| 64 | 18.4 | 4.96 |
| 70 | 18.0 | 5.38 |
| 76 | 17.5 | 5.85 |
| 82 | 17.2 | 6.24 |
| 88 | 16.7 | 6.73 |
| 94 | 16.5 | 7.04 |
| 100 | 16.2 | 7.45 |

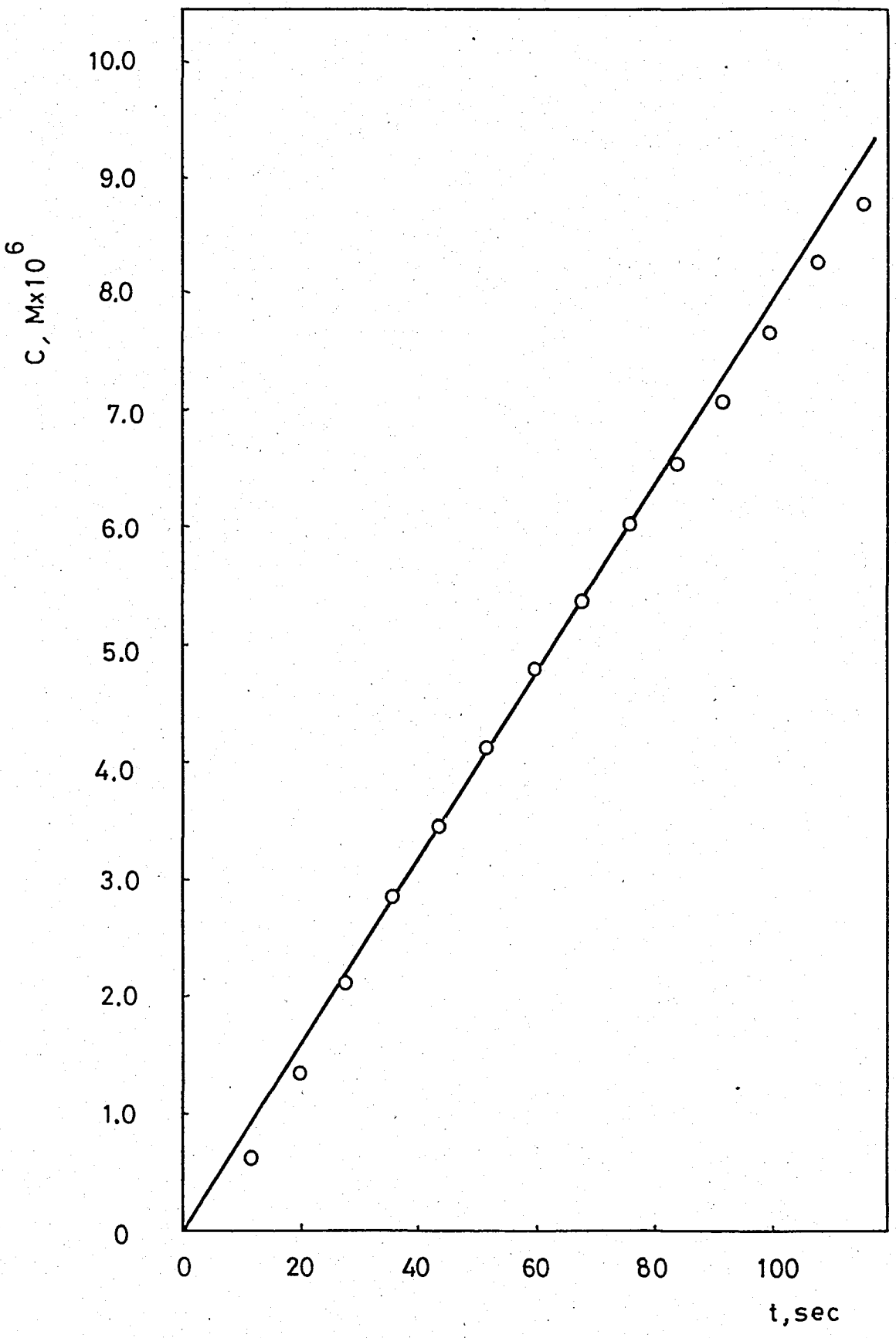


FIGURE 4.5.1. C v.s t Plot for the Dissolution of $Fe^{3+}$ Adsorbed $AgIO_3$ in Distilled $H_2O$.

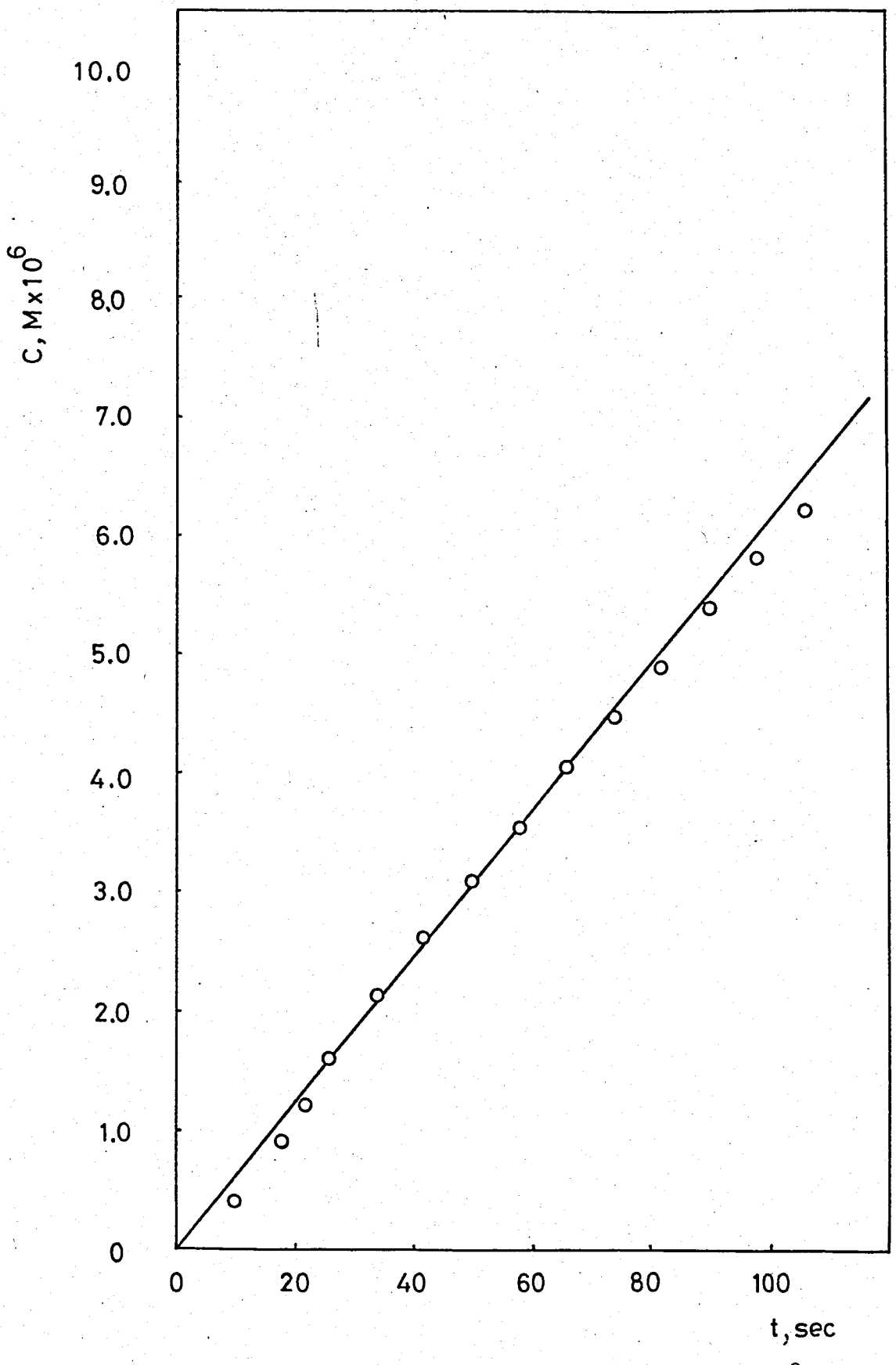


FIGURE 4.5.2. C v.s t Plot for the Dissolution of $Fe^{3+}$ Adsorbed $AgIO_3$ in $10^{-6}$ M $KNO_3$ Solution ($I=10^{-6}$) at 25°C.

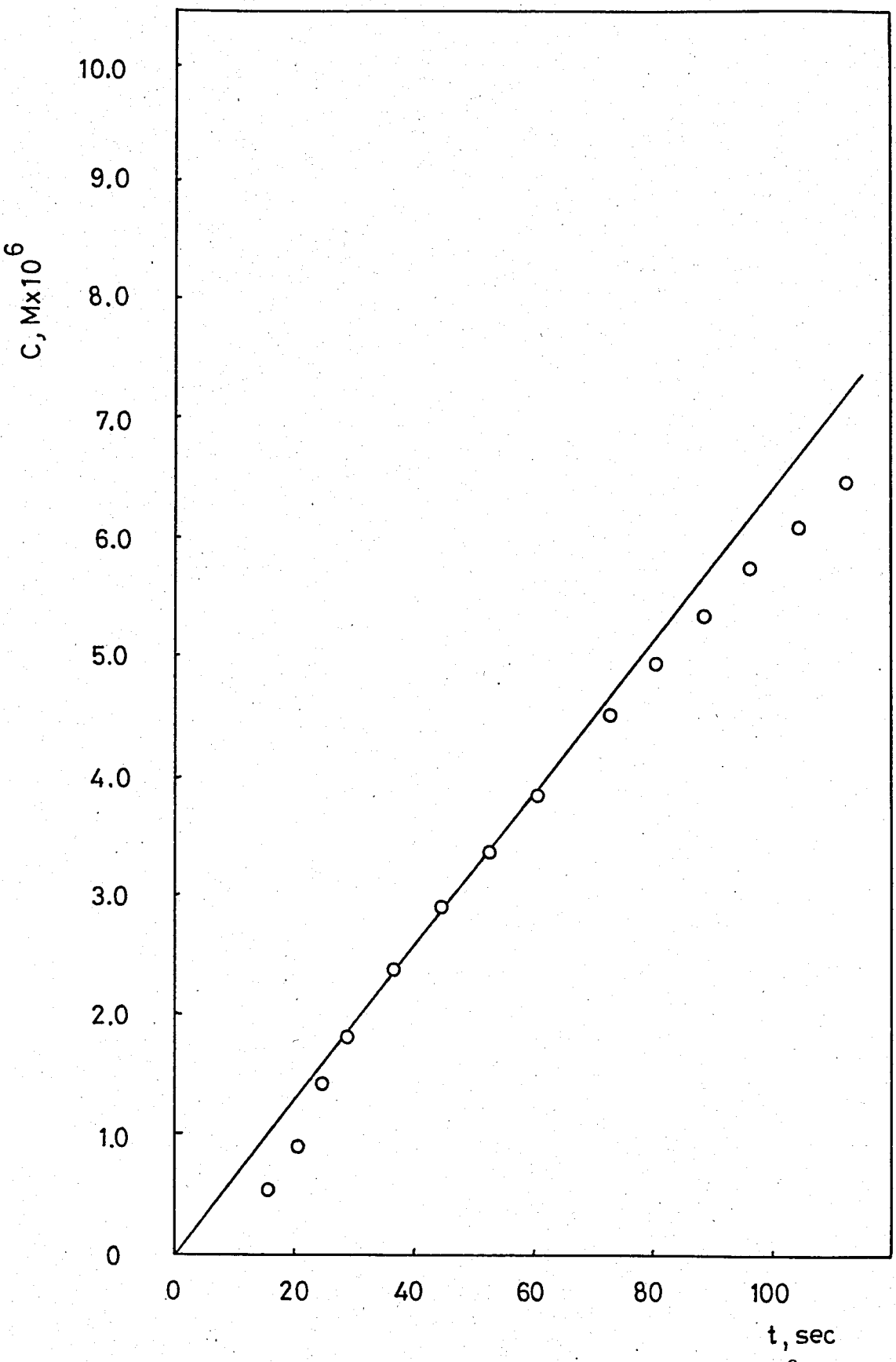


FIGURE 4.5.3. C v.s t Plot for the Dissolution of $Fe^{3+}$ Adsorbed $AgIO_3$ in $10^{-5}$ M $KNO_3$ Solution ($I=10^{-5}$) at 25°C.

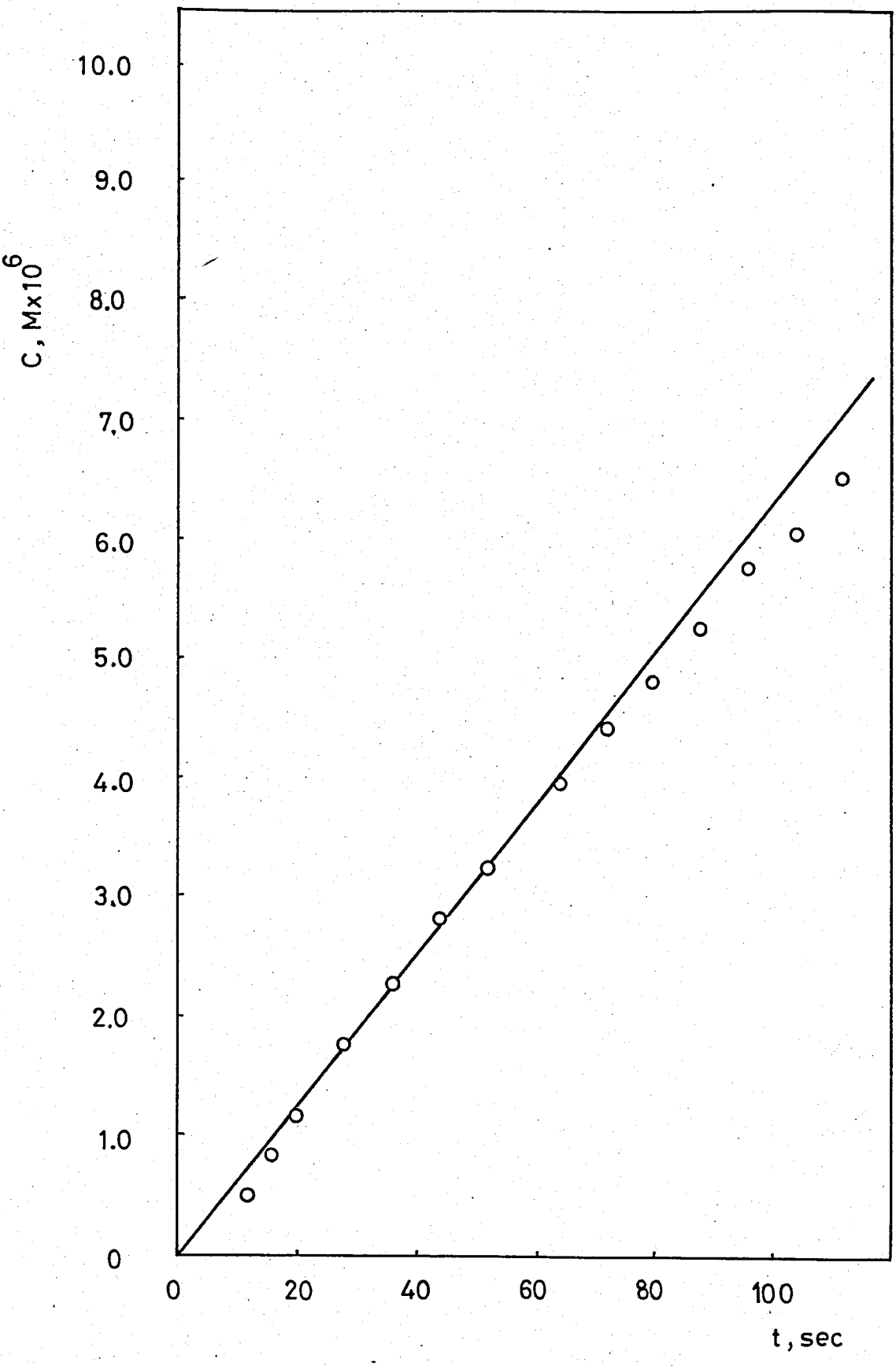


FIGURE 4.5.4. C v.s t Plot for the Dissolution of $Fe^{3+}$ Adsorbed $AgIO_3$ in $10^{-4}$ M $KNO_3$ Solution ($I=10^{-4}$) at 25°C.

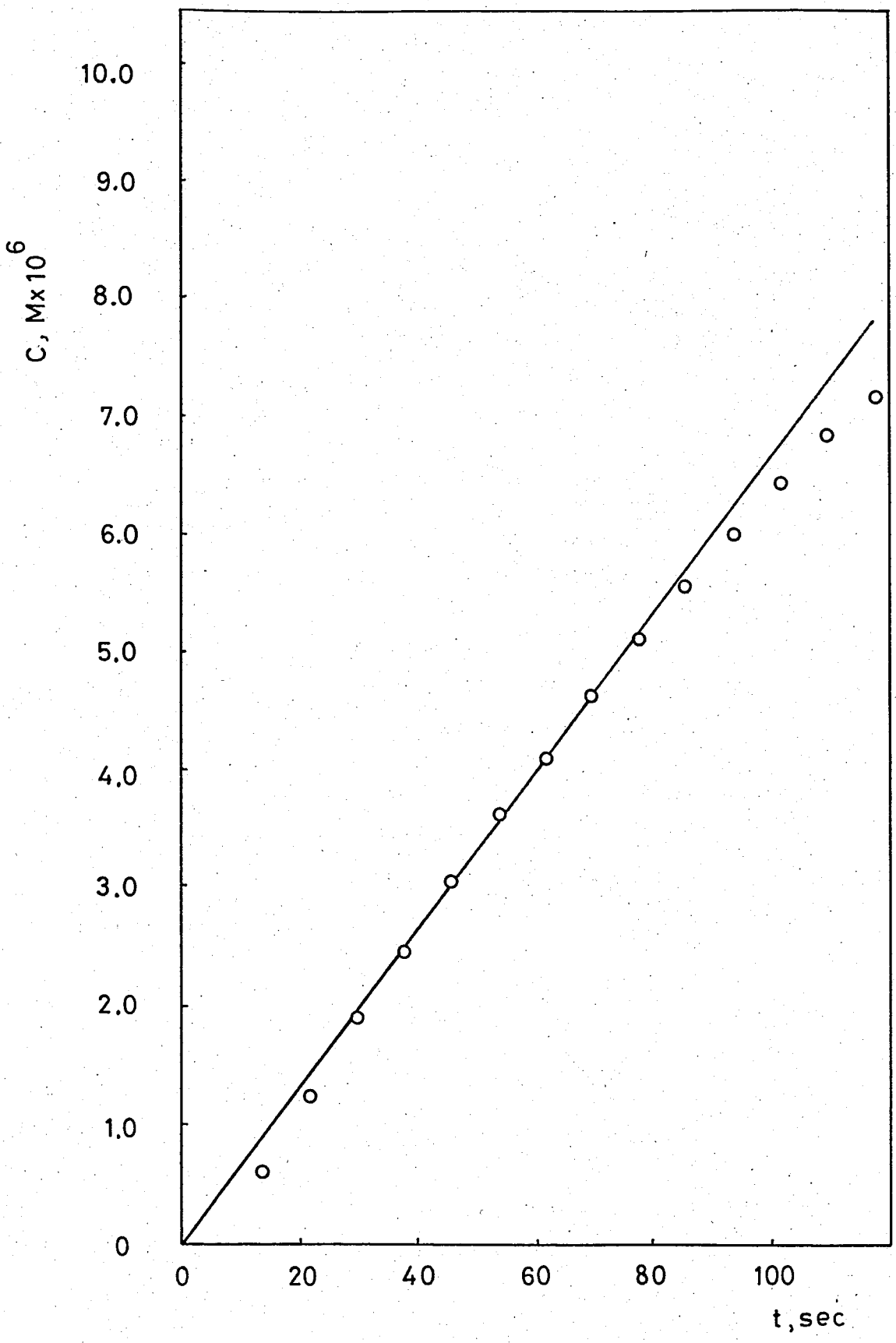


FIGURE 4.5.5. C v.s t Plot for the Dissolution of $Fe^{3+}$ Adsorbed $AgIO_3$ in $10^{-3}$ M $KNO_3$ Solution ($I=10^{-3}$) at $25^{o}C$.

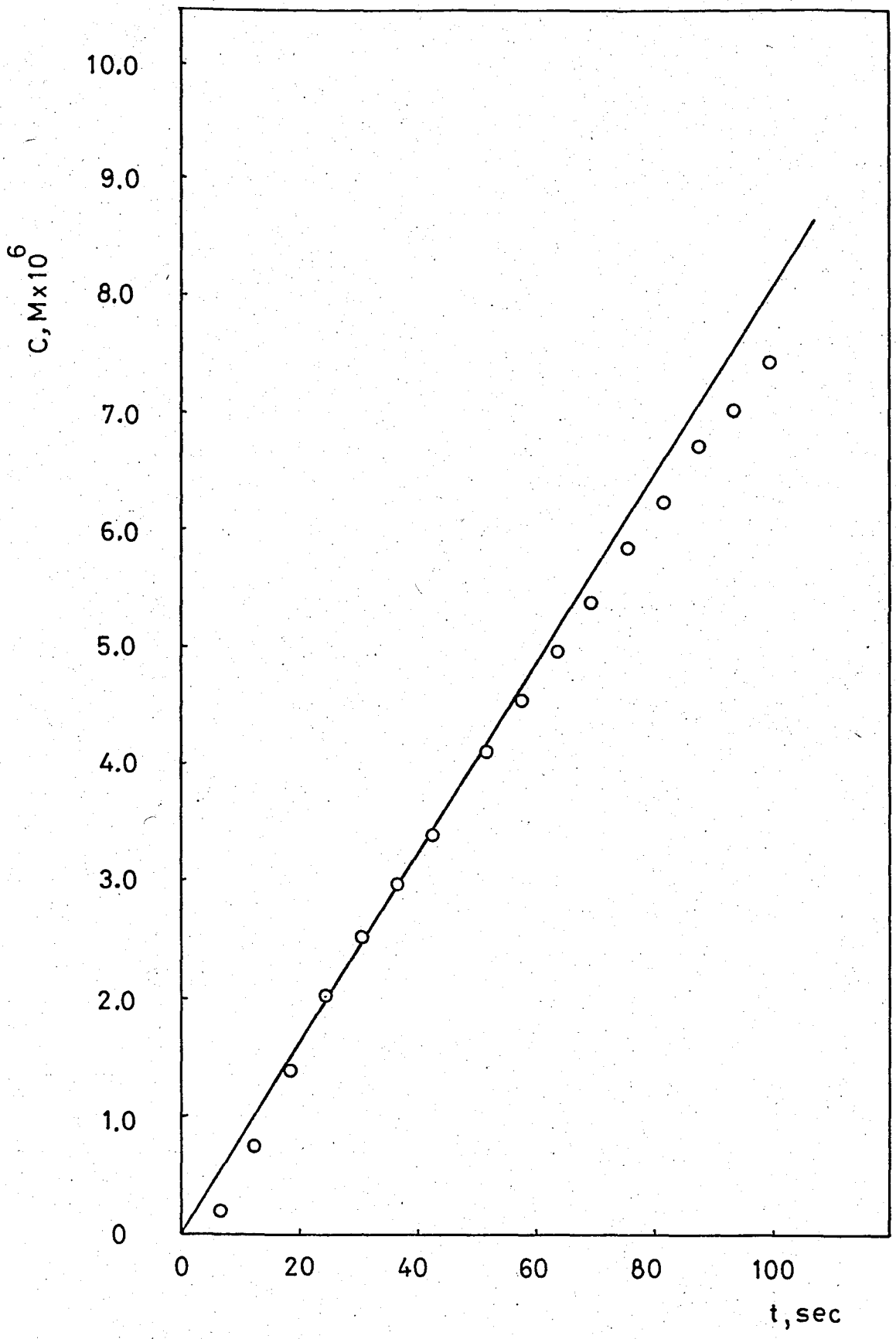


FIGURE 4.5.6. C v.s t Plot for the Dissolution of $Fe^{3+}$ Adsorbed $AgIO_3$ in $10^{-2}$ M $KNO_3$ Solution ($I=10^{-2}$) at 25°C.

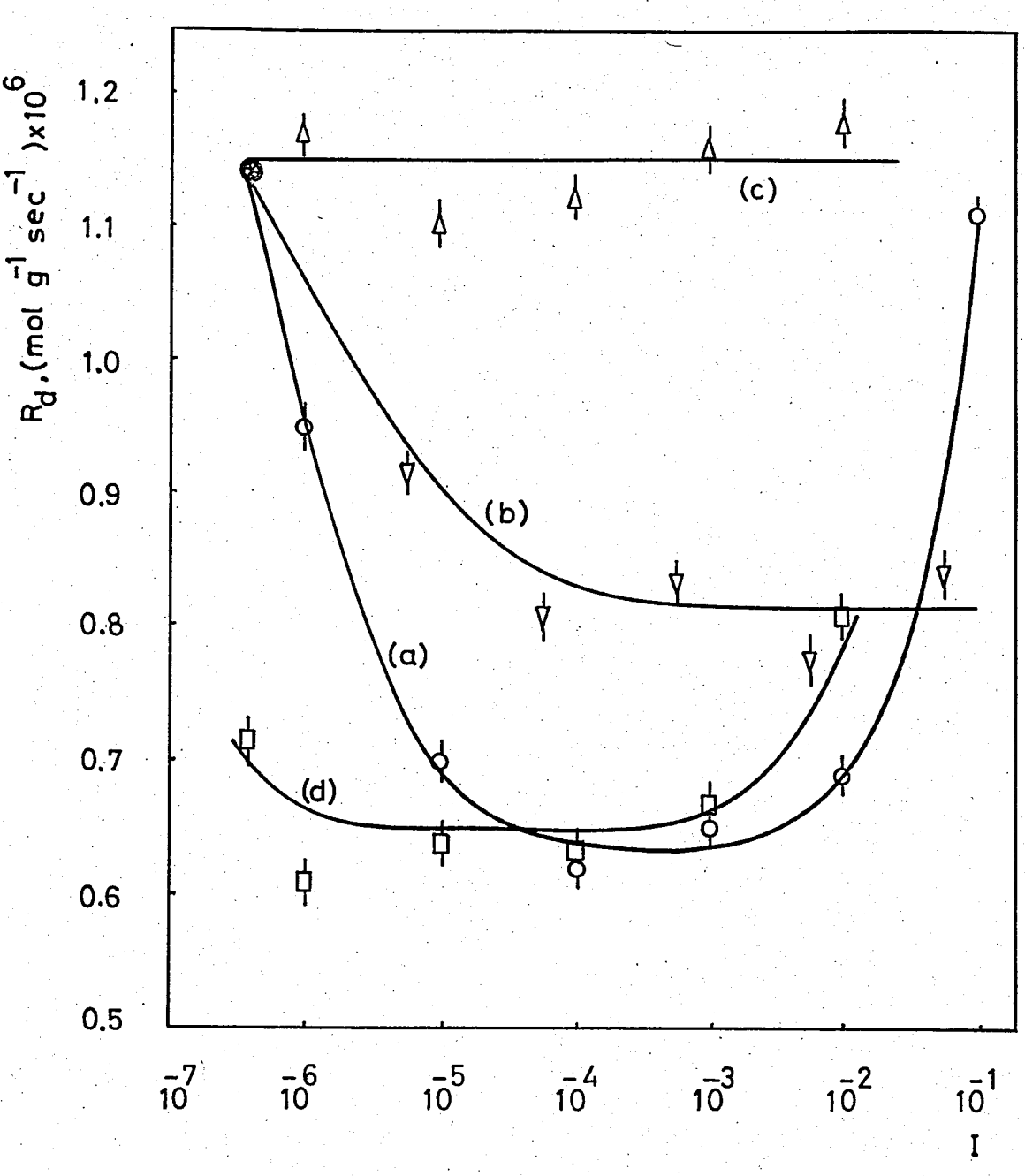


(a) $AgIO_3$ in $KNO_3$ Media

(b) $AgIO_3$ in $Al_2(SO_4)_3$ Media

(c) $Al^{3+}$ ads. $AgIO_3$ in $KNO_3$ Media

(d) $Fe^{3+}$ ads. $AgIO_3$ in $KNO_3$ Media

FIGURE 4.1. Dependence of the Initial Dissolution Rate of $AgIO_3$ on Ionic Strength of the Dissolution Medium at 25°C.

TABLE 4.5.7. Initial Dissolution Rates of $Fe^{3+}$ Adsorbed $AgIO_3$ in $KNO_3$ Media at 25°C

| Ionic Strength I | Initial Dissolution Rate, $R_d$, (mol $sec^{-1} gr^{-1}$)$\times 10^6$ |
|---|---|
| $10^{-6.4}$ (Distilled $H_2O$) | 0.79 |
| $10^{-6}$ | 0.61 |
| $10^{-5}$ | 0.64 |
| $10^{-4}$ | 0.63 |
| $10^{-3}$ | 0.67 |
| $10^{-2}$ | 0.81 |

The results of the experiments carried out with $Fe^{3+}$ adsorbed $AgIO_3$ in $KNO_3$ media resemble that of $AgIO_3$ in $KNO_3$ media in such a way that the corresponding dissolution rate - ionic strength curves nearly coincide between the ionic strengths $10^{-5}$ and $10^{-3}$. This is the interval in which the dissolution rate has its Gouy limiting value for the dissolution of $AgIO_3$ in $KNO_3$ media. According to the theory, at this limiting case, Gouy potential profile starts with a steep slope from the surface and continues with a practically horizontal tail in the vicinity of energy barriers. It may be concluded that for the dissolution of $Fe^{3+}$ adsorbed $AgIO_3$ in $KNO_3$ media a similar potential profile should exist within the ionic strength interval of $10^{-5}$ - $10^{-3}$. On the other hand, for this set of experiments, since the dissolution rate does not show any significant change from $I = 10^{-6}$ to $I = 10^{-3}$, this behavior should also be valid at $I = 10^{-6}$; but at a very low ionic strength like $10^{-6}$, a steep Gouy potential profile can not be expected. Therefore this steep part of the potential profile should be caused by a thin Stern layer produced by a very small amount of $Fe^{3+}$ in the medium. As a result, one can say that the electrical double layer is composed of a thin Stern layer which cannot reach the energy barriers and a Gouy layer with a flat profile from that point on. The positions of the Stern layer proposed in $Al^{3+}$ adsorbed

$AgIO_3$ and $Fe^{3+}$ adsorbed $AgIO_3$ cases can be explained by noting the hydrated radii of $Al^{3+}$ and $Fe^{3+}$ ions. The crystallographic radius of $Fe^{3+}$ is greater than that of $Al^{3+}$ and therefore because of the fact that the hydrated radii are in reverse order, the Stern layer produced by $Fe^{3+}$ is closer to the surface compared to that by $Al^{3+}$.

## 4.6. DISSOLUTION OF $AgIO_3$ IN ACIDIC MEDIA

In order to see the role played by $H^+$ ions in the dissolution of $AgIO_3$, experiments were carried out with a series of solutions having pH's between 1.5 and 6.0. The results of these experiments are given in Tables 4.6.1 through 4.6.6.(The calibration data for each pH is given in Table A.2.3). The C v.s t data for the dissolution of $AgIO_3$ in acidic media are plotted in Figures 4.6.1 through 4.6.6.

The initial rates of dissolution of $AgIO_3$ in acidic media were calculated from the initial slopes of the corresponding C v.s t plots. The range of pH values obtained by pH measurements is from 1.5 to 6.0. The pH values measured by pH meter are somewhat smaller than the pH values calculated from the concentrations of the solutions, the reason being due to $CO_2$ absorption from the atmosphere. The initial dissolution rates of $AgIO_3$ in acidic media are tabulated in Table 4.6.7. The data of Table 4.6.7 are plotted in Figure 4.2-a.

TABLE 4.6.1. Dissolution Data of $AgIO_3$ at pH = 6.0 ($2.5 \times 10^{-7}$ M $CH_3COOH$) at 25°C

Calibration Function: $\log C = -3.747 - 0.0875\ N_d$

| Time, t (sec) | Number of Divisions on Recorder Output, $N_d$ | Concentration of $AgIO_3$, C, ($M \times 10^6$) |
|---|---|---|
| 10 | 28.9 | 0.53 |
| 14 | 26.5 | 0.86 |
| 18 | 24.4 | 1.32 |
| 26 | 22.0 | 2.13 |
| 34 | 20.3 | 3.03 |
| 42 | 19.2 | 3.73 |
| 50 | 18.4 | 4.43 |
| 58 | 17.6 | 5.09 |
| 66 | 17.1 | 5.73 |
| 74 | 16.5 | 6.43 |
| 86 | 15.8 | 7.38 |
| 94 | 15.4 | 8.04 |
| 102 | 15.0 | 8.73 |

TABLE 4.6.2. Dissolution Data of $AgIO_3$ at pH = 5.0 ($4.2 \times 10^{-6}$ M $CH_3COOH$) at $25^oC$

Calibration Function: $\log C = -3.764 - 0.0894\ N_d$

| Time, t (sec) | Number of Divisions on Recorder Output, $N_d$ | Concentration of $AgIO_3$, C, ($M \times 10^6$) |
|---|---|---|
| 13 | 26.7 | 0.70 |
| 21 | 23.9 | 1.25 |
| 29 | 21.8 | 1.94 |
| 37 | 20.0 | 2.81 |
| 45 | 19.0 | 3.43 |
| 53 | 18.2 | 4.02 |
| 61 | 17.5 | 4.67 |
| 69 | 17.0 | 5.17 |
| 81 | 16.4 | 5.92 |
| 89 | 16.0 | 6.40 |
| 97 | 15.7 | 6.80 |
| 105 | 15.3 | 7.34 |

TABLE 4.6.3. Dissolution Data of $AgIO_3$ at pH=4.1 ($4.2 \times 10^{-4}$ M $CH_3COOH$) at $25^oC$

Calibration Function: $\log C = -4.022 - 0.073\ N_d$

| Time, t (sec) | Number of Divisions on Recorder Output, $N_d$ | Concentration of $AgIO_3$, C, ($M \times 10^6$) |
|---|---|---|
| 14 | 31.5 | 0.47 |
| 18 | 27.9 | 0.86 |
| 22 | 25.4 | 1.30 |
| 30 | 22.8 | 2.02 |
| 38 | 21.1 | 2.70 |
| 46 | 20.1 | 3.27 |
| 54 | 19.0 | 3.90 |
| 62 | 18.2 | 4.44 |
| 70 | 17.5 | 5.01 |
| 82 | 16.8 | 5.66 |
| 90 | 16.3 | 6.17 |
| 98 | 15.7 | 6.78 |
| 106 | 15.3 | 7.23 |
| 114 | 15.0 | 7.62 |

TABLE 4.6.4. Dissolution Data of $AgIO_3$ at pH=3.1 ($3.4 \times 10^{-2}$ M $CH_3COOH$) at $25^oC$

Calibration Function: $\log C = -3.994 - 0.083\ N_d$

| Time, t (sec) | Number of Divisions on Recorder Output, $N_d$ | Concentration of $AgIO_3$, C, ($M \times 10^6$) |
|---|---|---|
| 13 | 28.8 | 0.41 |
| 21 | 23.6 | 1.12 |
| 29 | 21.0 | 1.82 |
| 37 | 19.6 | 2.38 |
| 45 | 18.3 | 3.06 |
| 53 | 17.5 | 3.60 |
| 61 | 16.6 | 4.19 |
| 69 | 16.0 | 4.72 |
| 77 | 15.5 | 5.24 |
| 85 | 15.0 | 5.78 |
| 93 | 14.5 | 6.32 |
| 101 | 14.2 | 6.77 |
| 109 | 13.8 | 7.27 |
| 117 | 13.5 | 7.64 |

TABLE 4.6.5. Dissolution Data of $AgIO_3$ at pH=2.2 ($6.4 \times 10^{-3}$ M $HNO_3$) at 25°C

Calibration Function: $\log C = -3.425 - 0.0905\ N_d$

| Time, t (sec) | Number of Divisions on Recorder Output, $N_d$ | Concentration of $AgIO_3$, C, ($M \times 10^6$) |
|---|---|---|
| 17 | 28.9 | 0.91 |
| 21 | 26.3 | 1.55 |
| 25 | 25.8 | 1.74 |
| 33 | 24.0 | 2.51 |
| 41 | 23.1 | 3.06 |
| 49 | 22.2 | 3.68 |
| 57 | 21.4 | 4.36 |
| 65 | 20.9 | 4.84 |
| 73 | 20.4 | 5.36 |
| 81 | 20.0 | 5.88 |
| 89 | 19.5 | 6.40 |
| 97 | 19.3 | 6.77 |
| 105 | 18.7 | 7.53 |
| 113 | 18.4 | 8.03 |

TABLE 4.6.6. Dissolution Data of $AgIO_3$ at pH=1.5 ($3.2 \times 10^{-2}$ M $HNO_3$) at $25^oC$

Calibration Function: $\log C = -3.417 - 0.097\ N_d$

| Time, t (sec) | Number of Divisions on Recorder Output, $N_d$ | Concentration of $AgIO_3$, C, ($M \times 10^6$) |
|---|---|---|
| 17 | 26.8 | 0.96 |
| 25 | 23.9 | 1.85 |
| 33 | 22.1 | 2.77 |
| 41 | 20.7 | 3.80 |
| 49 | 19.7 | 4.73 |
| 57 | 19.0 | 5.55 |
| 65 | 18.4 | 6.34 |
| 73 | 17.9 | 7.05 |
| 81 | 17.5 | 7.75 |
| 89 | 17.2 | 8.26 |
| 97 | 16.9 | 8.83 |
| 105 | 16.6 | 9.48 |
| 113 | 16.3 | 10.03 |

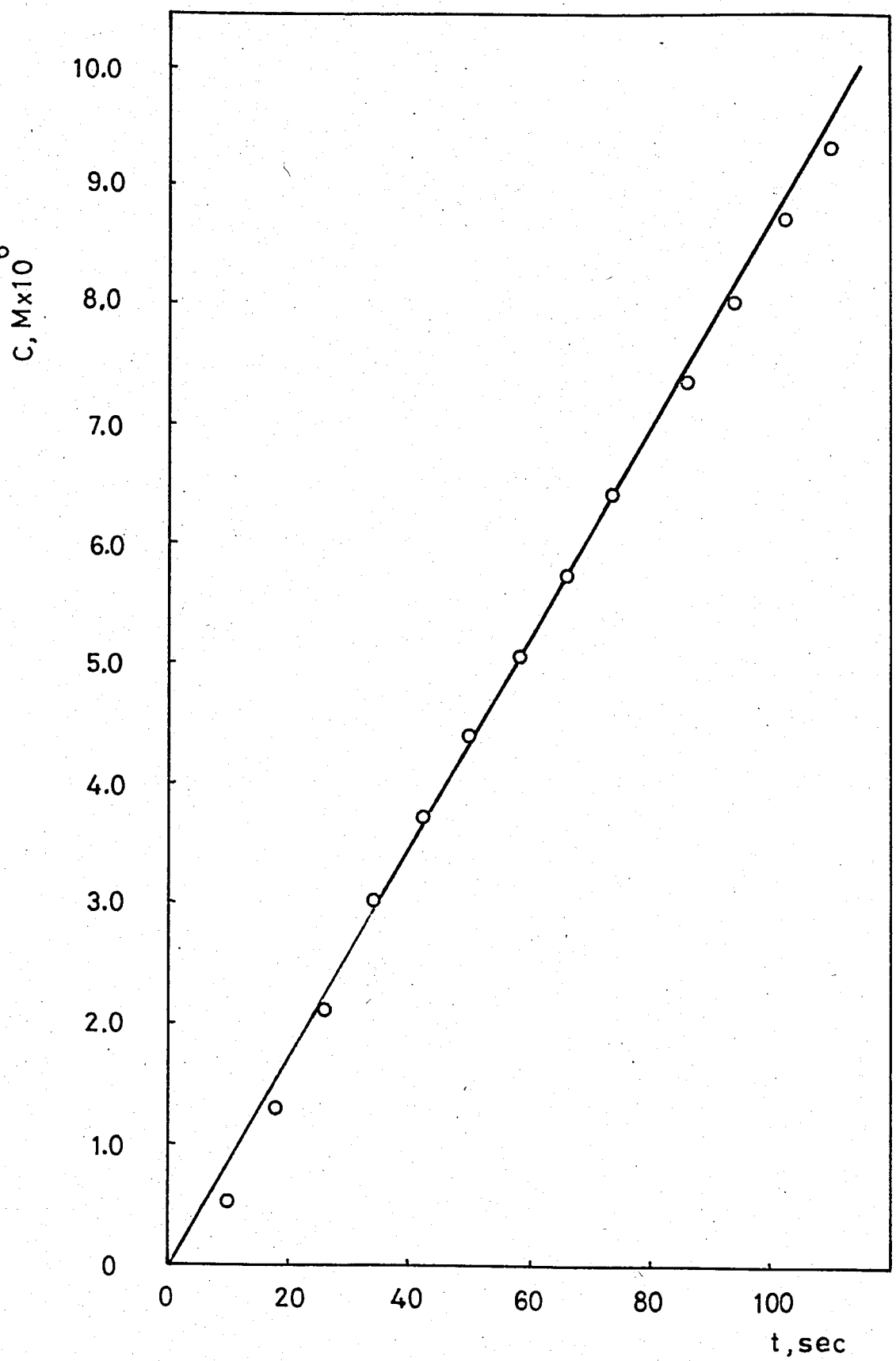


FIGURE 4.6.1. C v.s t Plot for the Dissolution of $AgIO_3$ at pH = 6.0 at 25°C.

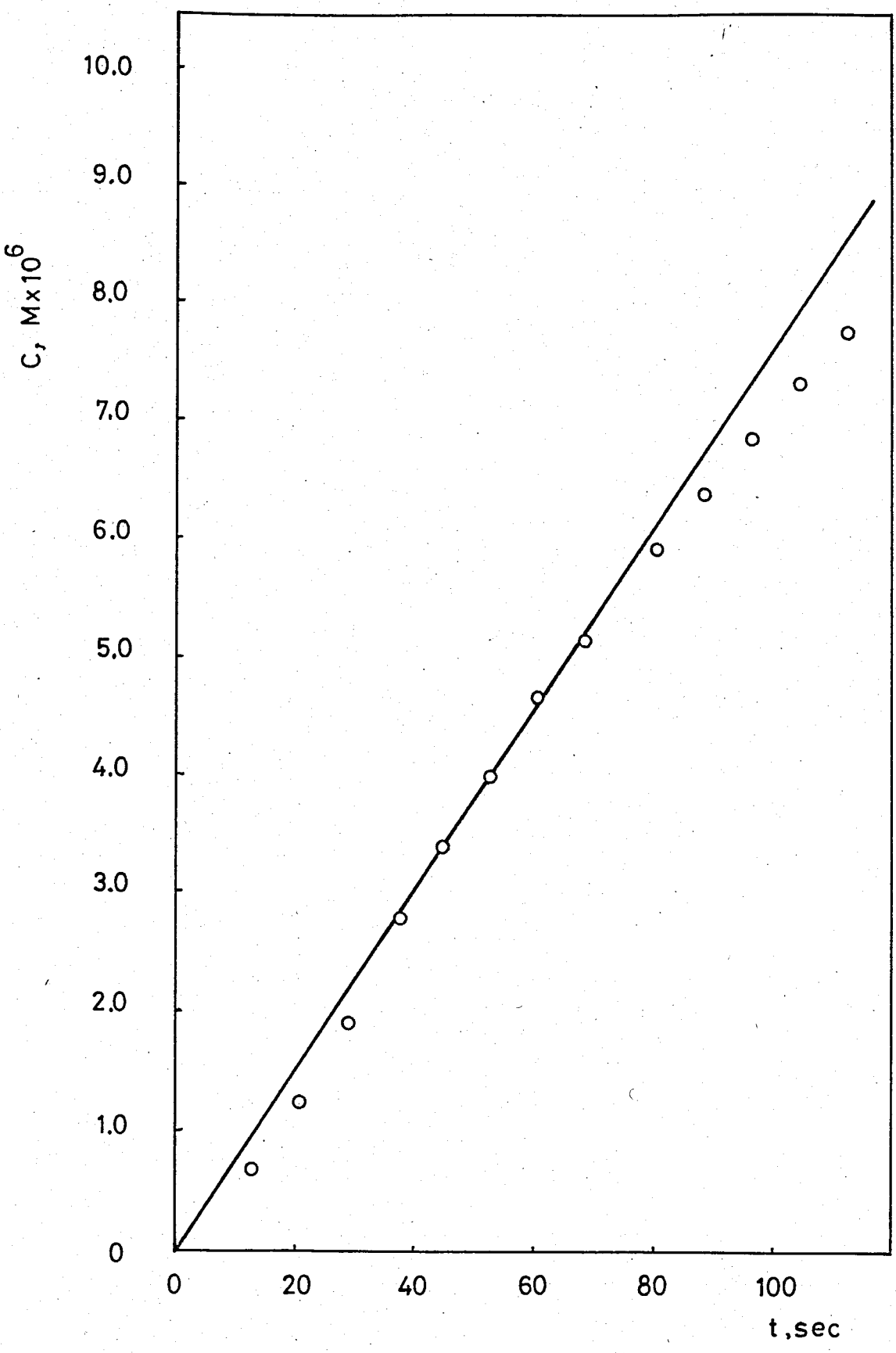


FIGURE 4.6.2. C v.s t Plot for the Dissolution of $AgIO_3$ at pH = 5.0 at 25°C.

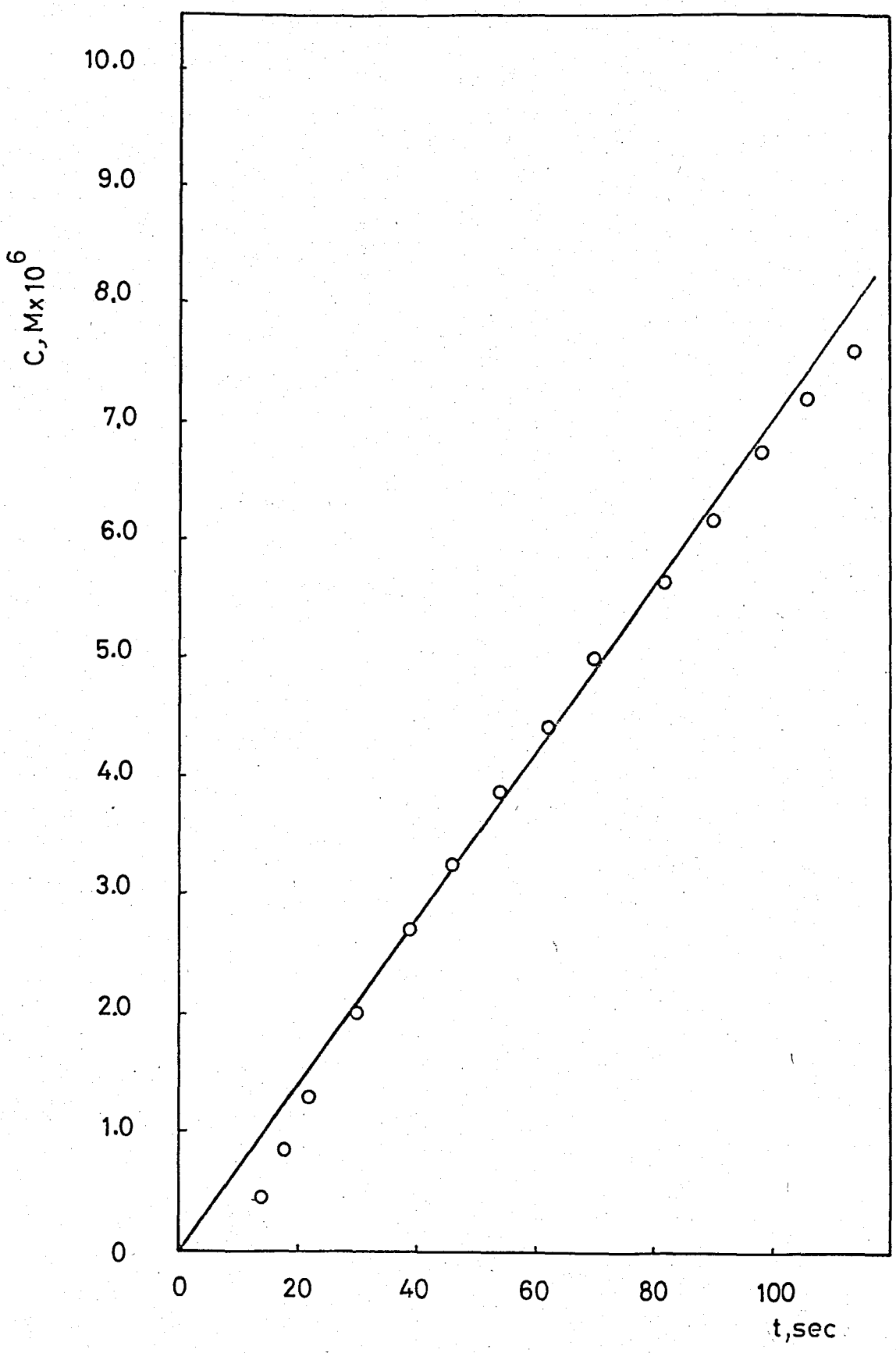


FIGURE 4.6.3. C v.s t Plot for the Dissolution of $AgIO_3$ at pH = 4.1 at 25°C.

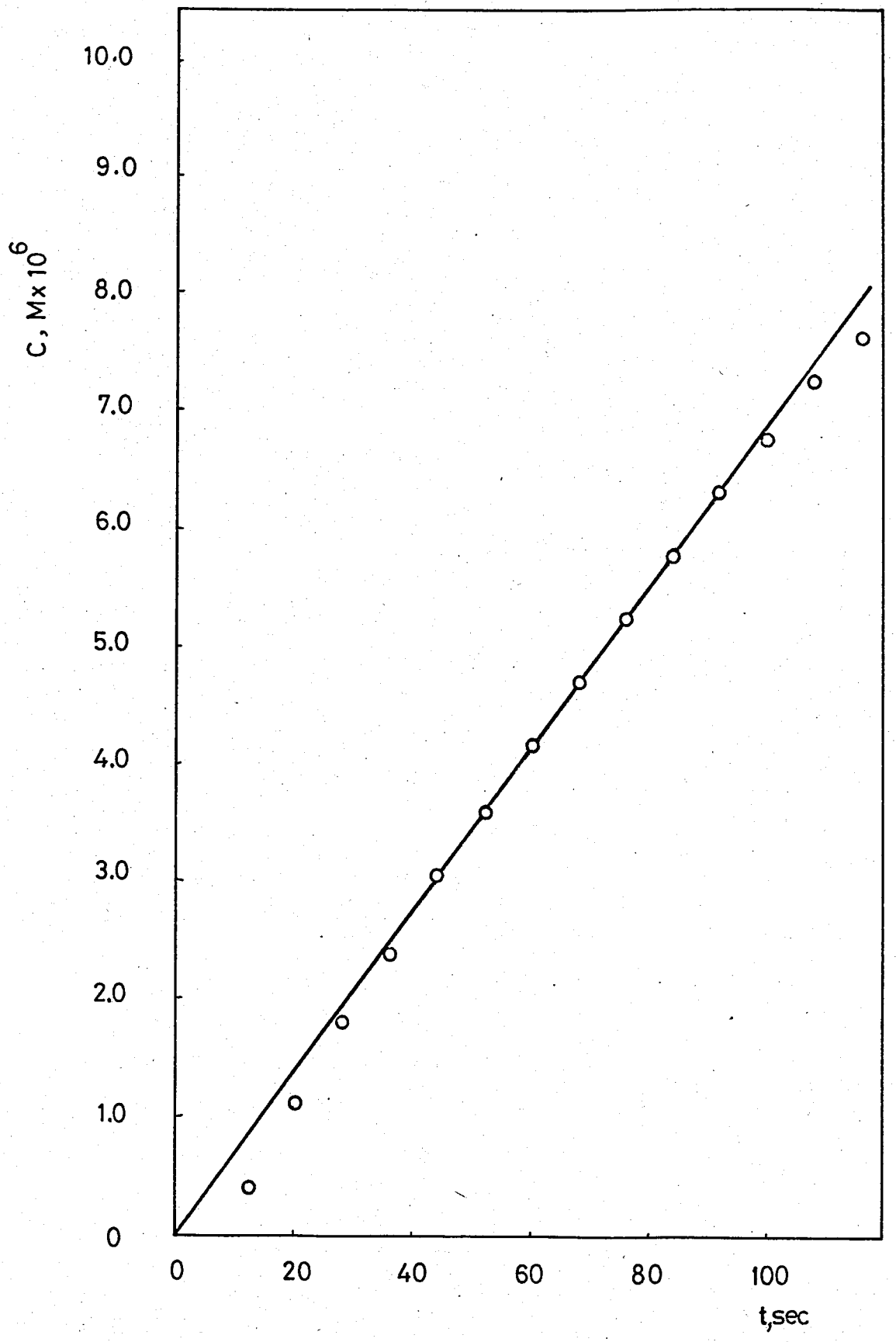


FIGURE 4.6.4. C v.s t Plot for the Dissolution of $AgIO_3$ at pH = 3.1 at 25°C

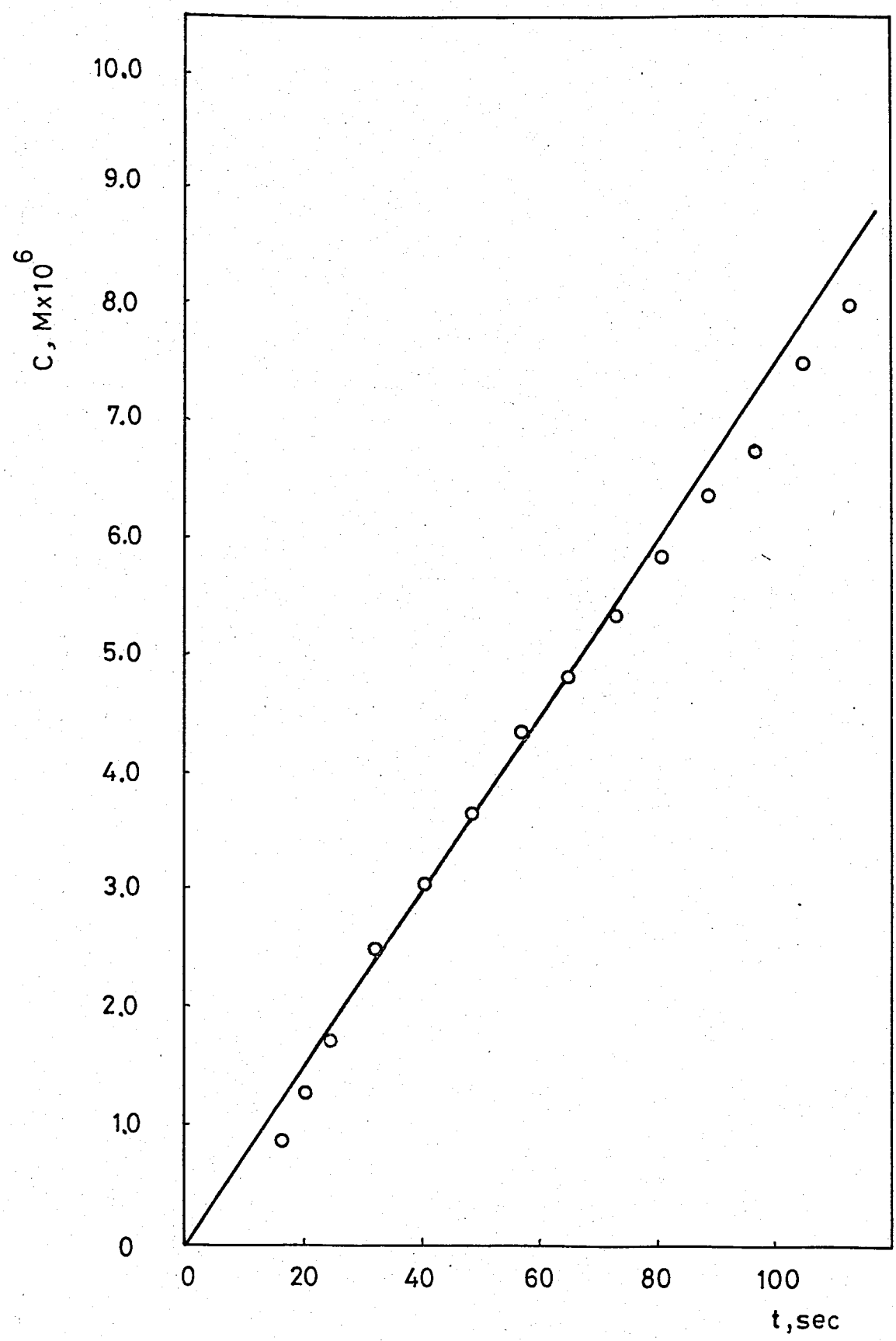


FIGURE 4.6.5. C v.s t Plot for the Dissolution of $AgIO_3$ at pH = 2.2 at 25°C.

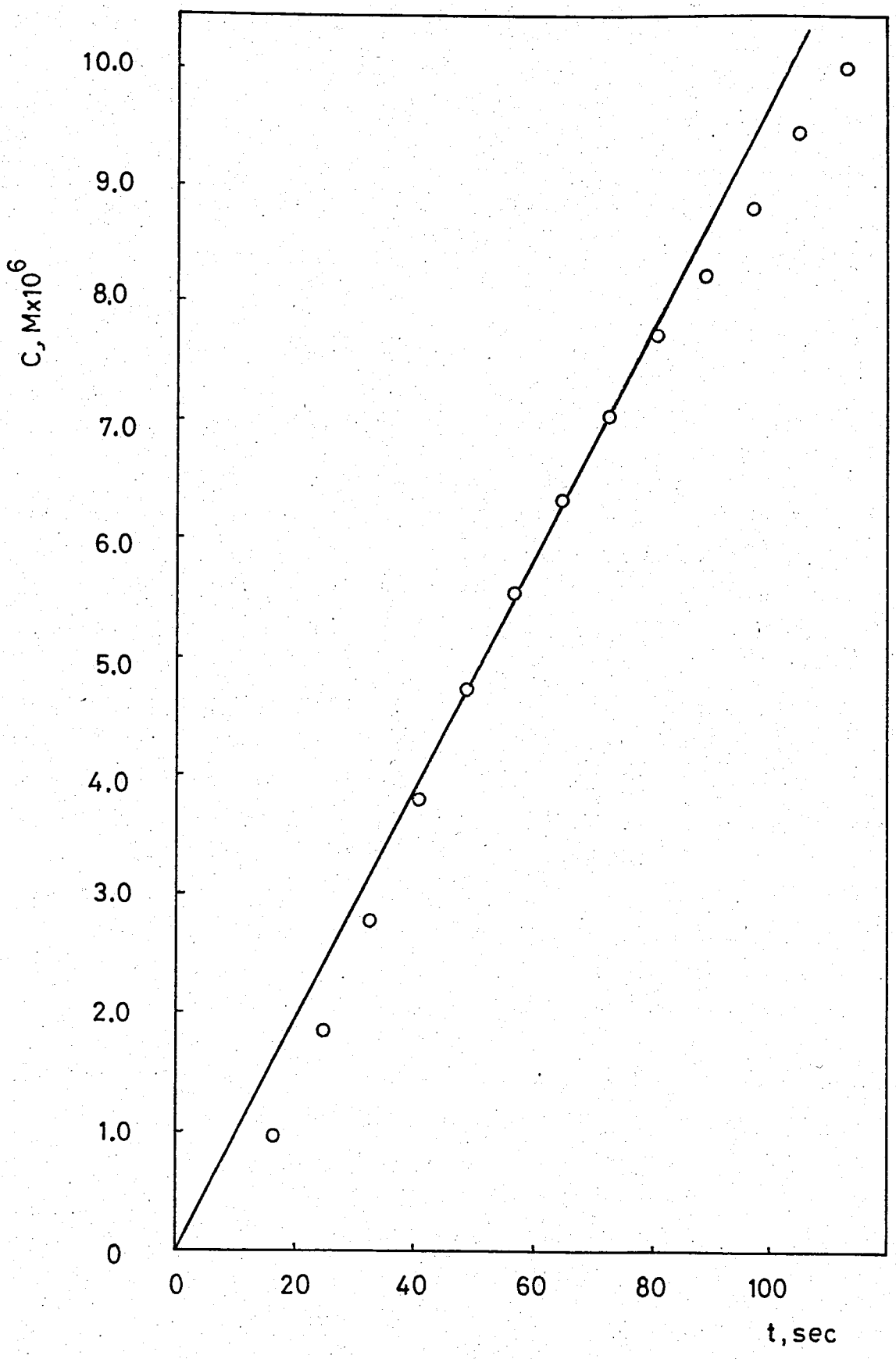


FIGURE 4.6.6. C v.s t Plot for the Dissolution of $AgIO_3$ at pH = 1.5 at 25°C

TABLE 4.6.7. Initial Dissolution Rates of $AgIO_3$ Acidic Media at 25°C

| pH | Initial Dissolution Rate, $R_d$, (mol $sec^{-1}gr^{-1}$)x$10^6$ |
|---|---|
| 6.0 | 0.89 |
| 5.0 | 0.76 |
| 4.1 | 0.71 |
| 3.1 | 0.68 |
| 2.2 | 0.75 |
| 1.5 | 0.98 |

An investigation of Figure 4.2-a shows that rate of dissolution drops by approximately 40 per cent from its value in distilled water up to a pH of about 4.0, and then remains constant till a pH of nearly 2.5 is reached. In terms of the theory this means that as pH decreases more and more $H^+$ ions enter into the region between the solid surface and energy barriers thus causing a continuous drop in rate to an asymptotic value. A comparison of this curve with that corresponding to the dissolution of $AgIO_3$ in $KNO_3$ media (Figure 4.1-a) shows that the per cent drops in rate are very close to each other meaning that the extents of $K^+$ and $H^+$ penetrations into the region between the solid surface and energy barriers are nearly equal. One would expect, however, that $H^+$ ions should exist in much less concentration compared to $K^+$ ions because of the larger hydrated radii of $H^+$ ions, and accordingly a much lesser drop in rate in acidic media (as is already known, the hydrated radii are greater for ions of smaller radii). The experimental observation may be explained on the basis of the already known unique mobility of unhydrated $H^+$ ions (protons). The hydrogen ions have an abnormally high mobility compared to other ions and this behavior is explained by a proton transfer mechanism through successive $H_2O$ molecules. The proton transfer picture of $H^+$ ions, thus, plays an important role in the $H^+$ ion incorporation into the region between the surface and energy barriers.

Around a pH of 2.5, the dissolution rate starts to increase towards its value in distilled water as in $KNO_3$ media, most probably because of the same reasons given in Section 4.2.

Finally a comparison of the results of dissolution experiments in acidic media and $Al_2(SO_4)_3$ media was made. For this purpose, the pH's of the $Al_2(SO_4)_3$ solutions given in Table 4.3.6 were measured and the initial dissolution rates at these pH's were found from Figure 4.2-a. Then these rates were compared with those in Table 4.3.6. The following table (Table 4.6.8) shows the differences between the two cases.

TABLE 4.6.8. Comparison of the Initial Dissolution Rates in $Al_2(SO_4)_3$ and Acidic Media

| Ionic Strength of $Al_2(SO_4)_3$ Solution | pH of $Al_2(SO_4)_3$ Solution | Initial Dissolution Rate in $Al_2(SO_4)_3$ Media, $R_d$ (mol $sec^{-1}gr^{-1} \times 10^6$ | Initial Dissolution Rate in Acidic Media, $R_d$ (mol $sec^{-1}gr^{-1}) \times 10^6$ |
|---|---|---|---|
| $7.5 \times 10^{-6}$ | 5.8 | 0.92 | 0.85 |
| $7.5 \times 10^{-5}$ | 5.1 | 0.81 | 0.75 |
| $7.5 \times 10^{-4}$ | 4.5 | 0.84 | 0.71 |
| $7.5 \times 10^{-3}$ | 3.9 | 0.78 | 0.70 |
| $7.5 \times 10^{-2}$ | 3.4 | 0.84 | 0.69 |

As can be observed from Table 4.6.8, the rates in $Al_2(SO_4)_3$ media are larger than those in acidic media at the same pH values. This is due to the difference in the nature of the electrical double layer in the two cases. The double layer behaves as a Gouy layer for the dissolution in acidic media whereas it is a combination of the Gouy and Stern layers for the dissolution in $Al_2(SO_4)_3$ media as explained previously.

## 4.7. DISSOLUTION OF $Al^{3+}$ ADSORBED $AgIO_3$ IN ACIDIC MEDIA

To investigate the effect of pH on the dissolution of $Al^{3+}$ adsorbed $AgIO_3$, experiments were carried out in solutions having pH's between 1.5 and 6.0. The results of these experiments are given in Tables 4.7.1 through 4.7.6 (the calibration data for each pH is given in Table A.2.3). The C v.s t data for the dissolution of $Al^{3+}$ adsorbed $AgIO_3$ in acidic media are plotted in Figures 4.7.1 through 4.7.6.

The initial rates of dissolution of $Al^{3+}$ adsorbed $AgIO_3$ in acidic media were calculated from the initial slopes of the corresponding C v.s t plots. These rates are tabulated in Table 4.7.7. The data of Table 4.7.7 are plotted in Figure 4.2-b.

TABLE 4.7.1. Dissolution Data of $Al^{3+}$ Adsorbed $AgIO_3$ at pH= 6.0 ($2.5 \times 10^{-7}$ M $CH_3COOH$) at 25°C

Calibration Function: $\log C = -3.747 - 0.0875\ N_d$

| Time, t (sec) | Number of Divisions on Recorder Output, $N_d$ | Concentration of $AgIO_3$, C, ($M \times 10^6$) |
|---|---|---|
| 14 | 26.2 | 0.92 |
| 22 | 23.1 | 1.71 |
| 30 | 21.1 | 2.57 |
| 38 | 19.8 | 3.34 |
| 46 | 18.5 | 4.28 |
| 54 | 17.7 | 5.03 |
| 62 | 17.1 | 5.77 |
| 70 | 16.5 | 6.48 |
| 78 | 16.0 | 7.10 |
| 86 | 15.6 | 7.80 |
| 94 | 15.1 | 8.49 |
| 102 | 14.6 | 9.22 |
| 110 | 14.2 | 9.96 |

TABLE 4.7.2. Dissolution Data of $Al^{3+}$ Adsorbed $AgIO_3$ at pH = 5.0 ($4.2 \times 10^{-6}$ M $CH_3COOH$) at 25°C

Calibration Function: $\log C = -3.764 - 0.0894\ N_d$

| Time, t (sec) | Number of Divisions on Recorder Output, $N_d$ | Concentration of $AgIO_3$, C, ($M \times 10^6$) |
|---|---|---|
| 10 | 28.3 | 0.51 |
| 18 | 24.4 | 1.13 |
| 26 | 21.9 | 1.88 |
| 34 | 20.0 | 2.83 |
| 42 | 18.9 | 3.54 |
| 50 | 18.2 | 4.09 |
| 58 | 17.4 | 4.80 |
| 66 | 16.7 | 5.48 |
| 74 | 16.2 | 6.06 |
| 82 | 15.8 | 6.65 |
| 90 | 15.4 | 7.24 |
| 98 | 15.0 | 7.87 |
| 106 | 14.6 | 8.44 |
| 114 | 14.3 | 9.02 |

TABLE 4.7.3. Dissolution Data of $Al^{3+}$ Adsorbed $AgIO_3$ at pH = 4.1 ($4.2 \times 10^{-4}$ M $CH_3COOH$) at 25°C

Calibration Function: $\log C = -4.022 - 0.0733\ N_d$

| Time, t (sec) | Number of Divisions on Recorder Output, $N_d$ | Concentration of $AgIO_3$, C, ($M \times 10^6$) |
|---|---|---|
| 12 | 30.3 | 0.57 |
| 20 | 25.7 | 1.25 |
| 28 | 22.8 | 2.02 |
| 36 | 21.1 | 2.71 |
| 44 | 19.9 | 3.29 |
| 52 | 18.9 | 3.91 |
| 60 | 18.1 | 4.51 |
| 72 | 17.0 | 5.40 |
| 80 | 16.4 | 5.96 |
| 88 | 15.9 | 6.49 |
| 96 | 15.4 | 7.03 |
| 104 | 15.0 | 7.62 |
| 112 | 14.6 | 8.07 |

TABLE 4.7.4. Dissolution Data of $Al^{3+}$ Adsorbed $AgIO_3$ at pH=3.1 ($3.4 \times 10^{-2}$ M $CH_3COOH$)

Calibration Function: $\log C = -3.994 - 0.083\ N_d$

| Time, t (sec) | Number of Divisions on Recorder Output, $N_d$ | Concentration of $AgIO_3$, C, ($M \times 10^6$) |
|---|---|---|
| 16 | 25.0 | 0.86 |
| 24 | 22.0 | 1.51 |
| 32 | 20.0 | 2.21 |
| 40 | 18.5 | 2.93 |
| 48 | 17.5 | 3.60 |
| 56 | 16.5 | 4.37 |
| 64 | 15.8 | 4.99 |
| 76 | 14.9 | 5.90 |
| 84 | 14.3 | 6.55 |
| 92 | 13.9 | 7.13 |
| 100 | 13.5 | 7.61 |
| 108 | 13.2 | 8.12 |
| 116 | 12.9 | 8.56 |

TABLE 4.7.5. Dissolution Data of $Al^{3+}$ Adsorbed $AgIO_3$ at pH = 2.2 ($6.4 \times 10^{-3}$ M $HNO_3$) at 25°C

Calibration Function: $\log C = -3.425 - 0.0905\ N_d$

| Time, t (sec) | Number of Divisions on Recorder Output, $N_d$ | Concentration of $AgIO_3$, C, ($M \times 10^6$) |
|---|---|---|
| 14 | 31.2 | 0.54 |
| 18 | 28.4 | 1.01 |
| 22 | 26.7 | 1.44 |
| 30 | 24.5 | 2.27 |
| 38 | 23.4 | 2.89 |
| 46 | 22.5 | 3.48 |
| 54 | 21.7 | 4.11 |
| 62 | 21.1 | 4.62 |
| 74 | 20.4 | 5.35 |
| 82 | 20.0 | 5.83 |
| 90 | 19.5 | 6.42 |
| 98 | 19.2 | 6.93 |
| 106 | 18.8 | 7.46 |
| 114 | 18.5 | 7.97 |

TABLE 4.7.6. Dissolution Data of $Al^{3+}$ Adsorbed $AgIO_3$ at pH = 1.5 ($3.2 \times 10^{-2}$ M $HNO_3$) at 25°C

Calibration Function: $\log C = -3.417 - 0.097\ N_d$

| Time, t (sec) | Number of Divisions on Recorder Output, $N_d$ | Concentration of $AgIO_3$, C, ($M \times 10^6$) |
|---|---|---|
| 12 | 30.8 | 0.40 |
| 20 | 25.6 | 1.26 |
| 28 | 23.5 | 2.04 |
| 36 | 21.7 | 3.00 |
| 44 | 20.4 | 4.05 |
| 52 | 19.7 | 4.75 |
| 60 | 19.0 | 5.52 |
| 68 | 18.4 | 6.25 |
| 76 | 18.0 | 6.94 |
| 84 | 17.6 | 7.60 |
| 92 | 17.2 | 8.30 |
| 100 | 16.9 | 8.87 |
| 108 | 16.6 | 9.46 |
| 116 | 16.4 | 9.86 |

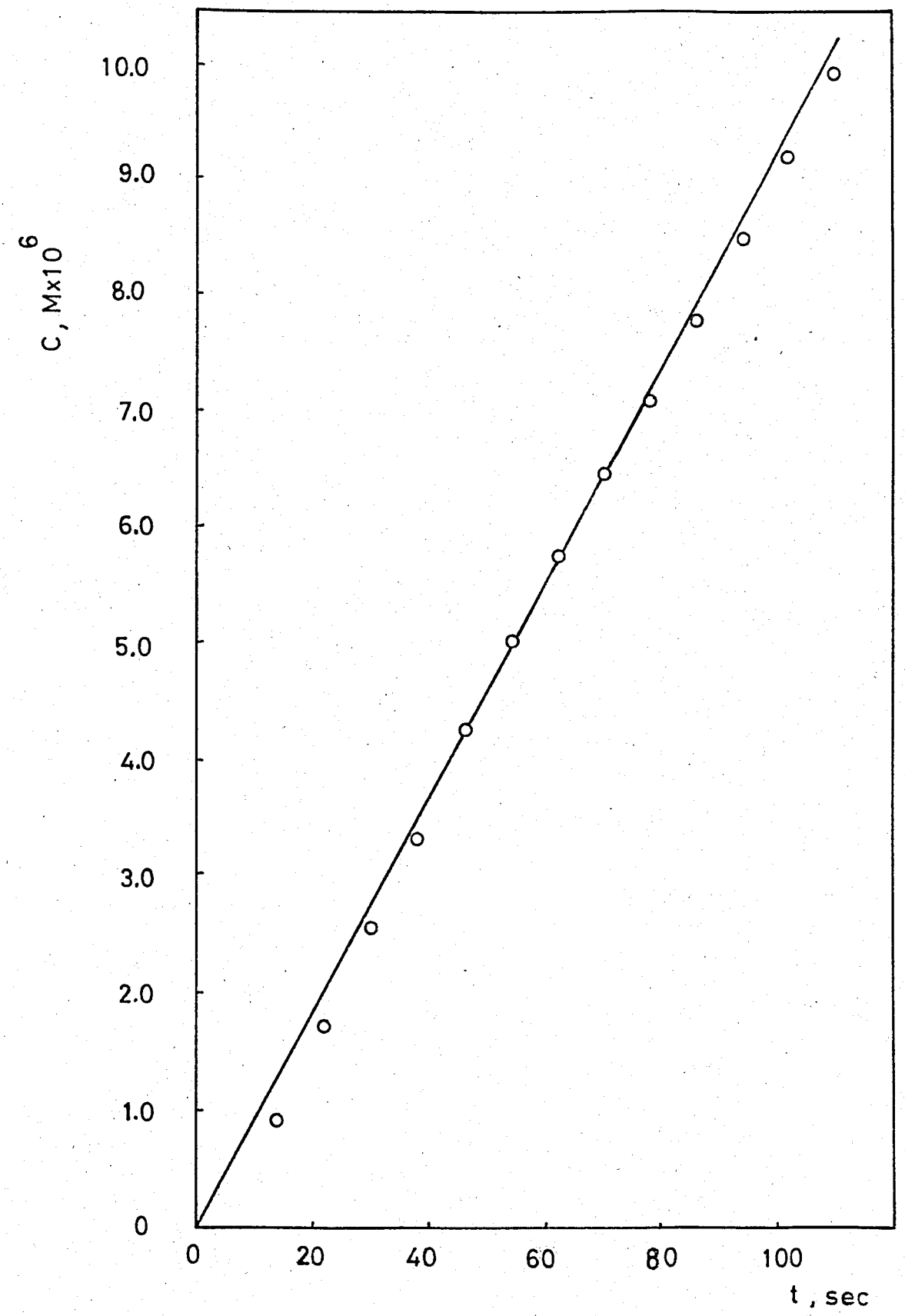


FIGURE 4.7.1. C v.s t Plot for the Dissolution of $Al^{3+}$ Adsorbed $AgIO_3$ at pH = 6.0 at 25°C.

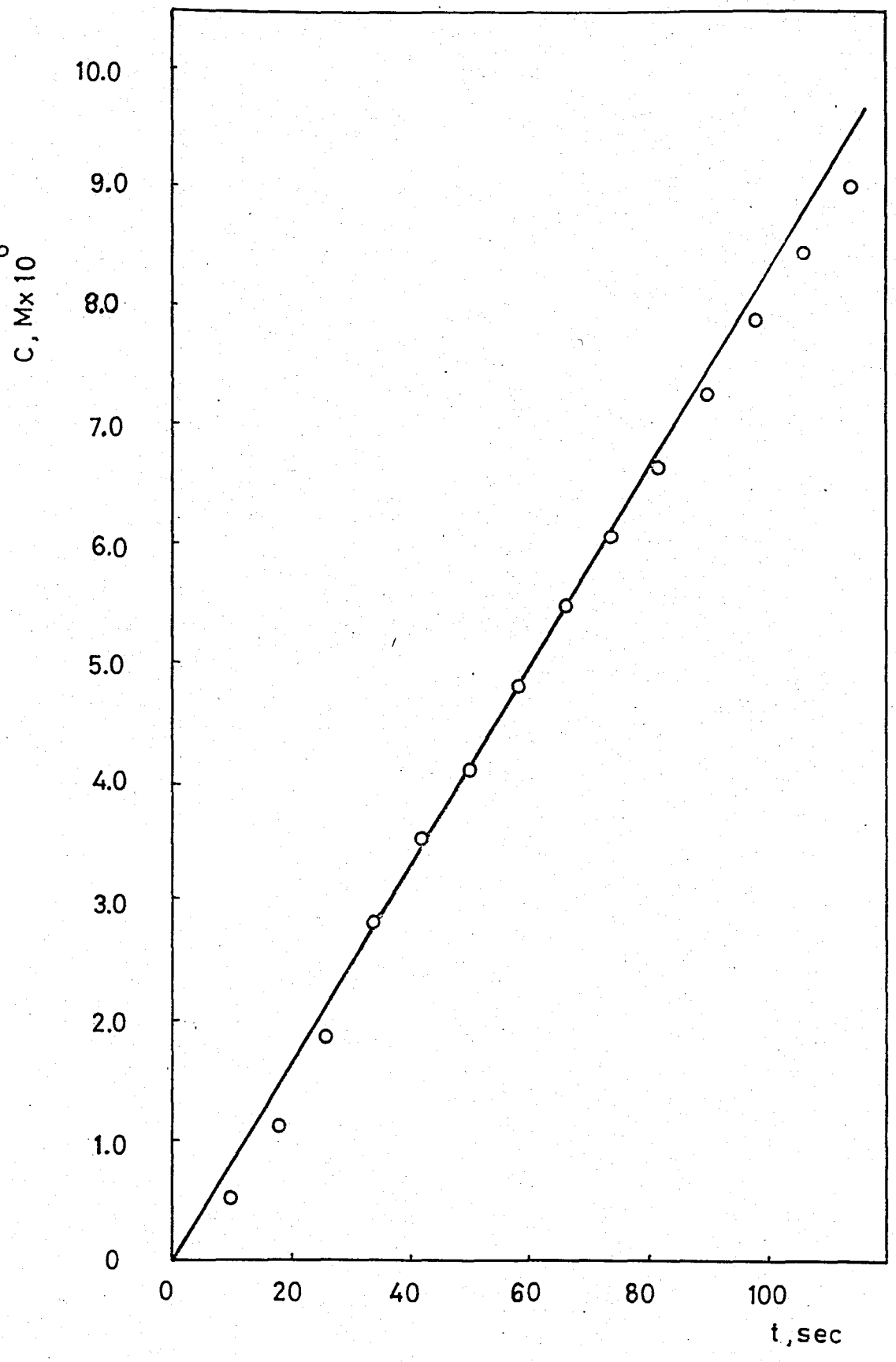


FIGURE 4.7.2. C v.s t Plot for the Dissolution of $Al^{3+}$ Adsorbed $AgIO_3$ at pH=5.0 at 25°C.

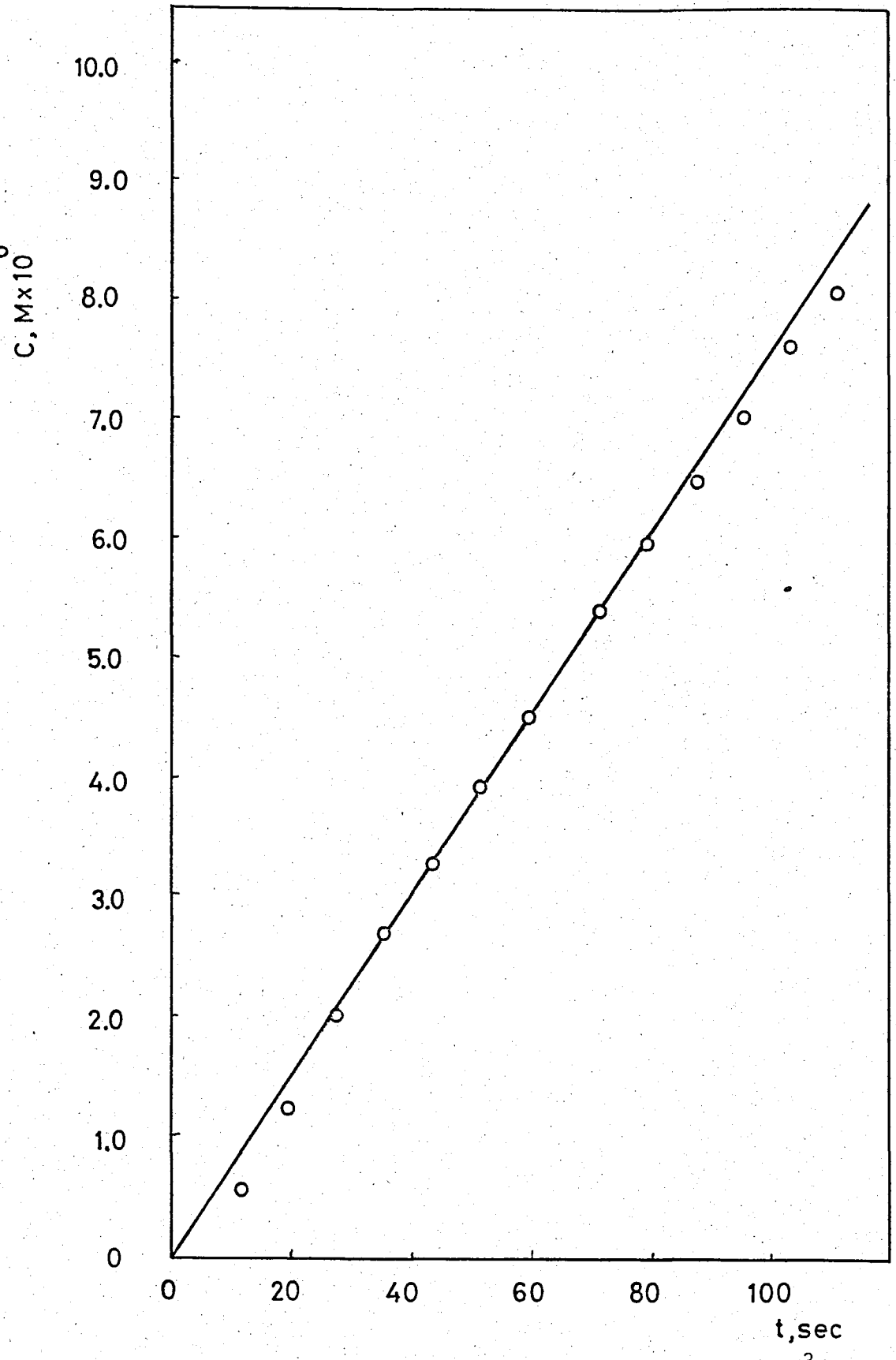


FIGURE 4.7.3. C v.s t Plot for the Dissolution of $Al^{3+}$ Adsorbed $AgIO_3$ at pH=4.1 at 25°C.

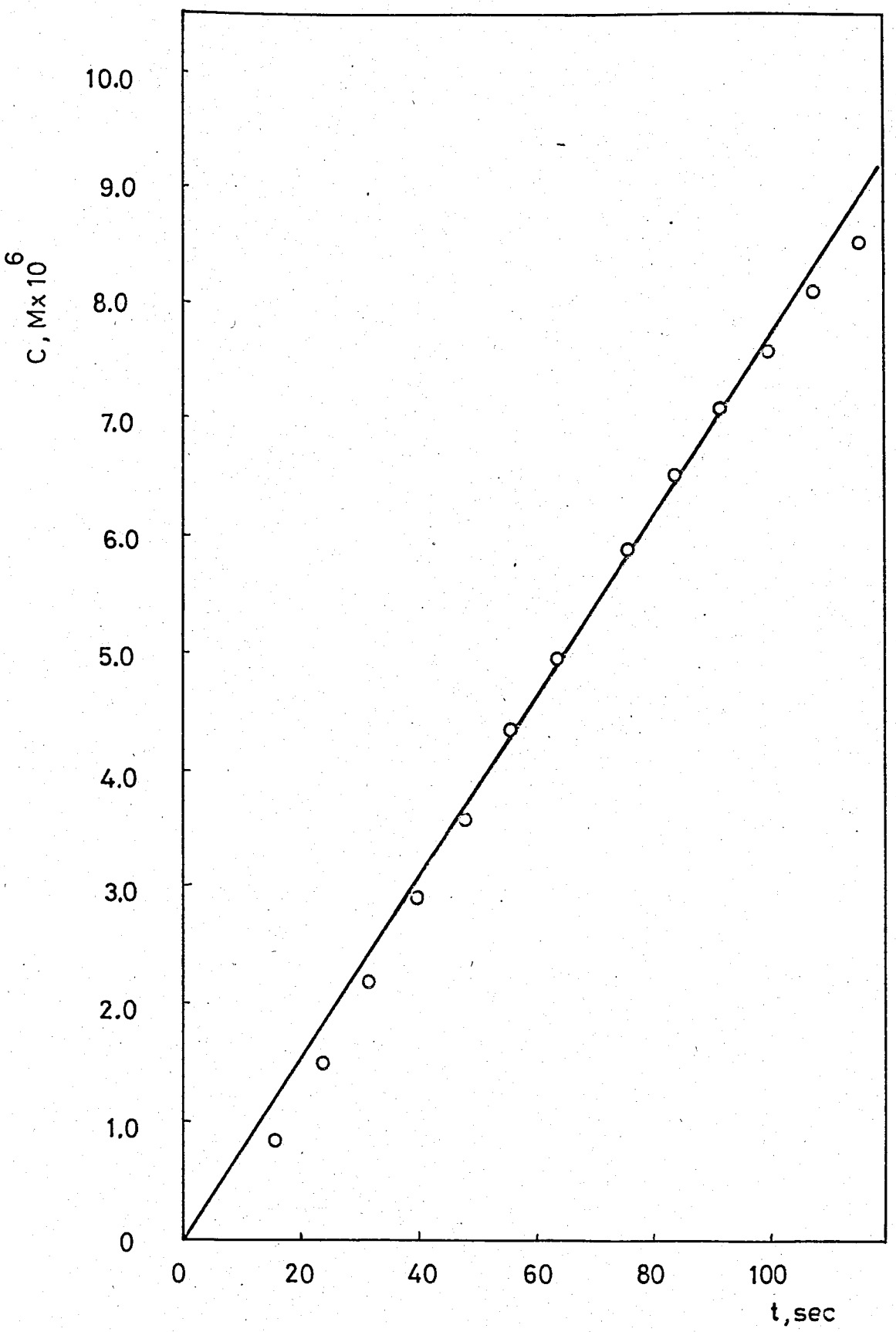


FIGURE 4.7.4. C v.s t Plot for the Dissolution of $Al^{3+}$ Adsorbed $AgIO_3$ at pH=3.1 at 25°C.

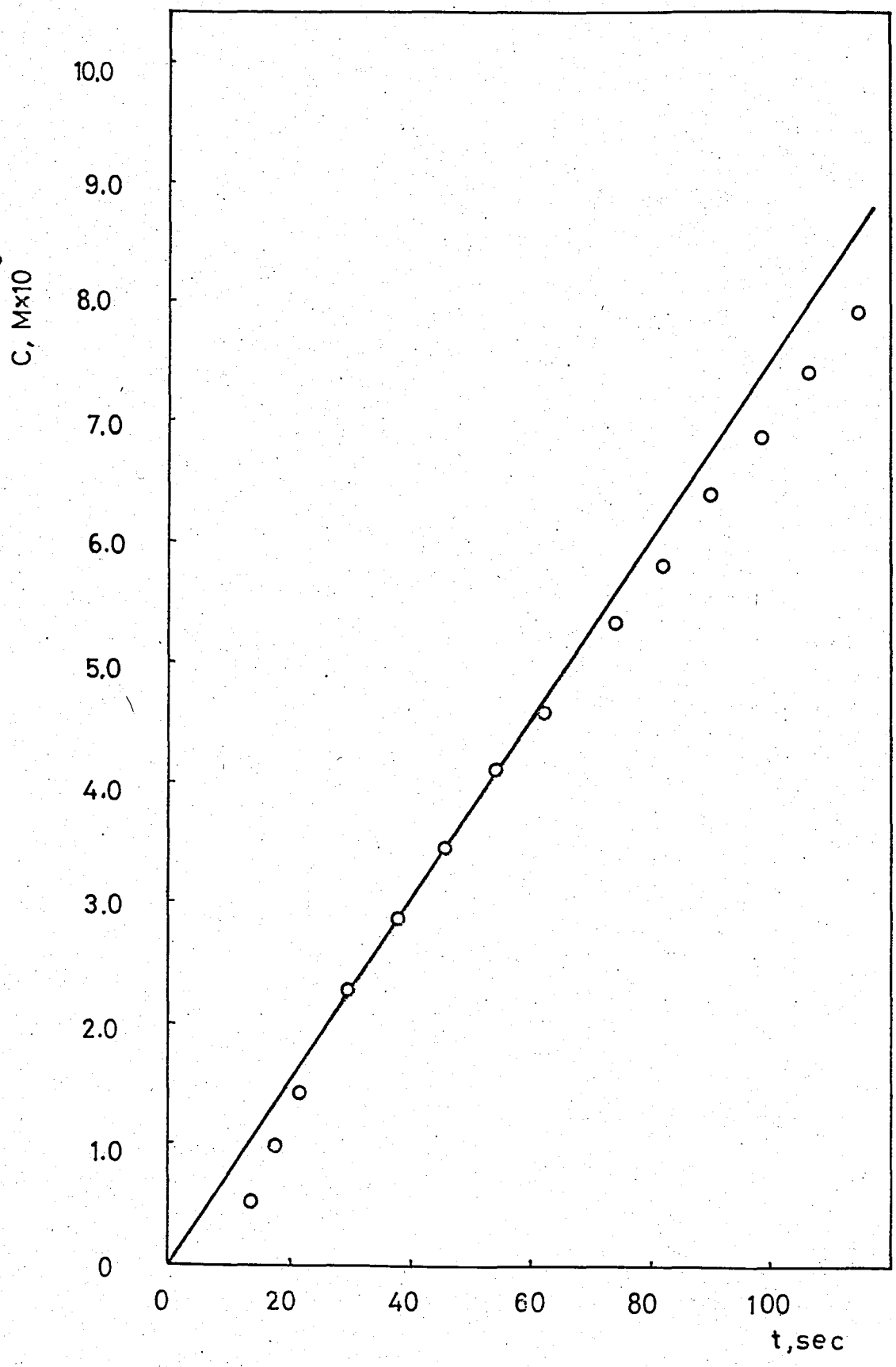


FIGURE 4.7.5. C v.s t Plot for the Dissolution of $Al^{3+}$ Adsorbed $AgIO_3$ at pH=2.2 at 25°C.

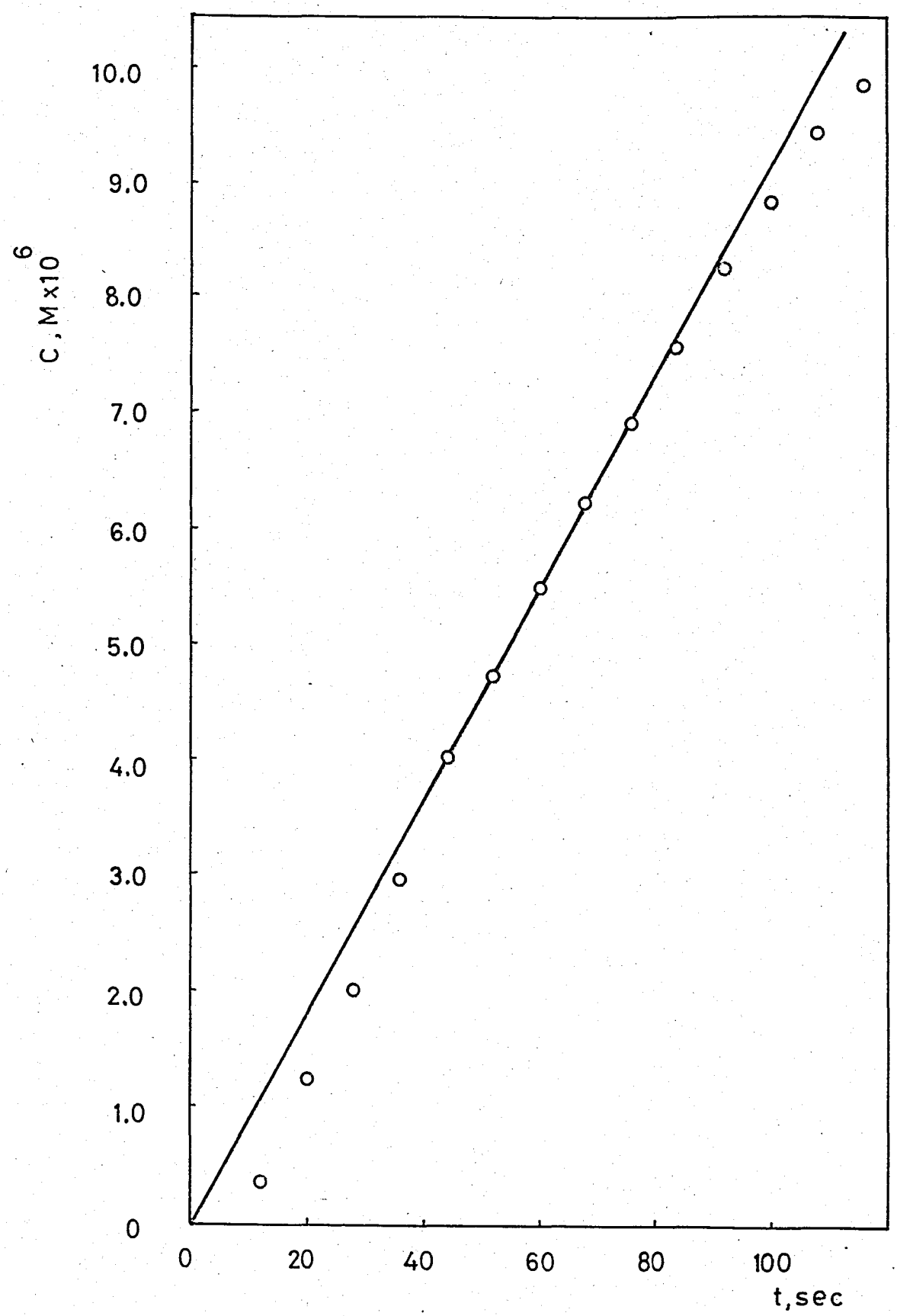


FIGURE 4.7.6. C v.s t Plot for the Dissolution of $Al^{3+}$ Adsorbed $AgIO_3$ at pH=1.5 at 25°C.

TABLE 4.7.7. Initial Dissolution Rates of $Al^{3+}$ Adsorbed $AgIO_3$ in Acidic Media at 25°C

| pH | Initial Dissolution Rate $R_d$, (mol $sec^{-1} gr^{-1}$) x $10^6$ |
|---|---|
| 6.0 | 0.93 |
| 5.0 | 0.83 |
| 4.1 | 0.75 |
| 3.1 | 0.78 |
| 2.2 | 0.76 |
| 1.5 | 0.92 |

From Figure 4.2-b, it can be seen that rate of dissolution decreases by approximately 32 per cent up to a pH of 4.0 and remains constant till a pH of 2.0. A comparison of this curve with that corresponding to dissolution of $Al^{3+}$ adsorbed $AgIO_3$ in $KNO_3$ media shows that although the penetration of $K^+$ ions into the Stern layer produced by adsorbed $Al^{3+}$ ions is not possible, $H^+$ ions can easily penetrate there thus causing a considerable drop in rate. If hydrated $H^+$ ions were responsible for the dissolution mechanism, the penetration of these ions into the Stern layer would be impossible because of the greater size of the hydrated $H^+$ ions compared to hydrated $K^+$ ions, and as a result dissolution rate would be unchanged irrespective of the pH values of the solutions. The appearance of a significant rate drop in acidic media can be explained on the basis of the proton nature of $H^+$ ions. As protons, the entrance of a considerable amount of $H^+$ ions into the Stern layer formed by adsorbed $Al^{3+}$ is expected thus causing the dissolution rate to decrease to an asymptotic value.

A comparison of the rate v.s pH plots for the dissolution of $AgIO_3$ and $Al^{3+}$ adsorbed $AgIO_3$ in acidic media reveals the fact that the per cent drop in rate in the former is larger. This means that, in the latter, the Stern layer formed by $Al^{3+}$ ions somewhat hinders the entrance of $H^+$ ions compared to the case where such a layer is not present. As a

result, the per cent drop in rate for the dissolution of $Al^{3+}$ adsorbed $AgIO_3$ in acidic media is smaller.

At about pH = 2.0, the dissolution rate of $Al^{3+}$ adsorbed $AgIO_3$ starts to increase as in other dissolution systems already discussed. The same reasonings apply here as in other cases.

## 4.8. DISSOLUTION OF $Fe^{3+}$ ADSORBED $AgIO_3$ IN ACIDIC MEDIA

The final set of experiments conducted in acidic media are those of dissolution of $Fe^{3+}$ adsorbed $AgIO_3$. In order to see the effect of pH on the initial dissolution rate of $Fe^{3+}$ adsorbed $AgIO_3$, experiments were carried out with solutions of pH's between 1.5 and 6.0. The results of these experiments are given in Tables 4.8.1 through 4.8.6 (the calibration data for each pH is given in Table A.2.3). The C v.s t data for the dissolution of $Fe^{3+}$ adsorbed $AgIO_3$ in acidic media are plotted in Figures 4.8.1 through 4.8.6.

The initial rates of dissolution of $Fe^{3+}$ adsorbed $AgIO_3$ in acidic media were calculated from the initial slopes of the corresponding C v.s t plots. These rates are tabulated in Table 4.8.7. The data of Table 4.8.7 are plotted in Figure 4.2-c.

TABLE 4.8.1. Dissolution Data of $Fe^{3+}$ Adsorbed $AgIO_3$ at pH=6.0 ($2.5 \times 10^{-7}$ M $CH_3COOH$) at 25°C

Calibration Function: $\log C = -3.747 - 0.0875 N_d$

| Time, t (sec) | Number of Divisions on Recorder Output, $N_d$ | Concentration of $AgIO_3$, C, ($M \times 10^6$) |
|---|---|---|
| 13 | 27.7 | 0.67 |
| 17 | 25.9 | 0.97 |
| 21 | 24.3 | 1.34 |
| 29 | 22.7 | 1.85 |
| 37 | 21.4 | 2.40 |
| 45 | 20.2 | 3.04 |
| 53 | 19.4 | 3.58 |
| 61 | 18.2 | 4.11 |
| 69 | 18.1 | 4.62 |
| 77 | 17.7 | 5.07 |
| 85 | 17.2 | 5.56 |
| 93 | 16.8 | 6.08 |
| 101 | 16.5 | 6.51 |

TABLE 4.8.2. Dissolution Data of $Fe^{3+}$ Adsorbed $AgIO_3$ at pH=5.0 ($4.2 \times 10^{-6}$ M $CH_3COOH$) at 25°C

Calibration Function: $\log C = -3.764 - 0.0894\ N_d$

| Time, t (sec) | Number of Divisions on Recorder Output, $N_d$ | Concentration of $AgIO_3$, C, ($M \times 10^6$) |
|---|---|---|
| 9 | 31.0 | 0.29 |
| 17 | 25.6 | 0.89 |
| 25 | 23.0 | 1.50 |
| 33 | 21.4 | 2.12 |
| 41 | 19.8 | 2.91 |
| 49 | 19.0 | 3.48 |
| 57 | 18.2 | 4.05 |
| 65 | 17.6 | 4.60 |
| 73 | 17.0 | 5.18 |
| 81 | 16.6 | 5.64 |
| 89 | 16.1 | 6.23 |
| 99 | 15.7 | 6.83 |
| 111 | 15.2 | 7.58 |

TABLE 4.8.3. Dissolution Data of $Fe^{3+}$ Adsorbed $AgIO_3$ at pH=4.1 ($4.2 \times 10^{-4}$ M $CH_3COOH$) at 25°C

Calibration Function: $\log C = -4.022 - 0.0733\ N_d$

| Time, t (sec) | Number of Divisions on Recorder Output, $N_d$ | Concentration of $AgIO_3$, C, ($M \times 10^6$) |
|---|---|---|
| 8 | 36.2 | 0.21 |
| 16 | 28.8 | 0.74 |
| 24 | 24.9 | 1.43 |
| 32 | 22.3 | 2.21 |
| 40 | 21.0 | 2.76 |
| 48 | 19.9 | 3.31 |
| 56 | 19.0 | 3.82 |
| 64 | 18.3 | 4.32 |
| 72 | 17.7 | 4.83 |
| 80 | 17.0 | 5.37 |
| 88 | 16.5 | 5.88 |
| 96 | 16.0 | 6.39 |
| 104 | 15.6 | 6.79 |

TABLE 4.8.4. Dissolution Data of $Fe^{3+}$ Adsorbed $AgIO_3$ at pH = 3.1 ($3.4 \times 10^{-2}$ M $CH_3COOH$) at 25°C

Calibration Function: $\log C = -3.994 - 0.083\ N_d$

| Time, t (sec) | Number of Divisions on Recorder Output, $N_d$ | Concentration of $AgIO_3$, C, ($M \times 10^6$) |
|---|---|---|
| 14 | 26.7 | 0.62 |
| 18 | 24.5 | 0.94 |
| 26 | 21.8 | 1.56 |
| 34 | 20.0 | 2.23 |
| 42 | 18.7 | 2.84 |
| 50 | 17.5 | 3.55 |
| 58 | 16.8 | 4.11 |
| 66 | 16.1 | 4.69 |
| 74 | 15.5 | 5.24 |
| 82 | 15.0 | 5.78 |
| 90 | 14.6 | 6.24 |
| 98 | 14.2 | 6.70 |
| 106 | 13.8 | 7.21 |
| 120 | 13.3 | 8.02 |

TABLE 4.8.5. Dissolution Data of $Fe^{3+}$ Adsorbed $AgIO_3$ at pH = 2.2 ($6.4 \times 10^{-3}$ M $HNO_3$) at 25°C

Calibration Function: $\log C = -3.425 - 0,0905\ N_d$

| Time, t (sec) | Number of Divisions on Recorder Output, $N_d$ | Concentration of $AgIO_3$, C, ($M \times 10^6$) |
|---|---|---|
| 17 | 28.3 | 1.03 |
| 25 | 25.7 | 1.77 |
| 33 | 23.9 | 2.58 |
| 41 | 22.9 | 3.21 |
| 49 | 21.9 | 3.89 |
| 57 | 21.2 | 4.50 |
| 65 | 20.7 | 4.98 |
| 73 | 20.2 | 5.55 |
| 81 | 19.8 | 6.08 |
| 89 | 19.3 | 6.68 |
| 97 | 19.0 | 7.12 |
| 105 | 18.6 | 7.73 |
| 113 | 18.4 | 8.18 |

TABLE 4.8.6. Dissolution Data of $Fe^{3+}$ Adsorbed $AgIO_3$ at pH=1.5 ($3.2 \times 10^{-2}$ M $HNO_3$)

Calibration Function: $\log C = -3.417 - 0.097\ N_d$

| Time, t (sec) | Number of Divisions on Recorder Output, $N_d$ | Concentration of $AgIO_3$, C, ($M \times 10^6$) |
|---|---|---|
| 18 | 28.0 | 0.74 |
| 26 | 24.4 | 1.65 |
| 34 | 22.6 | 2.46 |
| 42 | 21.2 | 3.37 |
| 50 | 20.1 | 4.30 |
| 58 | 19.4 | 5.02 |
| 66 | 18.9 | 5.70 |
| 74 | 18.4 | 6.38 |
| 82 | 17.9 | 7.00 |
| 90 | 17.5 | 7.66 |
| 98 | 17.2 | 8.26 |
| 106 | 16.9 | 8.77 |
| 114 | 16.7 | 9.31 |

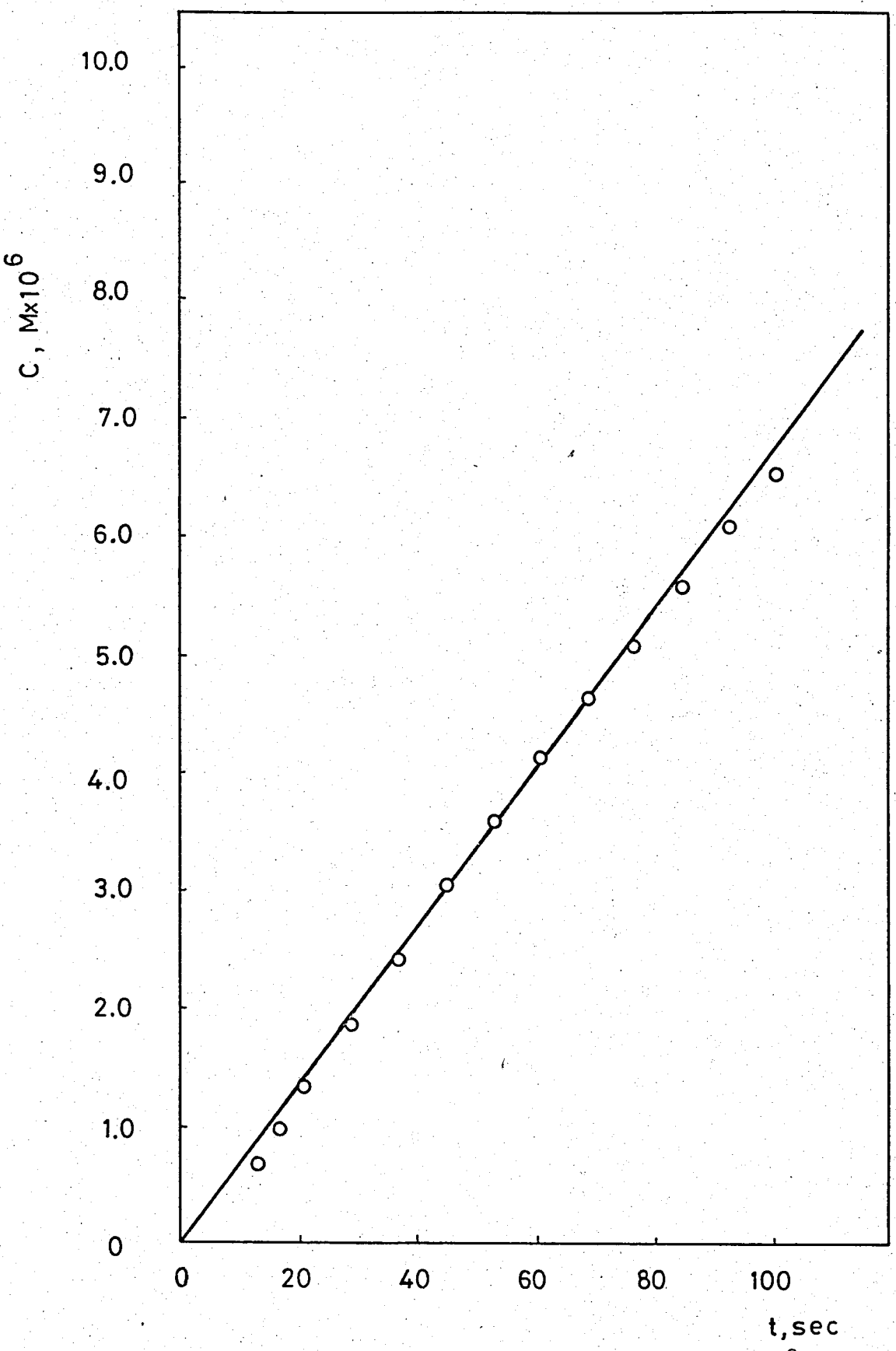


FIGURE 4.8.1. C v.s t Plot for the Dissolution of $Fe^{3+}$ Adsorbed $AgIO_3$ at pH=6.0 at 25°C.

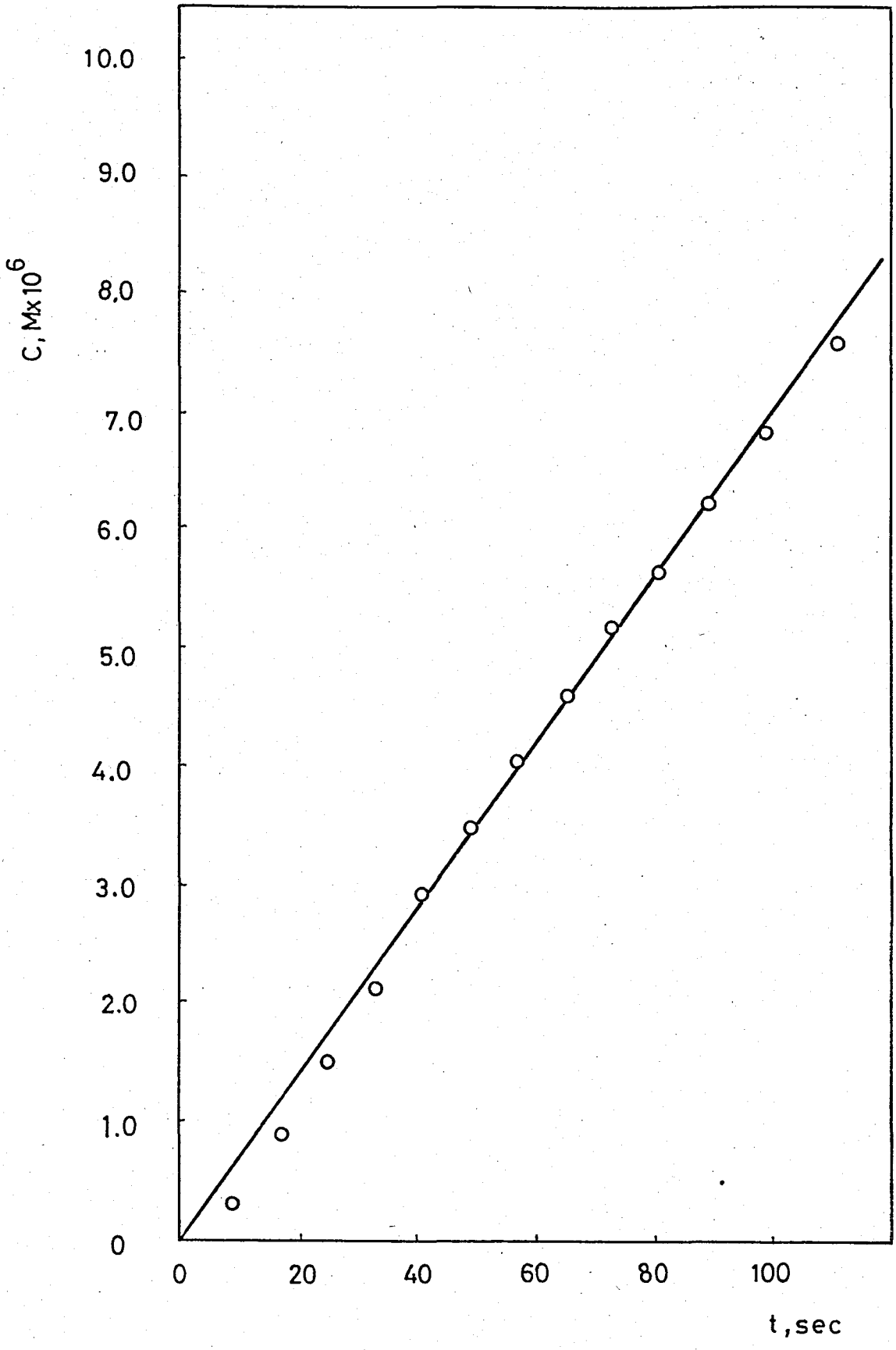


FIGURE 4.8.2. C v.s t Plot for the Dissolution of $Fe^{3+}$ Adsorbed $AgIO_3$ at pH=5.0 at 25°C

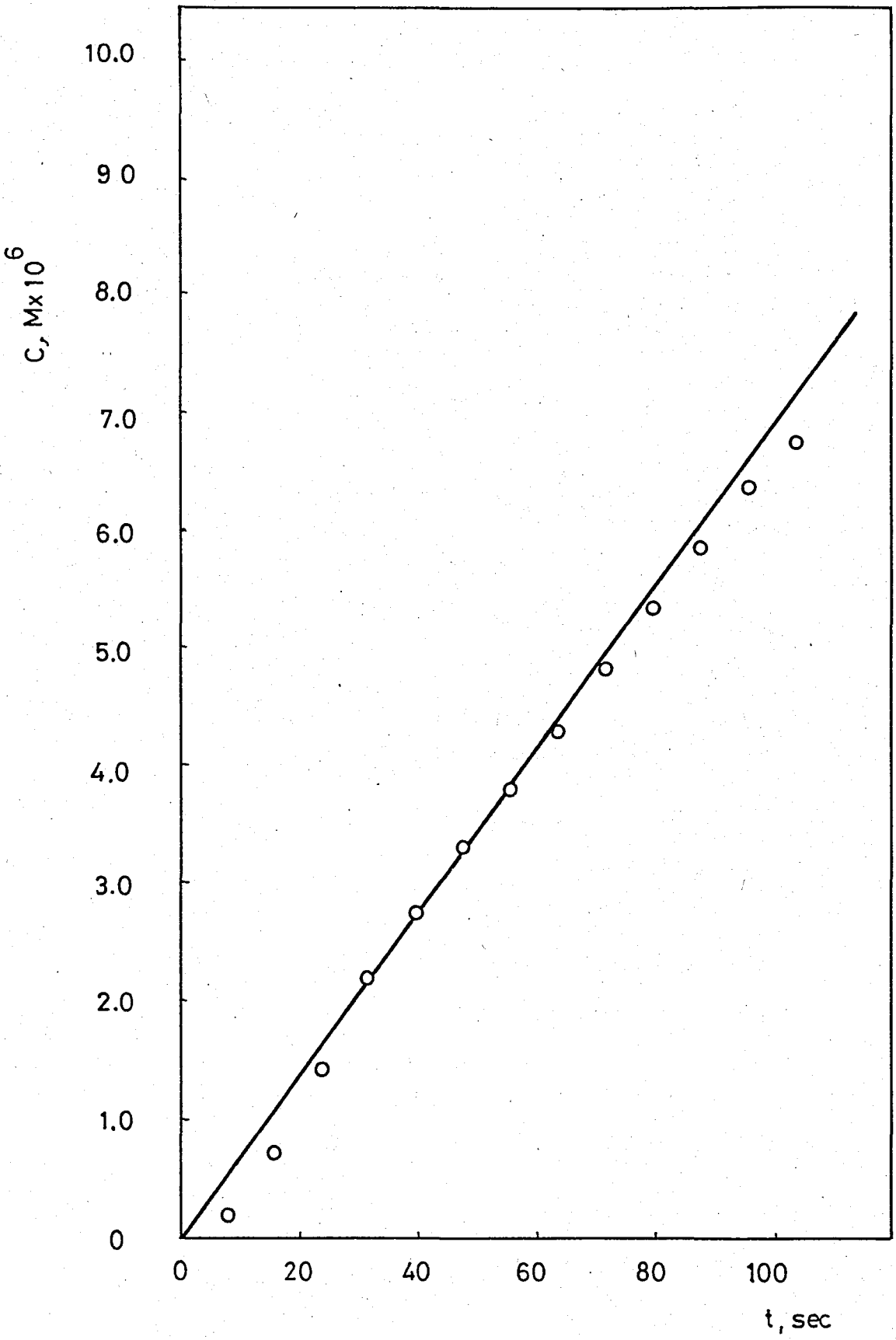


FIGURE 4.8.3. C v.s t Plot for the Dissolution of $Fe^{3+}$ Adsorbed $AgIO_3$ at pH=4.1 at 25°C.

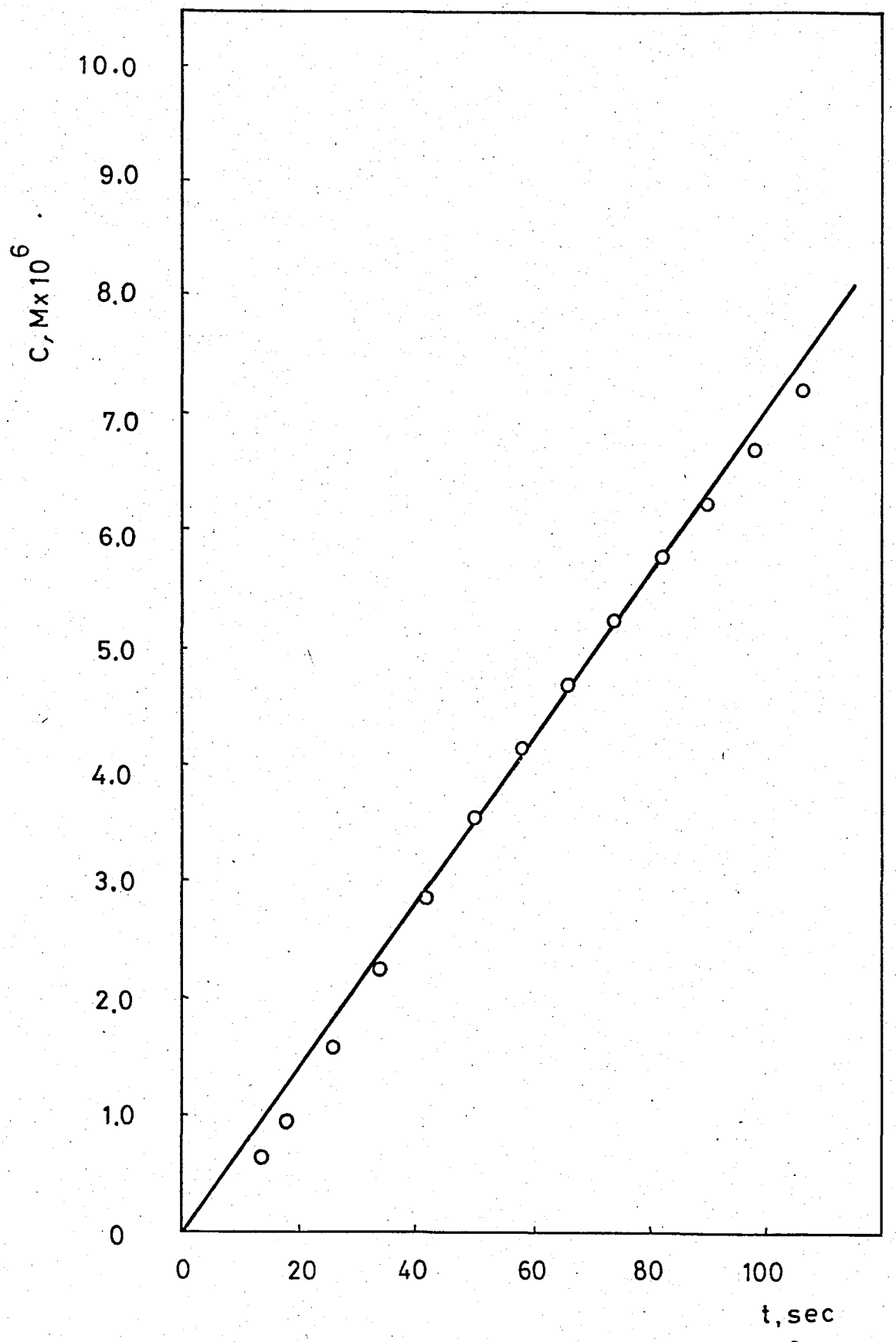


FIGURE 4.8.4. C v.s t Plot for the Dissolution of $Fe^{3+}$ Adsorbed $AgIO_3$ at pH=3.1 at 25°C.

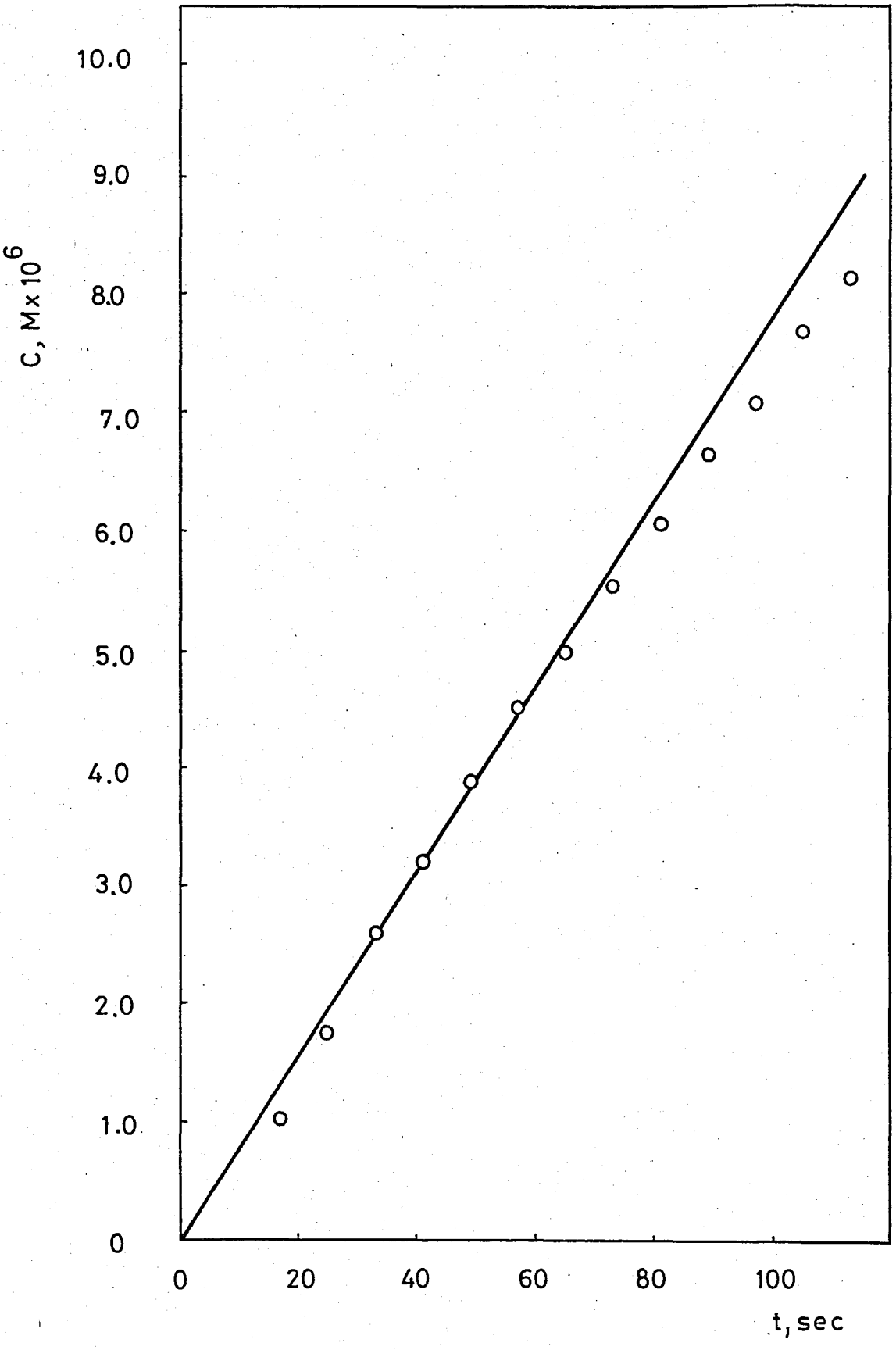


FIGURE 4.8.5. C v.s t Plot for the Dissolution of $Fe^{3+}$ Adsorbed $AgIO_3$ at pH=2.2 at 25°C.

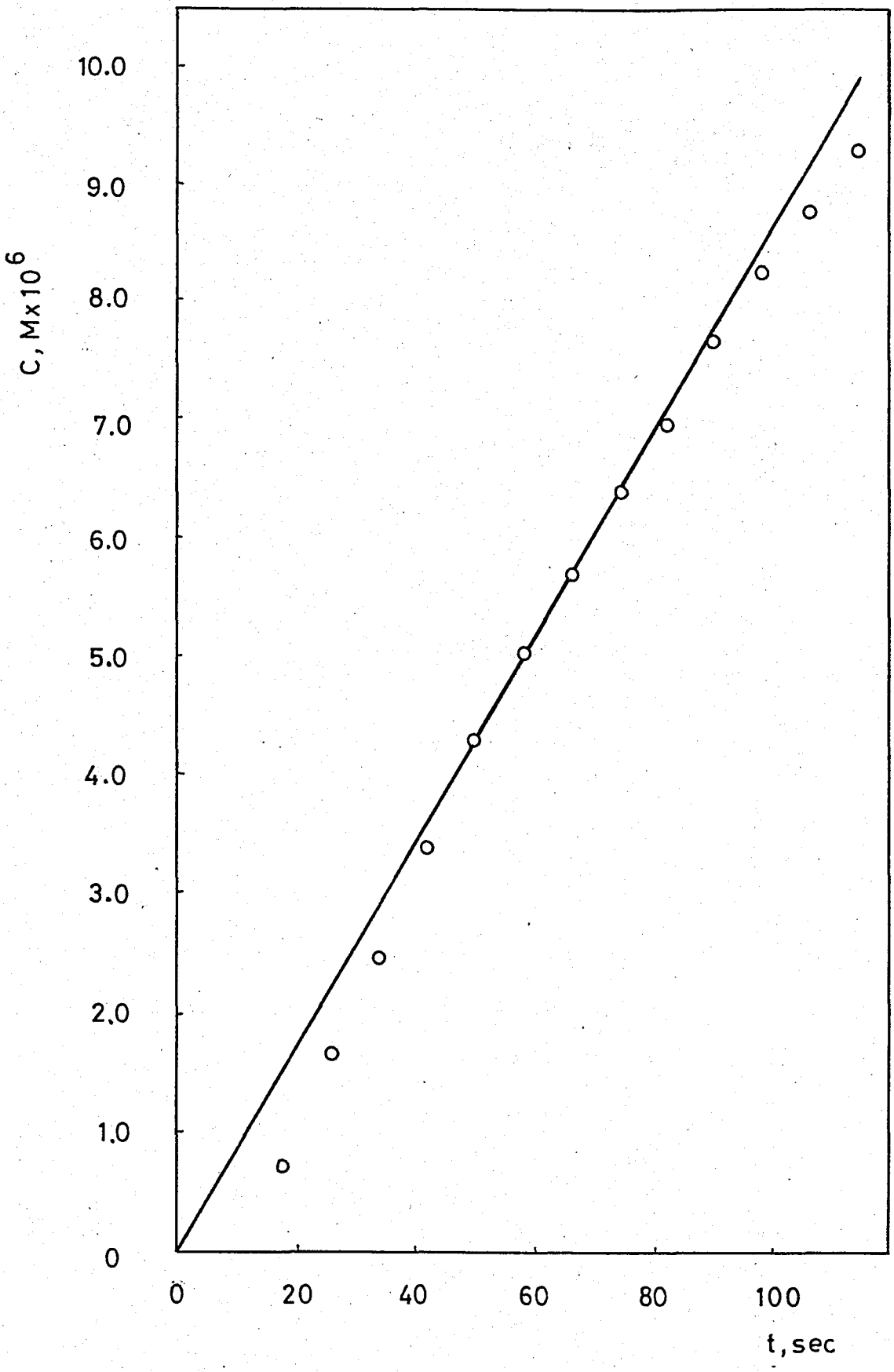


FIGURE 4.8.6. C v.s t Plot for the Dissolution of $Fe^{3+}$ Adsorbed $AgIO_3$ at pH=1.5 at 25°C.

The results of the experiments carried out with $Fe^{3+}$ adsorbed $AgIO_3$ in acidic media resemble that of the dissolution of $AgIO_3$ in acidic media in that the curves showing the pH dependence of initial dissolution rates nearly coincide between the pH's 5.0 and 3.0. This resemblance is of the same type as that between the dissolution behavior of $Fe^{3+}$ adsorbed $AgIO_3$ and $AgIO_3$ in $KNO_3$ media. The same reasonings apply, the only difference is that $K^+$ ions are replaced by $H^+$ ions in acidic media. The resultant picture consists of an electrical double layer which is composed of a thin Stern layer which cannot reach the energy barriers and a Gouy layer with a flat profile from there on.

TABLE 4.8.7. Initial Dissolution Rates of $Fe^{3+}$ Adsorbed $AgIO_3$ in Acidic Media at 25°C

| pH | Initial Dissolution Rate $R_d$, (mol $sec^{-1}gr^{-1}$) x $10^6$ |
|---|---|
| 6.0 | 0.68 |
| 5.0 | 0.71 |
| 4.1 | 0.69 |
| 3.1 | 0.71 |
| 2.2 | 0.79 |
| 1.5 | 0.86 |

## 4.9. DISSOLUTION OF $AgIO_3$ IN DISTILLED $H_2O$ AT VARIOUS TEMPERATURES

The dissolution kinetics of $AgIO_3$ was followed in distilled water at temperatures of 25°C, 30°C, 35°C and 40°C. The results of these experiments are given in Tables 4.9.1 through 4.9.3. The dissolution data in distilled water at 25°C was given in Table 4.2.1 (the calibration data for each temperature is given in Table A.2.4). The C v.s t data for the dissolution of $AgIO_3$ in distilled water at various temperatures are plotted in Figures 4.9.1 through 4.9.3.

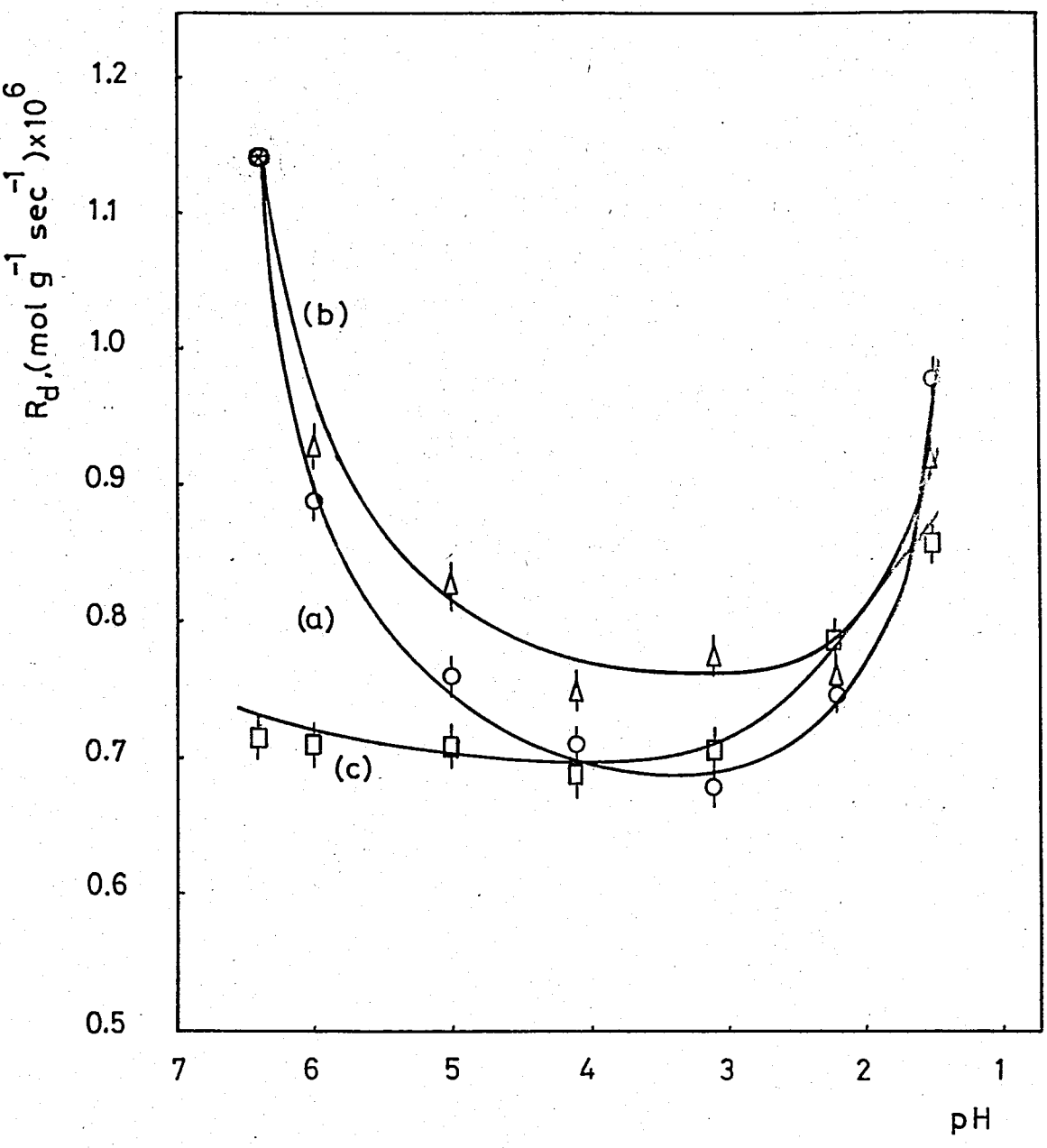


(a) $AgIO_3$ in Acidic Media

(b) $Al^{3+}$ ads. $AgIO_3$ in Acidic Media

(c) $Fe^{3+}$ ads. $AgIO_3$ in Acidic Media

FIGURE 4.2. Dependence of the Initial Dissolution Rate of $AgIO_3$ on pH of the Dissolution medium at $25^oC$.

The measured rate of dissolution per gram of the solid sample, $R_d$, can be expressed in terms of the specific rate, k, as

(4.2) $$R_d = k\sigma$$

where $\sigma$ is the specific surface of the sample. Therefore, neglecting the temperature dependence of the frequency factor, $k_B$ T/h, Equation 2.15 requires that a plot of ($\ell n$ $R_d$) v.s (1/T) must be linear, with a slope of $-\Delta H^*/R$. In order to verify Equation 2.15, the initial rates of dissolution of $AgIO_3$ in distilled water at various temperatures were calculated from the initial slopes of the corresponding C v.s t plots. These rates are tabulated in Table 4.9.4.

TABLE 4.9.1. Dissolution Data of $AgIO_3$ in Distilled $H_2O$ at $30^oC$

Calibration Function: $\log C = -3.689 - 0.0807\ N_d$

| Time, t (sec) | Number of Divisions on Recorder Output, $N_d$ | Concentration of $AgIO_3$, C, ($Mx10^6$) |
|---|---|---|
| 10 | 28.9 | 0.95 |
| 18 | 24.2 | 2.26 |
| 26 | 21.5 | 3.80 |
| 34 | 20.0 | 4.94 |
| 42 | 19.0 | 6.02 |
| 50 | 17.9 | 7.35 |
| 58 | 17.2 | 8.30 |
| 66 | 16.7 | 9.11 |
| 74 | 16.3 | 9.90 |
| 82 | 16.0 | 10.40 |

TABLE 4.9.2. Dissolution Data of $AgIO_3$ in Distilled $H_2O$ at $35^oC$

Calibration Function: $\log C = -3.415 - 0.087\ N_d$

| Time, t (sec) | Number of Divisions on Recorder Output, $N_d$ | Concentration of $AgIO_3$, C, ($Mx10^6$) |
|---|---|---|
| 8 | 28.9 | 1.17 |
| 12 | 26.2 | 2.03 |
| 16 | 24.3 | 2.99 |
| 24 | 22.2 | 4.55 |
| 32 | 20.7 | 6.14 |
| 40 | 19.7 | 7.50 |
| 48 | 19.0 | 8.52 |
| 56 | 18.1 | 10.25 |
| 64 | 17.4 | 11.82 |
| 72 | 16.8 | 13.30 |
| 80 | 16.3 | 14.69 |
| 88 | 15.8 | 16.17 |
| 96 | 15.4 | 17.60 |

TABLE 4.9.3. Dissolution Data of $AgIO_3$ in Distilled $H_2O$ at $40^oC$

Calibration Function: $\log C = -3.269 - 0.086\ N_d$

| Time, t (sec) | Number of Divisions on Recorder Output, $N_d$ | Concentration of $AgIO_3$, C, ($Mx10^6$) |
|---|---|---|
| 10 | 28.3 | 1.98 |
| 14 | 26.7 | 2.71 |
| 18 | 25.1 | 3.72 |
| 22 | 23.4 | 5.25 |
| 30 | 21.8 | 7.18 |
| 38 | 20.6 | 8.94 |
| 46 | 19.8 | 10.77 |
| 54 | 18.9 | 12.65 |
| 62 | 18.4 | 14.44 |
| 70 | 17.7 | 16.12 |
| 78 | 17.2 | 17.90 |
| 86 | 16.8 | 19.42 |

TABLE 4.9.4. Initial Dissolution Rates, $R_d$, of $AgIO_3$ in Distilled $H_2O$ at Various Temperatures

| T, $^oC$ | T, $^oK$ | $1/Tx10^3$, $^oK^{-1}$ | $R_d$, (mol $sec^{-1}gr^{-1}$)$x10^6$ | $\ell nR_d$ |
|---|---|---|---|---|
| 25 | 298 | 3.356 | 1.14 | -13.68 |
| 30 | 303 | 3.300 | 1.46 | -13.44 |
| 35 | 308 | 3.247 | 1.91 | -13.17 |
| 40 | 313 | 3.195 | 2.38 | -12.95 |

$\ell nR_d$ v.s 1/T data is plotted in Figure 4.9.4. As can be seen from the figure, the plot is a straight line. Thus, Equation 2.15 is experimentally verified. The slope of the straight line in Figure 4.9.1 is

$$\text{Slope} = \frac{-13.68 - (-13.44)}{3.356 \times 10^{-3} - 3.300 \times 10^{-3}}$$

$$\text{Slope} = -4.29 \times 10^3 \ ^oK$$

From the slope, the activation enthalpy for the dissolution, $\Delta H^*$, is calculated with R = 1.987 cal/mol.$^oK$ as

$$\Delta H^* = 4.29 \times 10^3 \times 1.987$$
$$\Delta H^* \cong 8{,}500 \text{ cal/mol ion}$$

A few values for $\Delta H^*$[15],[16] found in literature for $CaSO_4$ and $BaCO_3$ which are 10 kcal/mol and 8.45 kcal/mol respectively, are quite close to this value.

As far as the theory is concerned, it was of some interest to compare the experimental $\Delta H^*$ with what can be computed from the theory, at least approximately. For this purpose, neglecting Born repulsions, an approximate analytical expression for the Coulombic interaction curve in Figure 2.1 was derived. $AgIO_3$ was assumed to have a simple close packed cubic crystal structure (the actual crystal structure of $AgIO_3$ is rhombic bipyramidal[13] which would lead to an elaborate

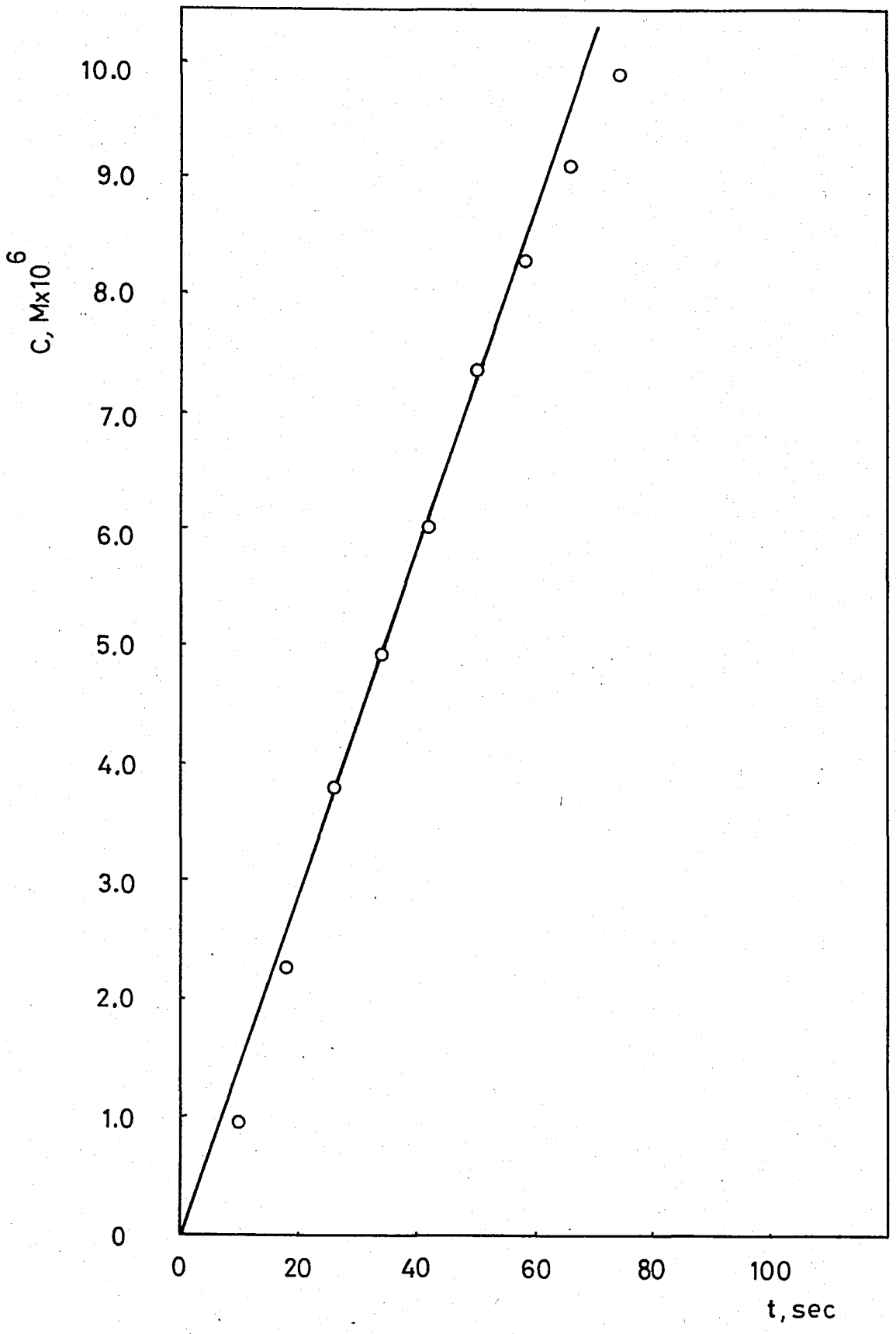


FIGURE 4.9.1. C v.s t Plot for the Dissolution of $AgIO_3$ in Distilled $H_2O$ at $30^oC$.

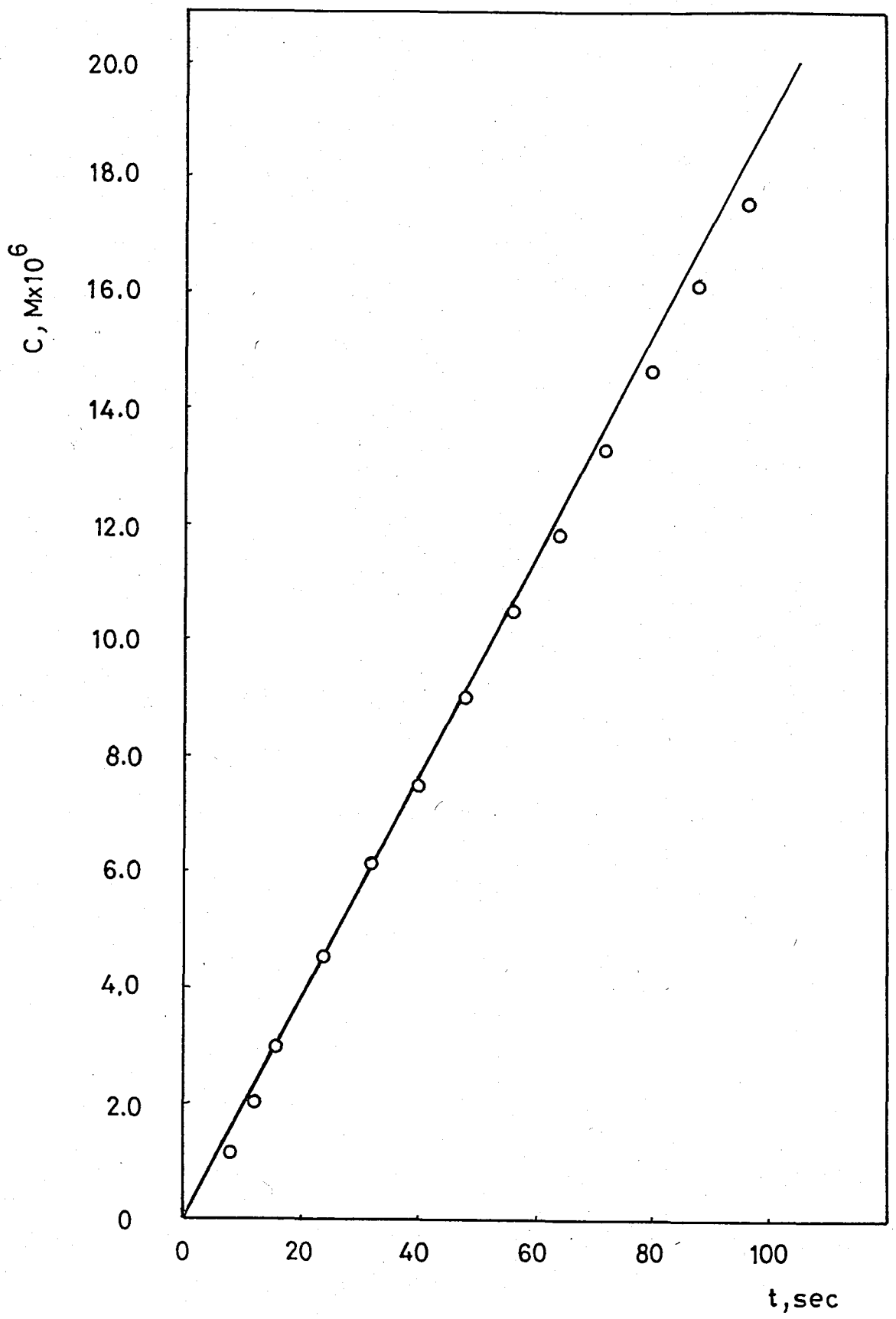


FIGURE 4.9.2. C v.s t Plot for the Dissolution of $AgIO_3$ in Distilled $H_2O$ at $35^oC$.

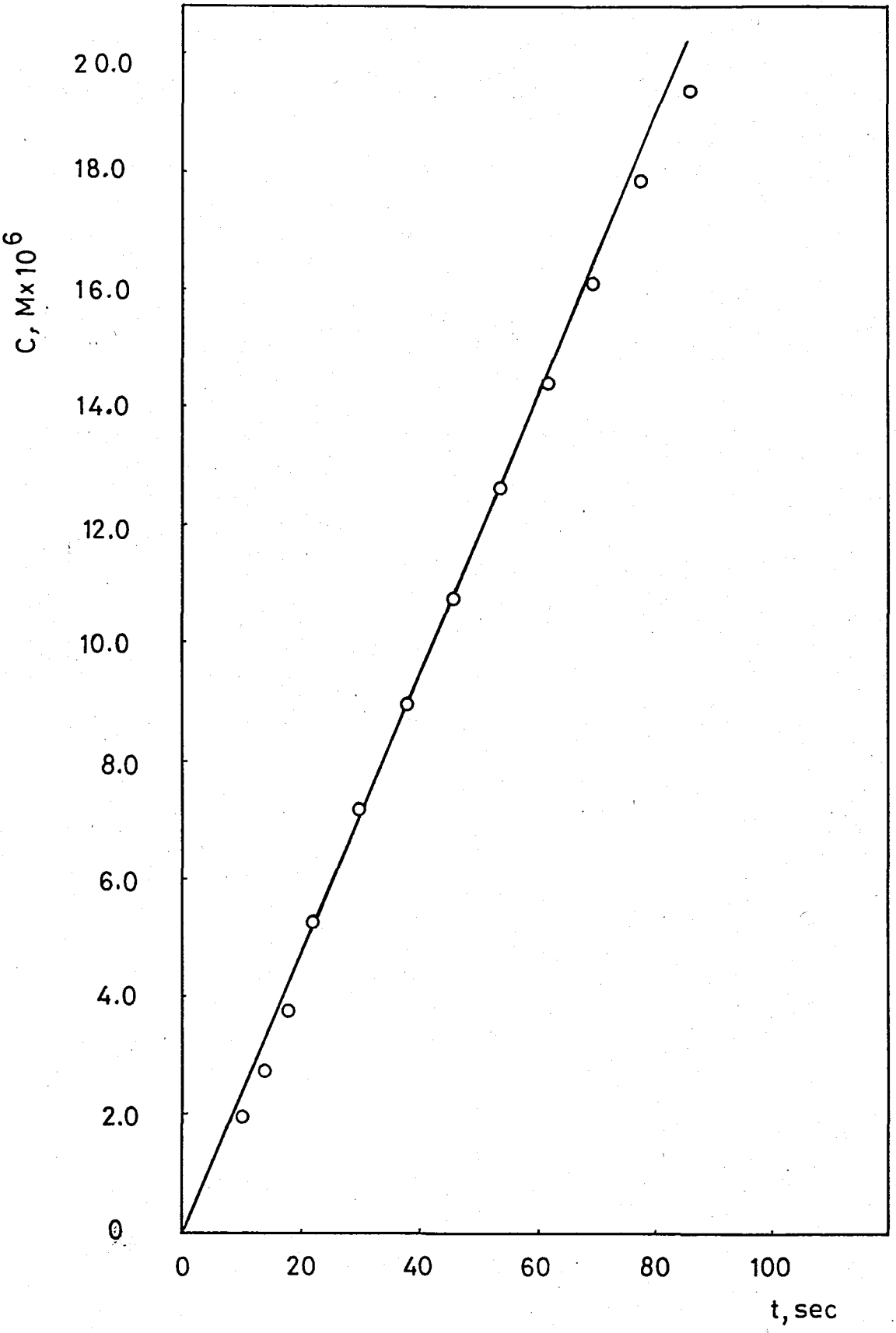


FIGURE 4.9.3. C v.s t Plot for the Dissolution of $AgIO_3$ in Distilled $H_2O$ at $40^oC$.

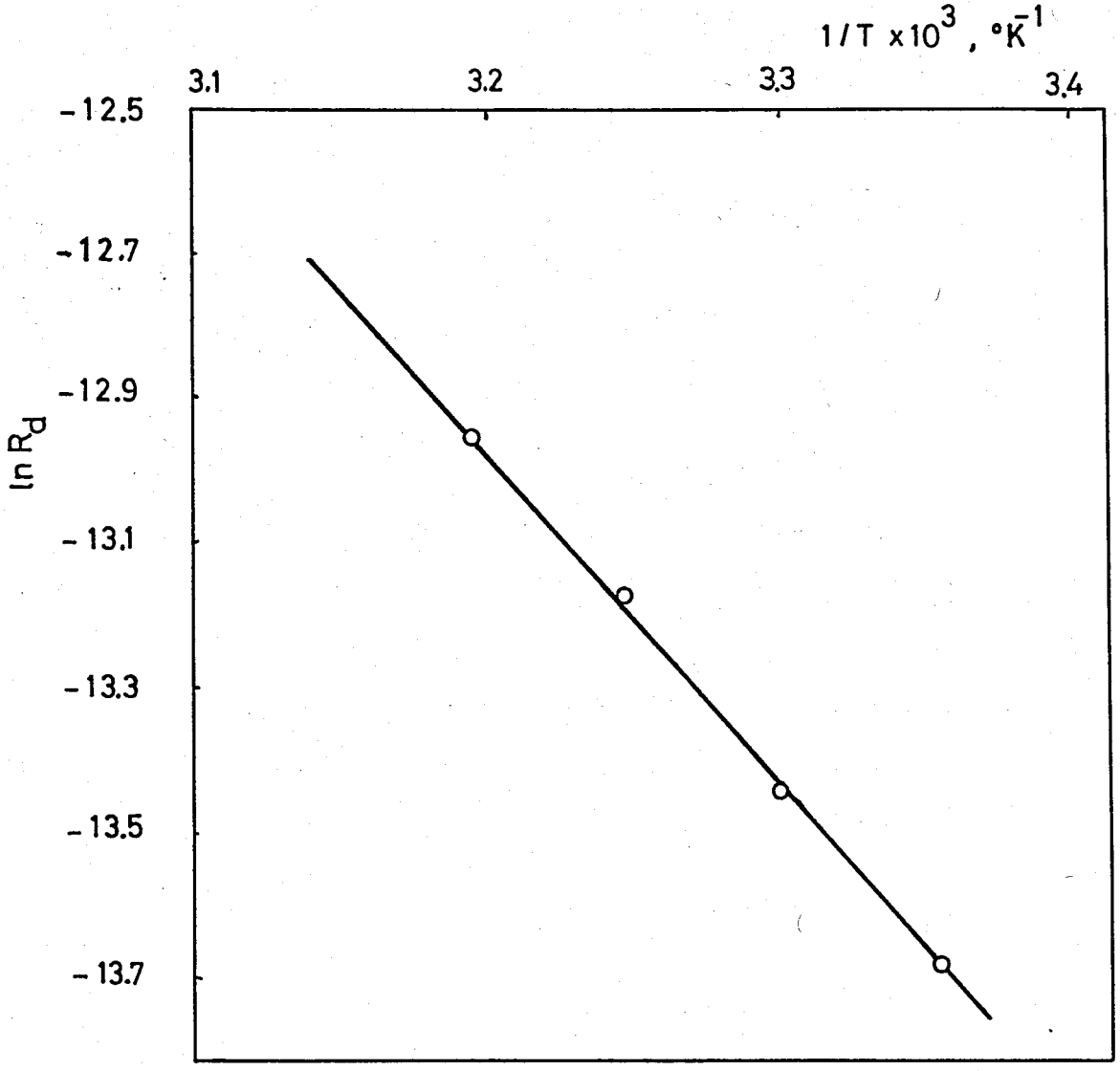


FIGURE 4.9.4. Arrhenius Plot for the Dissolution of $AgIO_3$ in Distilled $H_2O$

formulation). The ionic radii of $Ag^+$ and $IO_3^-$ are 1.26 Å and 1.28 Å respectively[17]. Considering displacement of a surface ion from a perfect crystal normal to the surface; and taking into account 5 nearest, 4 diagonal attractive neighbors; and 8 diagonal repulsive neighbors of this ion (Figure 4.9.5) a Coulombic energy expression can be derived which reads as

$$(4.3)\quad E_{coul} = \frac{e^2 x}{r_o(x+r_o)} + 4\,e^2\,\frac{(x^2+r_o^2)^{1/2}-r_o}{r_o(x^2+r_o^2)^{1/2}} + 4\,e^2\,\frac{\left[(x+r_o)^2+2r_o\right]^{1/2}-\sqrt{3}\,r_o}{\sqrt{3}\,r_o\left[(x+r_o)^2+2\,r_o^2\right]}$$

$$- 4\,e^2\,\frac{(2\,r_o^2+x^2)^{1/2}-\sqrt{2}\,r_o}{\sqrt{2}\,r_o\,(2\,r_o^2+x^2)^{1/2}} - 4\,e^2\,\frac{\left[(x+r_o)^2+r_o^2\right]^{1/2}-\sqrt{2}\,r_o}{\sqrt{2}\,r_o\left[(x+r_o)^2+r_o^2\right]^{1/2}}$$

where $r_o$ is the sum of the radii of cation and anion ($r_o = r_+ + r_- = 3.08$ Å), x is the perpendicular distance into the solution from the solid surface and e is the unit electrical charge ($e = 4.8 \times 10^{-10}$ e.s.u.)

Equation 4.3. is the most general case for the dissolution of a cation, i.e., the case in which a cation has the greatest number of neighbors. As is seen from Figure 2.1, the asymptotic value of the Coulombic energy curve is the limit of Equation 4.3 as r approaches infinity. Substituting the numerical values, this limit appears as

$$(4.4)\quad \lim_{x\to\infty} E_{coul} = \frac{e^2}{r_o}\left(5 + \frac{4}{\sqrt{3}} - \frac{8}{\sqrt{2}}\right) = 1.23 \times 10^{-11}\ \text{erg/ion}$$

The experimental activation enthalpy for dissolution was found as 8.500 cal/mol ion. When converted to "erg/ion" units, it becomes $5.9\times10^{-13}$ erg/ion. As can be observed from these numbers the activation enthalpy for dissolution is smaller than the asymptotic value of the Coulombic energy, an observation which is quite reasonable.

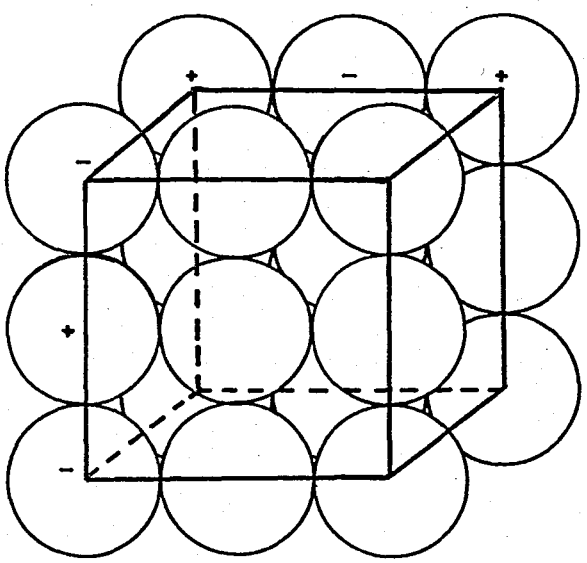


FIGURE 4.9.5. Schematic Representation of a Minimum Size of Unit of the Crystal Structure of $AgIO_3$.

As mentioned in Chapter 1, the dissolution theories in general assume that the dissolution spreads from the imperfections (e.g., kinks in steplines) on the surface. If this viewpoint is adopted, the number of neighbors of the dissolving ion decreases in such a manner that in Equation 4.3 the coefficients of the second and third terms become both 2. The asymptotic value of the Coulombic energy in such a case is calculated as

$$(4.5) \qquad \lim_{x\to\infty} E_{coul} = \frac{e^2}{r_o}\left(3 + \frac{4}{\sqrt{3}} - \frac{6}{\sqrt{2}}\right) = 7.86 \times 10^{-12} \text{ erg/ion}$$

The activation enthalpy for the dissolution is again smaller than the asymptotic value as expected.

In an extreme case where the dissolving ion is isolated on the surface in the sense that it has no lateral neighbor, in Equation 4.3 the second and fourth terms disappear. The asymptotic value of the Coulombic energy in this case is

$$(4.6) \qquad \lim_{x\to\infty} E_{coul} = \frac{e^2}{r_o}\left(1 + \frac{4}{\sqrt{3}} - \frac{4}{\sqrt{2}}\right) = 3.52 \times 10^{-12} \text{ erg}$$

The activation enthalpy for the dissolution is still smaller than the asymptotic value as expected.

The results of the experiments for the dissolution of $Al^{3+}$ adsorbed $AgIO_3$ and $Fe^{3+}$ adsorbed $AgIO_3$ in $KNO_3$ media indicated that the activation plane should be located between the outer boundaries of the Stern layers produced by hydrated $Fe^{3+}$ and hydrated $Al^{3+}$ ions. The hydrated radii of $Fe^{3+}$ and $Al^{3+}$ can be calculated from their ionic conductances assuming validity of Stokes' law, using the equation[18]

$$(4.7) \qquad (r_+)_h = \frac{e\, Z_+ F}{\lambda_+ (6\pi\eta)\ (300)}$$

Where $\lambda_+$ is the limiting equivalent ionic conductance and $\eta$ is the viscosity of the solvent. The $\lambda_+$ values for the $Fe^{3+}$ and $Al^{3+}$ ions are 68 and 61 $mho.cm^2.equivalent^{-1}$(19) respectively. Using these values in Equation 4.7, $(r_+)_h$ value for $Fe^{3+}$ was calculated as 1.35 Å and for $Al^{3+}$ as 1.50 Å.

If the point $(x_\pm, \Delta H^*)$ in Figure 2.1 is assumed approximately to fall on the Coulombic interaction curve, $x_\pm$ can be determined by equating the enthalpy of activation for dissolution to the Coulombic energy function given by Equation 4.3. Substituting $5.9 \times 10^{-13}$ erg/ion value for $E_{coul}$ in Equation 4.3 and replacing x by $x_\pm$, $x_\pm$ was calculated by trial and error as 0.7 Å, which is too small. This value of $x_\pm$ corresponds to the case in which an ion dissolves from a perfect surface. For the case of the dissolution from the kinks in steplines, the coefficients of the second and third terms in Equation 4.3 become both 2 as mentioned previously. In this case, a similar calculation for x resulted in a value of approximately 1.0 Å. This is again a too small value. At the extreme case where there is only one isolated ion on the solid surface which is dissolving, the second and fourth terms in Equation 4.3 disappear as mentioned previously. The value of $x_\pm$ which is similarly calculated comes out as 1.4 Å. This value is in good agreement with an estimate based on the hydrated radii of $Fe^{3+}$ and $Al^{3+}$ mentioned previously.

Although the last of these $x_\pm$ values falls between the hydrated radii of $Fe^{3+}$ and $Al^{3+}$, for the dissolution mode described in the last case, admittedly, it is hard to claim at this stage that dissolution mechanism involves a rate determining step in which laterally isolated surface ions dissolve, because of two reasons, namely

(1) The present treatment of activation enthalpy involves a number of approximations and assumptions,

(2) Such a claim would be internally inconsistent with the assumed model of dissolution of a perfect crystal.

Nevertheless, to illuminate the picture, it would be worthwhile to revise the theory to treat the case of dissolving isolated surface ions as "defect centers" and to see what remains in the intersection of consequences of the unrevised and revised theories.

# CHAPTER V
# CONCLUSIONS

The results obtained in this study can be summarized as follows:

(1) The presence of small hydrated cations such as $K^+$ decreases the dissolution rate of $AgIO_3$ asymptotically to a limiting value with increasing ionic strength at low and medium ionic strengths. This is characteristic of Gouy layer.

(2) The presence of large hydrated cations such as $Al^{3+}$ decreases the dissolution rate of $AgIO_3$ asymptotically to a lesser degree with increasing ionic strength at low and medium ionic strengths. This is a situation in which $Al^{3+}$ ions form a Stern layer extending beyond the activation planes and in the inner parts the double layer shows some Gouy character due to $H^+$ formed by hydrolysis of $Al^{3+}$.

(3) The presence of small and large hydrated cations such as in the case of the dissolution of $Al^{3+}$ adsorbed $AgIO_3$ in $K^+$ containing media have no effect on the dissolution rate of $AgIO_3$, independent of the ionic strength of the medium.

(4) The dissolution of $AgIO_3$ in acidic media follows a Gouy layer pattern almost with the same drop in rate as that in $K^+$ containing media at low and medium pH's. Such a picture can be explained by a proton transfer mechanism

of $H^+$ ions causing the potential drop between the solid surface and activation plane.

(5) The dissolution of $Al^{3+}$ adsorbed $AgIO_3$ in acidic media follows a Gouy layer pattern showing a significant drop in rate at low and medium pH's. Although $K^+$ ions cannot penetrate into the Stern layer produced by $Al^{3+}$ ions, $H^+$ ions can manage this because of their proton nature thus causing the drop in rate.

(6) The dissolution of $Fe^{3+}$ adsorbed $AgIO_3$ in $K^+$ containing and acidic media resemble that of $AgIO_3$ in corresponding media at medium ionic strengths. For these cases the electrical double layer is composed of a Stern layer formed by $Fe^{3+}$ ions, which cannot reach the activation planes and a Gouy layer with a flat profile from that point on.

(7) In all dissolution experiments, the dissolution rate at high ionic strengths shows an increase up to the value in distilled water, which is a deviation from the theory resulting most probably because the theory is valid for a sufficiently dilute medium.

(8) The dependence of dissolution rate of $AgIO_3$ in distilled water on temperature follows an Arrhenius type expression resulting in an activation enthalpy for dissolution of 8500 cal/mol which is well correlated with other values found in literature for other ionic substances. The activation enthalpy for dissolution is also checked on the basis of the theory and found to be reasonable.

# APPENDIX I
# DERIVATION OF THE EXPRESSION FOR THE ENTROPY OF ACTIVATION GIVEN BY EQUATION 2.9

The expression for the entropy of activation is given by Equation 2.9.

$$(2.9) \qquad \Delta S^*_{\pm} = -R \ln \left[ X^*_{\pm} / (1-X^*_{\pm}) \right]$$

where R is the gas constant and $X^*_{\pm}$ is the mole fraction of the available sites occupied by the activated ions on the respective activation plane. This equation can be derived from statistical thermodynamic considerations for one type of ion as follows.

Let N be the total number of sites available on the activation plane, assumed to be equal to that of ions on the solid surface occupied by activated ions. From statistics the number of ways of distributing N' identical things on N labelled sites is given by

$$(A.1.1) \qquad \Omega = N! / \left[ N'!(N-N')! \right]$$

The configurational entropy of the assembly consisting of each type of ions on the activation plane can be expressed in the usual way as

$$(A.1.2) \qquad S = k_B \ln \Omega$$

where $k_B$ is the Boltzmann constant. Inserting Equation A.1.1 into Equation A.1.2, S becomes

(A.1.3) $$S = k_B \left[ \ell nN! - \ell nN'! - \ell n(N-N')! \right]$$

Since N, N', and (N-N') are very large numbers the logarithmic terms within the brackets may be expanded by Stirling's approximation in the following way

(A.1.4) $$\ell nN! = N\ell nN - N$$

(A.1.5) $$\ell nN'! = N'\ell nN' - N'$$

(A.1.6) $$\ell n(N-N')! = (N-N')\ \ell n(N-N') - (N-N')$$

Substituting Equations A.1.4, A.1.5 and A.1.6 into Equation A.1.3 one gets

(A.1.7) $$S = k_B \left[ N\ell nN - N'\ell nN' - (N-N')\ell n(N-N') \right]$$

Let

(A.1.8) $$N = n\ N_o$$

and

(A.1.9) $$N' = n'N_o$$

where n is the number of moles of sites on the surface, n' is the number of moles of ions in activation plane and $N_o$ is the Avogadro number With Equations A.1.8, A.1.9 and also

(A.1.10) $$k_B = R/N_o$$

Equation A.1.7 becomes

(A.1.11) $$S = R \left[ n\ell n\ n - n\ell n(n-n') - n'\ell n\ n' + n'\ell n(n-n') \right]$$

after simplifications. The configurational partial molal entropy of the ions in the activation plane, $\bar{S}$, is defined in the following manner

(A.1.12) $\bar{S} = \left(\frac{\partial S}{\partial n'}\right)_n$

Differentiating Equation A.1.11 with respect to n' at constant n and combining with Equation A.1.12 gives

(A.1.13) $\bar{S} = -R \ln \frac{n'}{n-n'}$

Defining

(A.1.14) $X^* = n'/n$

where $X^*$ is the mole fraction of the activated ions on the activation plane, Equation A.1.13 becomes

(A.1.15) $\bar{S} = -R \ln \left[X^*/(1-X^*)\right]$

Assuming that the configurational partial molal entropy of an ion on the solid surface is zero (assumption of perfect crystal) the differential entropy of activation per mole of ion becomes

(A.1.16) $\Delta S^*_{\pm} = \bar{S}_{\pm} - 0 = -R \ln \left[X^*_{\pm} / (1-X^*_{\pm})\right]$

which is the desired result.

# APPENDIX II
# THE CALIBRATION DATA

The procedure for the calibration experiments was described in Section 3.3.4. In this section, the calibration data consisting of the amounts of dilution of saturated $AgIO_3$ solutions and the corresponding number of divisions on the recorder output are tabulated for each dissolution medium.

TABLE A.2.1. Calibration Data in $KNO_3$ Media at 25°C

| Dilution of Saturated $AgIO_3$ Solution, (fold) | Number of Divisions on Recorder Output, $N_d$ | | | | | |
|---|---|---|---|---|---|---|
| | $I=10^{-6}$ | $I=10^{-5}$ | $I=10^{-4}$ | $I=10^{-3}$ | $I=10^{-2}$ | $I=10^{-1}$ |
| 25.0 | 18.9 | 18.0 | 15.2 | 18.0 | 16.5 | 18.0 |
| 33.3 | 20.7 | 20.2 | 16.8 | 20.0 | 18.0 | 19.8 |
| 50.0 | 22.8 | 22.4 | 19.2 | 22.2 | 20.3 | 22.0 |
| 62.5 | 24.2 | 24.0 | 20.4 | 24.0 | 21.4 | 23.5 |
| 100.0 | 27.2 | 27.5 | 23.2 | 27.0 | 24.1 | 26.1 |

TABLE A.2.2. Calibration Data in $Al_2(SO_4)_3$ Media at 25°C

| Dilution of Saturated $AgIO_3$ Solution, (fold) | Number of Divisions on Recorder Output, $N_d$ | | | | |
|---|---|---|---|---|---|
| | $I=7.5\times10^{-6}$ | $I=7.5\times10^{-5}$ | $I=7.5\times10^{-4}$ | $I=7.5\times10^{-3}$ | $I=7.5\times10^{-2}$ |
| 25.0 | 18.6 | 17.6 | 17.3 | 16.1 | 15.8 |
| 33.3 | 20.1 | 19.1 | 18.6 | 17.4 | 17.0 |
| 50.0 | 22.6 | 21.4 | 20.5 | 19.4 | 18.8 |
| 62.5 | 24.1 | 22.5 | 21.6 | 20.5 | 19.6 |
| 100.0 | 27.0 | 25.0 | 23.9 | 22.8 | 21.6 |

TABLE A.2.3. Calibration Data in Acidic Media at 25°C

| Dilution of Saturated $AgIO_3$ Solution, (fold) | Number of Divisions on Recorder Output, $N_d$ | | | | | |
|---|---|---|---|---|---|---|
| | pH=6 | pH=5 | pH=4.1 | pH=3.1 | pH=2.2 | pH=1.5 |
| 25.0 | 16.1 | 15.5 | 15.4 | 13.9 | 19.0 | 17.9 |
| 33.3 | 17.4 | 17.0 | 17.1 | 15.5 | 20.4 | 19.1 |
| 50.0 | 19.3 | 18.7 | 19.3 | 17.4 | 22.4 | 21.0 |
| 62.5 | 20.6 | 19.8 | 20.8 | 18.6 | 23.5 | 21.9 |
| 100.0 | 22.9 | 22.3 | 23.6 | 21.2 | 25.6 | 24.1 |

TABLE A.2.4. Calibration Data in Distilled $H_2O$ at Various Temperatures

| Dilution of Saturated $AgIO_3$ Solution, (fold) | Number of Divisions on Recorder Output, $N_d$ | | | |
|---|---|---|---|---|
| | $T=25^oC$ | $T=30^oC$ | $T=35^oC$ | $T=40^oC$ |
| 25.0 | 16.3 | 17.1 | 18.0 | 19.2 |
| 33.3 | 17.7 | 18.5 | 19.6 | 20.7 |
| 50.0 | 20.1 | 20.9 | 21.6 | 22.8 |
| 62.5 | 21.3 | 22.0 | 22.7 | 23.9 |
| 100.0 | 23.8 | 24.5 | 25.0 | 26.1 |

# APPENDIX III
# SAMPLE CALCULATION FOR THE INITIAL DISSOLUTION RATE OF $AgIO_3$ IN DISTILLED $H_2O$ AT 25°C

## A.3.1. THE CALIBRATION FUNCTION FOR THE DISSOLUTION OF $AgIO_3$ IN DISTILLED $H_2O$ AT 25°C

The concentration cell used in the dissolution experiments is

$$Ag|AgIO_3(C)||AgIO_3(C_s)|Ag$$

as given in Section 3.1. The cell potential for this system can be expressed in the following form

$$\varepsilon = p' \log \frac{a_s}{a} \qquad (A.3.1)$$

where p' is a constant group involving transference number of the anion, temperature, and universal constants. $a_s$ and a are the activities of the right and left half-cells respectively. Since the solutions used in this system are quite dilute, activities may be replaced by concentrations and Equation A.3.1 takes the following form

$$\varepsilon = p' \log \frac{C_s}{C} \qquad (A.3.2)$$

The number of divisions on the recorder output, $N_d$, changes linearly with the cell potential developed, $\varepsilon$. By introducing this linearity, Equation A.3.2 may be rearranged to give

(A.3.3) $\log c = p + qN_d$

where p and q are the constants of the calibration function. The calculation of p and q requires calibration data for the dissolution of $AgIO_3$ in distilled water at 25°C which is given in Table A.2.4. The extents of dilution given in Table A.2.4. are converted into concentrations using the solubility of $AgIO_3$ in water at 25°C ($C_s = 1.785 \times 10^{-6}$M), and the following table is constructed.

TABLE A.3.1. Calibration Data for the Dissolution of $AgIO_3$ in Distilled $H_2O$ at 25°C

| Dilution (fold) | C ($M \times 10^6$) | logc | $N_d$ |
|---|---|---|---|
| 25 | 7.14 | -5.15 | 16.3 |
| 33.3 | 5.36 | -5.27 | 17.7 |
| 50 | 3.57 | -5.45 | 20.1 |
| 62.5 | 2.86 | -5.54 | 21.3 |
| 100 | 1.79 | -5.75 | 23.8 |

A plot of logc v.s. $N_d$ is in Figure A.3.1. The function represented by Equation A.3.3 can be obtained by linear least square analysis of the data in Table A.3.1. Denoting logc values by "y" and $N_d$ values by "x", the constants p and q are calculated through the use of Equations A.3.4 and A.3.5

(A.3.4) $$q = \frac{\Sigma yx - \Sigma x \Sigma y/n}{\Sigma x^2 - (\Sigma x)^2/n}$$

(A.3.5) $$p = \frac{\Sigma y - q\Sigma x}{n}$$

Substituting the values of y and x into Equations A.3.4 and A.3.5 one gets

$$q = \frac{-541.63-(99.2)(-27.16)/5}{2003.12-(99.2)^2/5} = -0.0793$$

$$p = \frac{-27.16-(-0.0793)(99.2)}{5} = 3.859$$

Therefore the calibration function is obtained as

$$\log c = -3.859 - 0.0793\ N_d$$

## A.3.2. THE INITIAL DISSOLUTION RATE OF $AgIO_3$ IN DISTILLED $H_2O$ AT 25°C

The dissolution of 20 mg of $AgIO_3$ in 200 ml of distilled $H_2O$ was followed at 25°C and the recorder output given in Figure A.3.2 was obtained. The chart speed for this run was 6 cm/min and hence each small division represents 2 sec. With this information at hand, the number of divisions were read from the curve at every four seconds. Then $N_d$ values were converted into C values through the use of the calibration function. The results are tabulated in Table 4.2.1. The C v.s t data for the dissolution of $AgIO_3$ in distilled $H_2O$ are plotted in Figure 4.2.1.

The points in Figure 4.2.1 fell on a straight line through the origin within a short region at the middle section of the curve because of the reasons given in Section 4.1. The initial slope is obtained by extrapolating the straight line to the origin as follows:

$$\text{Slope} = \frac{7.30\times10^{-6}-5.46\times10^{-6}}{64-48} = 1.14\times10^{-7}\ \text{mol lt}^{-1}\text{sec}^{-1}$$

The initial dissolution rate per gram of $AgIO_3$ is calculated by multiplying the initial slope by the volume of the solution (200 ml) and dividing the result by the mass of $AgIO_3$ initially present in the dissolution medium (20 mg). The result is

$$R_d = 1.14\times10^{-7}\ \frac{\text{mol}}{\text{lt-sec}} \times \frac{0.200\ \text{lt}}{0.020\ \text{gr}}$$

$$R_d = 1.14\times10^{-6}\ \text{mol sec}^{-1}\text{gr}^{-1}$$

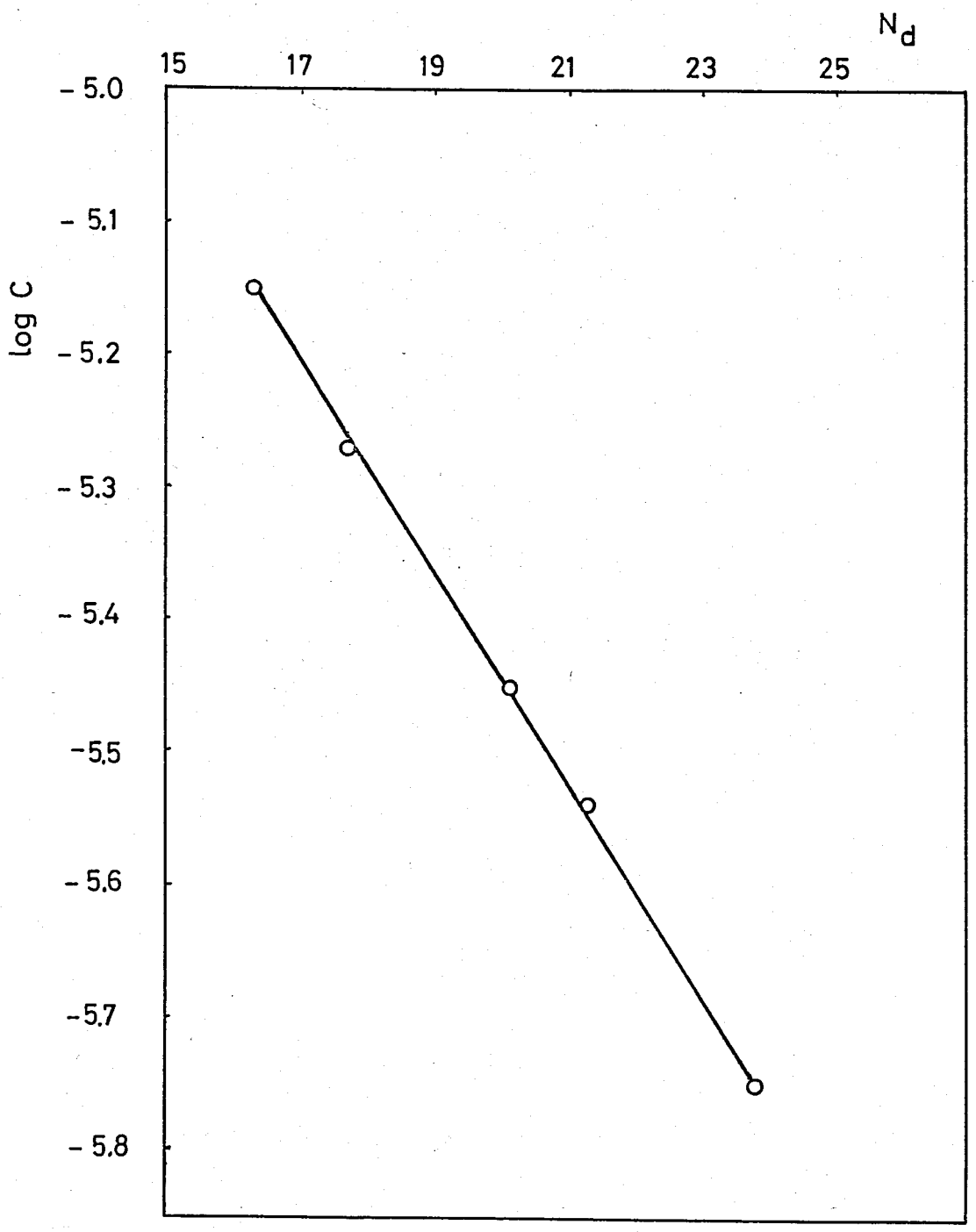


FIGURE A.3.1. Calibration Plot for the Dissolution of $AgIO_3$ in Distilled $H_2O$ at 25°C.

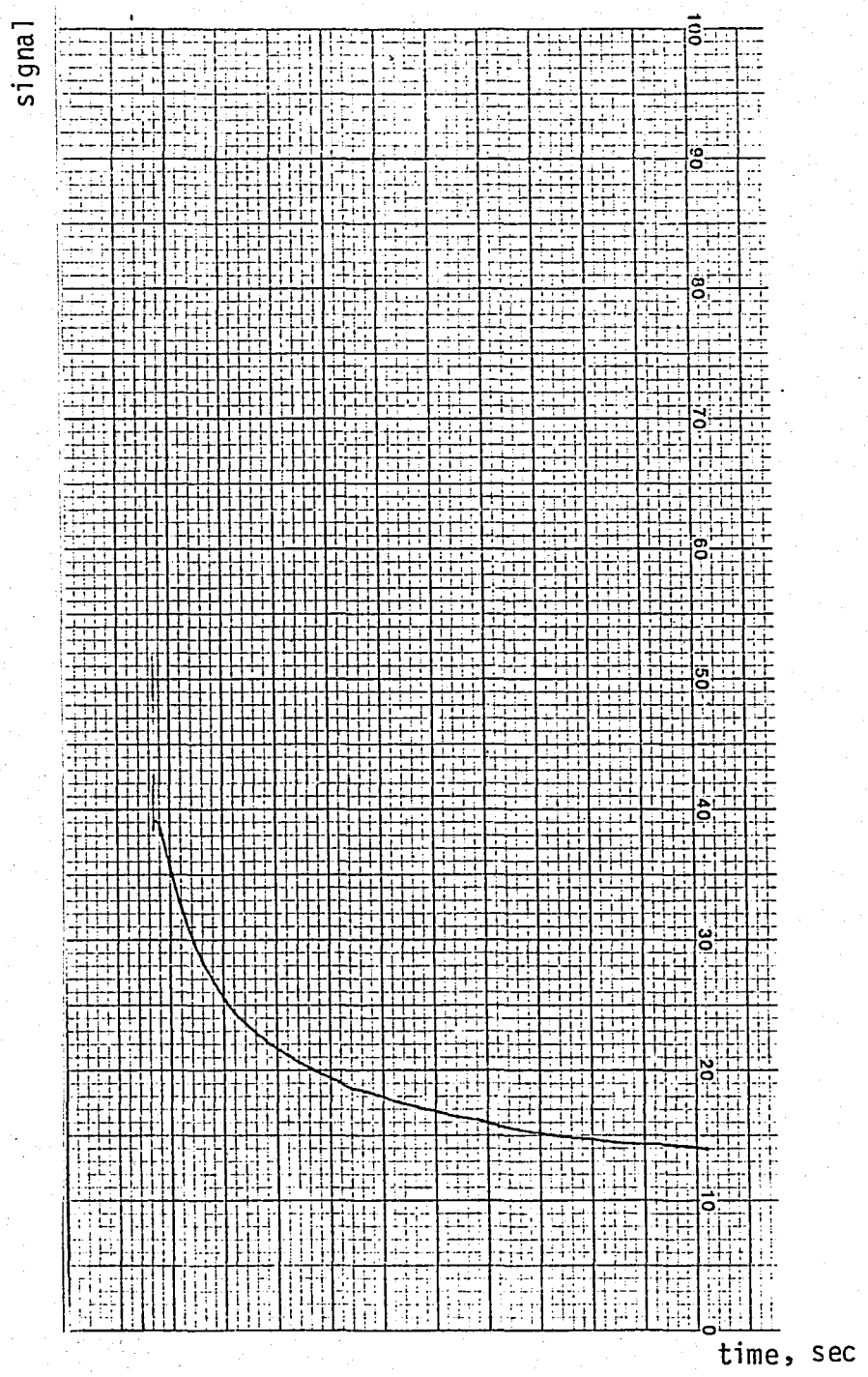


FIGURE A.3.2. Recorder Output for the Dissolution of $AgIO_3$ in Distilled $H_2O$ at 25°C.

# APPENDIX IV
# DELAY IN EQUILIBRIATION AT THE SILVER ELECTRODE

A $AgIO_3$ solution of concentration $C_1 = 1.2 \times 10^{-6}$M (corresponding to $N_d = 64.9$) was placed in sample cell. Then another solution of $AgIO_3$ was quickly poured into the cell to give rise to a concentration of $C_2 = 6.85 \times 10^{-6}$M (corresponding to $N_d = 41.2$). Figure A.4.1 is the recorder output of this experiment. Although a tail is observed on this figure, almost 90 per cent of $C_2$ is reached before tailing occured. Therefore the overall picture can be thought of as two baselines connected by a very steep straight line. The concentration at any point on this line is the "apparent" concentration denoted by "C". "$C_2$" is the "actual" concentration, i.e., the concentration which would occur if there was no delay in equilibriation at the silver electrode.

Figure A.4.1. suggests the following expression among the various concentrations and time

$$\text{(A.4.1)} \qquad \frac{dC}{dt} = k_d (C_2 - C)$$

Here, $k_d$ is the rate constant for the delay in equilibriation at the silver electrode. Rearranging Equation A.4.1 and integrating between the concentration limits from $C_1$ to C and the time limits from 0 to t, one gets

$$\text{(A.4.2)} \qquad \int_{C_1}^{C} \frac{dC}{C_2 - C} = \int_{0}^{t} k_d dt$$

(A.4.3) $$\ln \frac{C_2-C_1}{C_2-C} = k_d t$$

Evaluation of $k_d$ from Equation A.4.3 requires C v.s t data for Figure A.4.1 which is given in Table A.4.1. The data of Table A.4.1 is plotted in Figure A.4.2 in $\ln\left[(C_2-C_1)/(C_2-C)\right]$ v.s t coordinates. The slope of this plot gives $k_d$.

$$\text{Slope} = k_d = \frac{1.155 - 0}{0.8 - 0}$$

$$k_d = 1.45 \text{ sec}^{-1}$$

TABLE A.4.1. C v.s t Data for the Delay in Equilibriation at the Silver Electrode

$C_1 = 1.20 \times 10^{-6} M$ ($N_1 = 64.9$)
$C_2 = 6.85 \times 10^{-6} M$ ($N_2 = 41.2$)

Calibration Function: $\log c = -3.859 - 0.0317\ N_d$ (Sensitivity doubled)

| Time, t (sec) | Number of Divisions, $N_d$ | Concentration of $AgIO_3$, c, ($M \times 10^6$) | $\ln \frac{C_2-C_1}{C_2-C}$ |
|---|---|---|---|
| 0 | 64.9 | 1.20 | 0 |
| 0.1 | 58.0 | 2.01 | 0.155 |
| 0.2 | 53.6 | 2.76 | 0.323 |
| 0.3 | 52.2 | 3.07 | 0.402 |
| 0.4 | 49.7 | 3.69 | 0.581 |
| 0.5 | 48.6 | 3.98 | 0.677 |
| 0.6 | 46.9 | 4.52 | 0.886 |
| 0.7 | 46.1 | 4.77 | 0.999 |
| 0.8 | 45.3 | 5.07 | 1.155 |

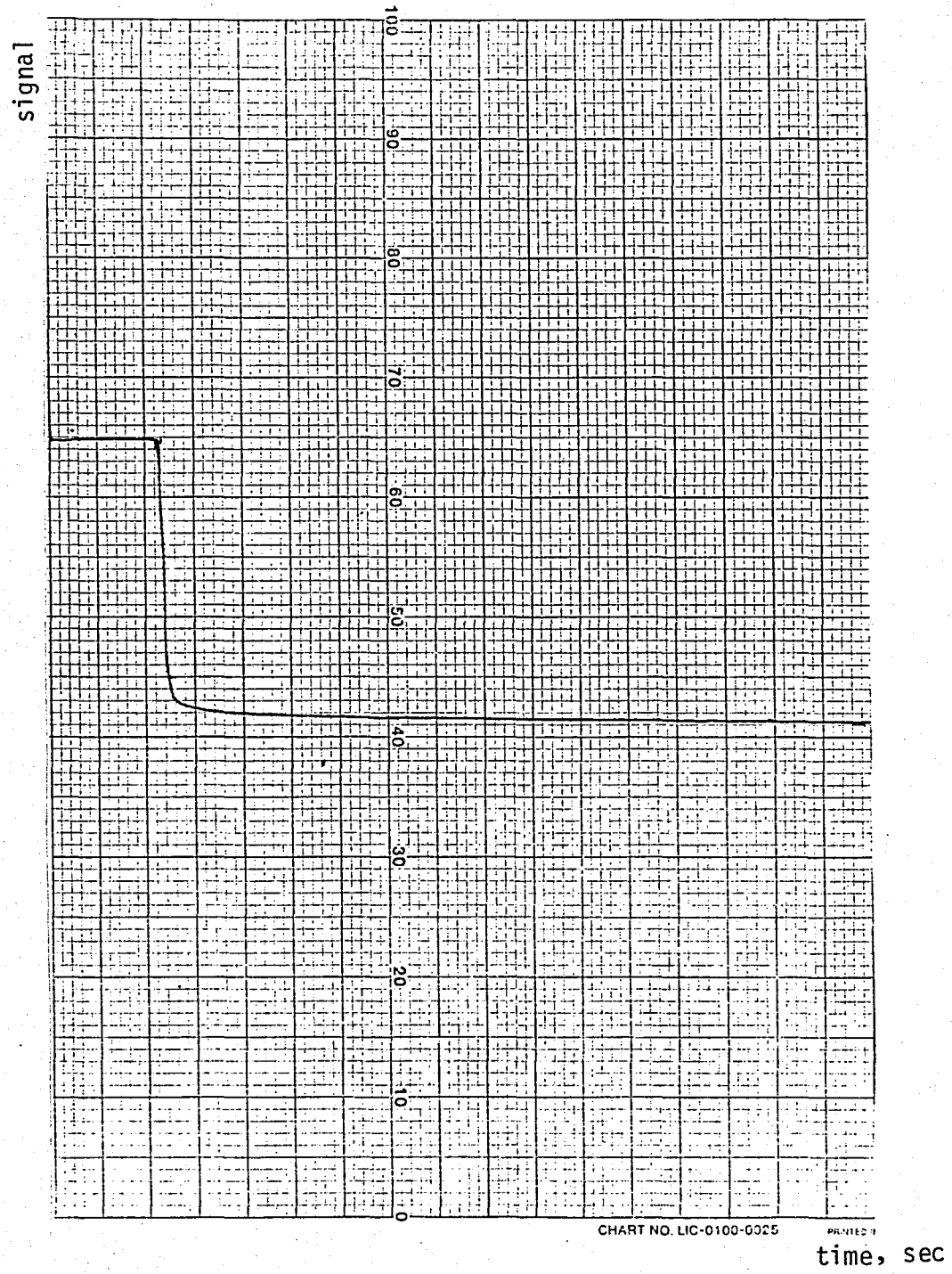


FIGURE A.4.1. Recorder Output for the Delay in Equilibriation at the Silver Electrode.

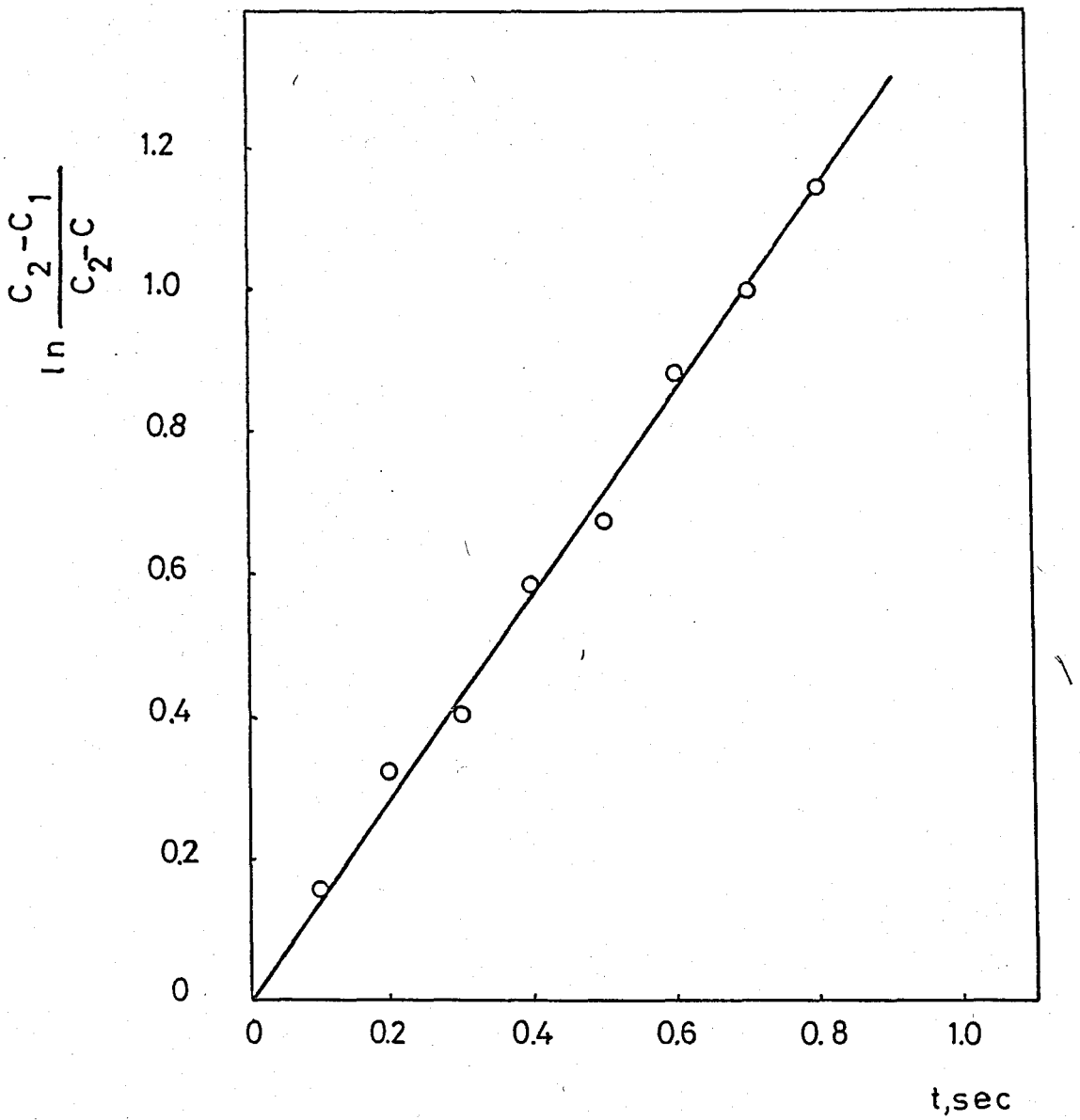


FIGURE A.4.2. Plot for the Evaluation of the Rate Constant for the Delay in Equilibriation at the Silver Electrode.

The actual concentration, $C_2$, changes linearly with time in the intermediate stages of dissolution (see the concentration v.s time plots given in Chapter 4). This can be expressed as follows

$$\frac{dC_2}{dt} = k' \qquad (A.4.4)$$

or integrating between the concentration limits from 0 to $C_2$ and the time limits from 0 to t,

$$\int_0^{C_2} dC_2 = k' \int_0^t dt \qquad (A.4.5)$$

$$C_2 = k't \qquad (A.4.6)$$

where k' is the rate constant for the dissolution. Substituting the value of $C_2$ in Equation A.4.6 into Equation A.4.1 and rearranging, the following differential equation is obtained

$$\frac{dC}{dt} + k_d C = k_d k't \qquad (A.4.7)$$

Equation A.4.7 is a linear differential equation whose solution is of the following form

$$C = \exp(-\int k_d dt)\left[\int \exp(\int k_d dt) k_d k't\, dt + \gamma\right] \qquad (A.4.8)$$

where $\gamma$ is integration constant Performing the necessary integrations and using the boundary condition (t=0; C=0), the following solution is reached

$$C = \left[t + \exp(-k_d t)/k_d - 1/k_d\right]k' \qquad (A.4.9)$$

Evaluation of k' from Equation A.4.9 requires the data given in Table A.4.2 which is obtained by using the dissolution data in distilled $H_2O$ at $25^oC$ and the value of $k_d$ obtained from delay experiments. The data of Table A.4.2 is plotted in Figure A.4.3 in proper coordinates. The slope of this plot gives k'

$$\text{Slope} = k' = \frac{6.9\times10^{-6} - 2.9\times10^{-6}}{58.41-26.41}$$

$$k' = 1.25\times10^{-7} \text{ mol/lt-sec}$$

A comparison of $k_d$ and $k'$ shows that $k' << k_d$. In other words, rate of dissolution is much smaller than the delay in equilibriation at the silver electrode. Therefore no correction is needed.

TABLE A.4.2. Data for the Evaluation of k'

| Time, t (sec) | Concentration of $AgIO_3$, c ($M\times10^6$) | $t + [\exp(-1{,}45\ t)-1]/0.63$ | $k' \times 10^7$ ($sec^{-1}$) |
|---|---|---|---|
| 20 | 1.9 | 18.41 | 1.03 |
| 28 | 2.9 | 26.41 | 1.10 |
| 36 | 4.0 | 34.41 | 1.16 |
| 44 | 5.0 | 42.41 | 1.18 |
| 52 | 6.0 | 50.41 | 1.19 |
| 60 | 6.9 | 58.41 | 1.18 |
| 68 | 7.9 | 66.41 | 1.19 |
| 80 | 9.1 | 78.41 | 1.16 |
| 88 | 9.7 | 86.41 | 1.12 |

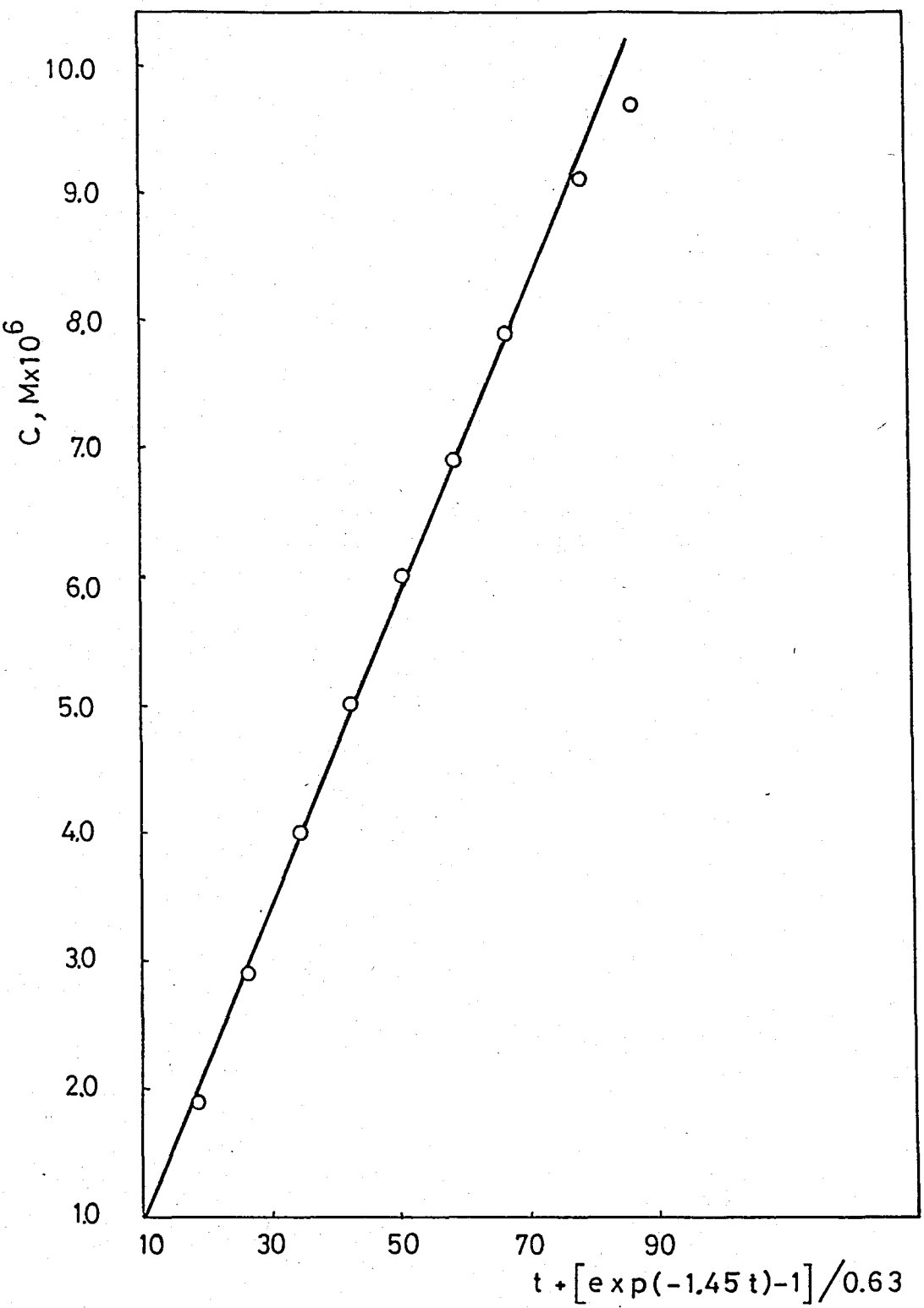


FIGURE A.4.3. Plot for the Evaluation of k'.

# BIBLIOGRAPHY


1. Jones,A.L., "Tracer Study of the Kinetics of Solution of AgCl," Transactions Faraday Society, Vol.59, pp.2355-2361, 1963.

2. Linge,H.G., "Dissolution of Ionic Crystal Surfaces," Advances in Colloid and Interface Science, Vol.14, pp.239-250, 1981.

3. Burton,W.K., Cabrera,N., Frank,F.C., "The Growth of Crystals and Equilibrium Structure of their Surfaces," Philosophical Transactions Royal Society, London, Ser. A243, pp.299-306, 1951.

4. Bennema,P., "Importance of Surface Diffusion for Crystal Growth from Solution," Journal of Crystal Growth, Vol.5, pp.29-36, 1969.

5. Davies,C.W., Jones,A.L., "A New Discussion on Surface Dissolution: Adsorption Layers," Transactions Faraday Society, Vol.51, pp.812-820, 1955.

6. Engell,H.J., "The Solution of Oxides in Dilute Acids. The Electrochemistry of Ion Crystals," Zeitschrift für physikalische Chemie, N.F., Vol.7, pp.158-165, 1956.

7. Vermilyea,D.A., "Electronic Conduction in Anode Films-Role of Forming Solution," Journal of Electrochemical Society, Vol.113, pp.1067-1071, 1966.

8. Lee,C.H., Yeager,E., "Electrochemical Aspects of the Dissolution of Ionic Crystals," Technical Reports, No.5, Case Western Reserve University, Cleveland, Ohio, p.83, 1969.

9. Landsberg,R., Fürtig,H., "Passivation Experiments on Nickel Anodes in Potassium Cyanide Solutions," Zeitschrift für physikalische Chemie (East German), Vol. 216, pp.212-219, 1961.

10. Enüstün,B.V., "Rate of Dissolution of an Ionic Solid," M.E.T.U.Journal of Pure and Applied Sciences, Vol.9, No. 2, pp.133-143, 1976.

11. Adamson,A.W., Physical Chemistry of Surfaces. 2nd.ed., Interscience Publishers, p.240, 1968.

12. Enüstün,B.V., Ayrancı,E., "Solubility Rate of Silver Iodate," Bilim Kongresi Matematik-Fizik-Biyolojik Bilimler Araştırma Grubu Tebliğleri, T.B.T.A.K., 1977, Kimya Seksiyonu, pp.233-239, 1979.

13. Gmelins Handbuch der Anorganischen Chemie, 8. Auflage, Vol.61, pp.434-445.

14. C.R.C. Handbook of Chemistry and Physics, 51st ed., p.B-210, 1969.

15. Liu,Sung-Tsuen, Noncollas,G.H., "Kinetics of Dissolution of Calcium Sulfate Dihydrate," Journal of Inorganic Nucleation Chemistry, Vol.33(8), pp.2311-2316, 1971.

16. Eksen,O., Constable,F.H., "The Analysis of the Solution Kinetics of Barium Carbonate and Its Determination by Its Heat of Activation,", Istanbul Üniversitesi Fen Fakültesi Mecmuası, Seri C, Vol.39-40-41(1-3), pp.161-167, 1977.

17. Huheey,J.E. Inorganic Chemistry, 2nd.ed., Harper and Row, Publishers, p.74, 1978.

18. Castellan,G.W. Physical Chemistry, 2nd ed., Addison Wesley Co., p.723, 1971.

19. Harnet,H.S., Owen,B.B. The Physical Chemistry of Electrolytic Solutions. 3rd.ed., Reinhold Publishing Corporation, p.253, 1958.